Control of High Precision Roll-to-Roll Printing Systems

by

Zhiyi Chen

A dissertation submitted in partial fulfillment
of the requirements for the degree of
Doctor of Philosophy
(Mechanical Engineering)
in the University of Michigan
2023

Doctoral Committee:

Professor Jun Ni, Chair
Associate Professor Neil Dasgupta
Professor Stephen Forrest
Associate Professor Gabor Orosz

Zhiyi Chen
chzhiyi@umich.edu
ORCID iD: 0000-0002-4414-2030

To my family

ACKNOWLEDGMENTS

As I reflect on my journey leading up to this moment, I am filled with a sense of gratitude and accomplishment. The past few years spent in Ann Arbor, at the University of Michigan, have shaped me both academically and personally. This vibrant city has become my second home, and I am proud to say that I am ready to embrace the next chapter of my life, knowing that I am about to earn this degree through dedication and hard work.

I would like to begin by expressing my gratitude to my advisor, Professor Jun Ni. As the founder of the UM-SJTU Joint Institute, he has played an instrumental role in bringing me to this pivotal stage in my life. Professor Ni's mentorship extends far beyond scientific problem-solving; he has shared with me his wisdom on approaching challenges and making life-defining choices. From helping me select the graduate program to guiding me in choosing a research topic and career path, Professor Ni has been an unwavering source of support and guidance.

I would also like to extend my sincere gratitude to Professor Stephen Forrest, one of the co-founders of the Joint Institute. His generosity in offering me the opportunity to collaborate on my first comprehensive research project has had a significant impact on my subsequent studies.

To my dissertation committee members, Professor Gabor Orosz and Professor Neil Dasgupta, I am grateful for their willingness to serve and provide invaluable feedback. Without their help, I would not have been able to bring my dissertation to its current state of completeness.

I would like to acknowledge Dr. Shantonio Birch for inspiring me to embark on this degree journey; Prof. Xun Huan for his guidance on my research projects; Dr. Huanyi Shui for her support throughout this entire process; and Boning Qu for being an exceptional collaborator. I extend my appreciation to Dr. Yulong Cao, for being my former roommate and providing technical support; Dr. Yuxin Chen for being a close friend since my undergraduate years.

I am grateful for the collaborations with our industry partners, especially Dr. Harshal Maske, Dr. Devesh Upadhyay, Michael Hopka, and David Porter. Their involvement has added valuable real-world perspectives to my research.

I am thankful for the moments shared with my labmates, Dr. Yangbing Lou, Dr. Baoyang Jiang, Dr. Kai Chen, Dr. Hao Lei, Dr. Farhang Momeni, Dr. Ankush Bansal, Dr. Xingjian Lai, Dr. Joseph Cohen, Tianchen Qiu, Tianxing Ma, Yuzhang Liu, Haozhen Chen, and Shuyu Long. Their presence and shared experiences have made our lab an inspiring and supportive environment. Additionally, I would like to thank my friends Zhengyang Lyu, Xiaheng Huang, Yifan Wei, Kaiwen Liu, Keyi Cai, Ji Qiu, Ziyang Zhong, Weilun Peng, Dr. Jingxuan Lyu, Dr. Tianshu Dong, Pinyi Wu, Dr. Ying Luo, Dr. Bowei Li, and Jianbo Gu for their support and friendship throughout this journey.

Lastly, I want to express my heartfelt appreciation to my parents, Lingsong Chen and Xiaoke Jing, and my grandparents, Guixiang Chen, Libin Zhuo, Fengrui Jing, and Yuying Yue. Your love, support, and belief in my abilities have been the foundation of my success. I know you all have been anticipating this moment, and the time you are awaiting is now within reach.

TABLE OF CONTENTS

LIST OF FIGURES

FIGURE

LIST OF TABLES

TABLE

ABSTRACT

Roll-to-Roll (R2R) printing technology offers high-speed and continuous processing of substrate-based products, making it attractive for various industries. However, R2R processes often suffer from lower precision compared to traditional batch processes, limiting their widespread adoption in high-precision production.

This dissertation aims to develop advanced control strategies to improve the finished product quality in R2R printing systems. Solutions are developed firstly from the process-level and then to the system-level to achieve this purpose. In Chapter 2, a robust tension control scheme is proposed to ensure consistent tension levels throughout the R2R system. The control approach employs a linear parameter-varying model predictive control framework, specifically designed to handle model uncertainties and slowly-changing dynamics that can affect tension control performance.

Chapter 3 introduces a constrained registration accuracy control scheme, aiming to achieve precise alignment of printed layers in R2R systems. The proposed control synthesis framework utilizes an algebraic Riccati equation and control barrier functional techniques to eliminate registration errors while maintaining system safety. This control strategy directly addresses product quality concerns and enhances the accuracy of the printing process.

In Chapter 4, the focus shifts to system-level optimization through the design of deep Koopman modeling and supervisory control. The deep Koopman model learns the system dynamics and propagates quality characteristics across different stages of the R2R process. A supervisory control scheme is developed based on the learned model, enabling accurate prediction of potential quality disruptions and proactive adjustment decisions to improve overall system performance.

The proposed control strategies are validated using datasets collected from real or simu-

lated R2R production systems. Overall, this dissertation contributes to the advancement of control strategies for R2R manufacturing, providing valuable insights and tools to enhance efficiency, reliability, and enable the adaptation of R2R processes to various industrial applications.

CHAPTER 1

Introduction to Roll-to-Roll Processes

1.1 Motivation

Roll-to-Roll (R2R) printing technology is a highly efficient method for continuous processing of substrate-based products. This manufacturing process utilizes rollers to transport and/or process substrate materials at high speeds. In the technological review of 2015, the Department of Energy has already recognized the critical role of R2R in addressing environmental and economic challenges [1]. While there are alternative methods to produce similar products, R2R processes offer advantages such as high production rates, automation, and potential for cost reduction. R2R systems can be integrated with various processing technologies, making them highly versatile in many industries. Traditionally, R2R processes have been utilized for producing paper, sheet metal, and fabrics [2, 3]. Beyond these, recent developments have demonstrated the potential of utilizing R2R production lines for new industrial applications such as battery manufacturing [4], photovoltaics production [5], and flexible electronic device production [6].

Figure 1.1 illustrates different designs for substrate-based product manufacturing, including sheet-to-sheet and sheets-on-shuttle methods. They are representatives of discrete manufacturing processes which involve distinct finished products that can be easily separated and counted. However, in these processes, semi-finished products undergo a cycle of processing, transferring, storing, and waiting for subsequent processing, which can lead to production inefficiencies and delays. In contrast, R2R processes produce a continuous flow of products that are not immediately

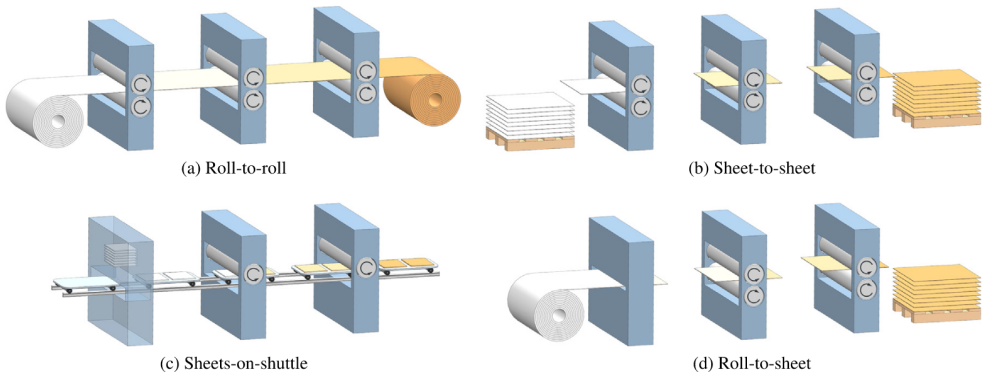

Figure 1.1: Overview of the substrate transport mechanisms [7].

cut into individual units, although a boundary can be set between each unit. In R2R processes, substrates are connected from the unwind roller, where raw materials are released, all the way to the rewind roller, where finished products are collected. Note that operation machines can be placed as intermediate stages to process the substrates.

A recent study compared the production costs of organic light emitting devices (OLEDs), specifically white OLEDs, using conventional discrete processing methods versus R2R manufacturing [8]. The findings showed that R2R manufacturing, along with the corresponding processing methods, significantly reduced the cost of producing white OLEDs. The estimated cost decreased from at least $\$50/\mathrm{klm}$ [9] using conventional methods to $\$12.5/\mathrm{klm}$ with R2R manufacturing. Further improvements in device quality and incremental reductions in miscellaneous costs are expected to further decrease the cost to $\$6.3/\mathrm{klm}$ in the near future. This cost reduction will make R2R-based OLED products an economical solution for lighting applications. It is important to recognize that this study represents just a glimpse of the potential benefits of R2R manufacturing for flexible electronic applications, indicating the vast opportunities it holds in various industries.

In many applications, R2R processes can be integrated into a production line, providing more flexibility in designing the manufacturing processes. For example, roll-to-sheet (R2S) production combines R2R processes with sheet-to-sheet technologies, where substrate sheets are delivered by high-speed R2R processes. A case study by Yang and Von Olmen demonstrated the use of a R2S process to fabricate multilayer ceramic capacitors (MLCC) [10]. One would notice

that the conversion from roller-based to sheet-based methods occurs between the screen printing process and the layer stacking process. While using sheet-based methods can significantly slow down the process compared to R2R methods, it becomes the preferable way to ensure the accuracy and precision of the stacking process in many scenarios that involve multilayer patterning.

A significant problem with R2R systems, in general, is that the consistency of their finished products is relatively low (or, in other words, they provide poor product quality) compared to traditional discrete processes. This issue is particularly vital when using R2R to print high-precision devices. For example, thin films fabricated by R2R processes typically suffer from large variations in registration quality, as noted in [7]. Although many laboratory studies have successfully implemented R2R processes for the complete production of flexible thin-film devices, their application in real semiconductor industry is still limited. This is because when producing small batches of devices in laboratories, the impact of ambient noise is less severe. During industrial mass production, significant environmental noise or unexpected disturbances can lower the yield of a R2R manufacturing system and can even cause the system to fail. Therefore, enhancing the performance of R2R printing systems under disturbances is crucial to enable their adoption in mass production.

This dissertation aims to develop advanced control strategies that are specifically designed for R2R printing systems. Standing on the shoulders of existing R2R hardware designs (as demonstrated in [5], [11], [12]), the proposed methodologies approach from algorithmic perspectives to improve the system reliability and ending product quality.

1.2 Research Issues

In R2R systems, multiple machines are often connected together to form a continuous production line. Due to this fact, R2R processes pose some distinct challenges in addition to those usually encountered in discrete manufacturing systems. The challenges include but are not limited to:

1. *Machine coupling* refers to the interconnected nature of R2R systems, making it difficult to isolate an individual machine from its neighbors and identify the impact of key process characteristics. The interconnection of the R2R machines also means that the failure of one machine can quickly affect the whole production line, leading to downtime and decreased productivity. This is essentially the most significant property that causes troubles in designing high-performance R2R systems.

2. *Nonlinearity* is a common issue in R2R processes, which can result from the nonlinear dynamics of processing machines and their interaction with each other. Such nonlinearities can cause unexpected behavior and performance degradation, making it difficult to design and control R2R systems. For instance, nonlinearities in the coating/deposition process make it hard to obtain uniform layer thickness, which causes variations in the mechanical and electrical properties of the printed films.

3. *Time delay* refers to the delay between the printing of one layer and subsequent layers in R2R systems. Various factors, such as substrate speed, layer printing time, and curing time can cause this delay. Time delay can have a significant impact on the final properties of the printed film, particularly in terms of the registration accuracy of the layers. While in sheet-to-sheet processes, operators can design registration markers to achieve good layer alignment, achieving high registration accuracy during the continuous movement of the substrate is extremely challenging.

4. *Unknown system dynamics* commonly happens especially when R2R systems involve solution/vapor treatments. The behavior of the solution or vapor, as well as its interaction with the substrate and other materials in the system, can be complex and difficult to predict. In practice, rule-based methods can be used to characterize process properties. However, these methods have limited capability to interpolate a large design space, which can lead to conservative process performance. Therefore, this issue is particularly challenging for large-scale systems.

These challenges can significantly degrade system performance and ultimately lead to disruptions in product quality.

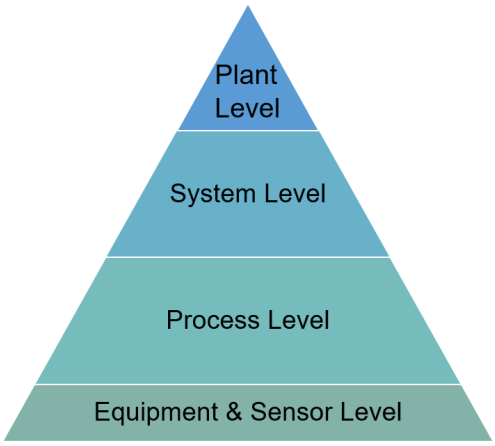

Figure 1.2: The research pyramid for developing R2R systems.

To achieve high-performance and automated production, researchers have proposed a hierarchical approach known as the "automation pyramid." This approach aims to organize the five different levels of automation in a manufacturing system, including field level, control level, supervisory level, management level, and enterprise level [13]. Similar to the automation pyramid, the operation of high-performance R2R processes requires efforts from four different levels, as shown in Figure 1.2. Each level involves different types of research work that contribute to the overall success of the process.

Level I involves the fundamental design of equipment and sensors necessary for R2R processing, including the development of thin-film processing technologies [5, 14], system configuration [15, 16], and sensors [17, 18] for monitoring the process parameters. The goal of this level is to establish a reliable and robust R2R process design.

Level II focuses on developing models [19, 20] and process control schemes [21, 22] for R2R systems. This includes developing dynamics models that describe the system behavior and control strategies that can adjust the process to maintain desired performance levels. The goal of level II is to improve process stability and produce quality products by monitoring the system status and enabling real-time feedback control.

Level III involves research on integrating a R2R stage into a larger manufacturing system. It covers topics such as developing decision-making tools for identifying bottlenecks [23], optimizing production schedules [24], and coordinating process parameters [25] so that the incorporated subsystems can better cooperate with each other. The goal of this level is to find the optimal settings for large-scale R2R systems and maximize their efficiency.

Level IV concerns managing manufacturing facilities and optimizing their performance as a whole, from raw material acquisition to final product delivery, through effective management and coordination of all related processes. This level includes topics such as designing the layout of a factory [26], supply chain management [27], and managing inventory levels [28]. The goal of Level IV is to ensure that all manufacturing systems are streamlined and coordinated for maximum efficiency, productivity, and profitability.

The objective of this dissertation is to propose solutions that enhance the performance of R2R processes by addressing critical issues in Level II and Level III. By doing so, the goal is to achieve a higher level of automation in R2R processes, which can lead to improved product quality. The proposed solutions can serve as a basis for future research that can further optimize the processes from economic and operational perspectives. More specifically, the rest of this dissertation will present work regarding: (1) Tension control; (2) Registration accuracy control; and (3) Quality propagation modeling and supervisory control.

1.3 Research Objectives

One of the most important objectives in mass production is to reduce the quality variation between individual products. In R2R systems, substrate tension is the most important process parameter that operators would pay attention to. Therefore, this dissertation will start by designing a robust tension control scheme that will benefit most R2R printing systems. This considers the process control of a R2R system.

However, tension control is, after all, an indirect means of performing quality control. To

further improve quality control, it is important to also consider direct quality measures of printed materials. One such measure is registration accuracy, which is extensively considered in this dissertation. A novel framework will be introduced to address the limitations of conventional process control schemes. The framework places significant emphasis on directly targeting quality-related characteristics, while simultaneously ensuring that the process characteristics remain within desired control limits to ensure system safety.

Tension control and registration control are both considered process-level studies in the research hierarchy (Figure 1.2) because they involve real-time control of process characteristics by commanding actuators (i.e., motors in our case). These control techniques can be applied to different parts of a R2R system for local control. For example, the tension controller can be applied to the winding and rewinding subsystems, while the registration controller is applied to the printing subsystem. However, the optimal cooperation across all subsystems requires a supervisory controller responsible for the system-level control. The third part of this research focuses on developing a data-driven system-level control algorithm to supervise and coordinate lower-level controllers. This approach enables the R2R system to achieve optimal efficiency and reduce quality variations, which is critical for industrial applications.

The three topics covered in this dissertation are conducted following a bottom-up routine, where each level is built upon the previous one. An overview of the topics is shown in Figure 1.3.

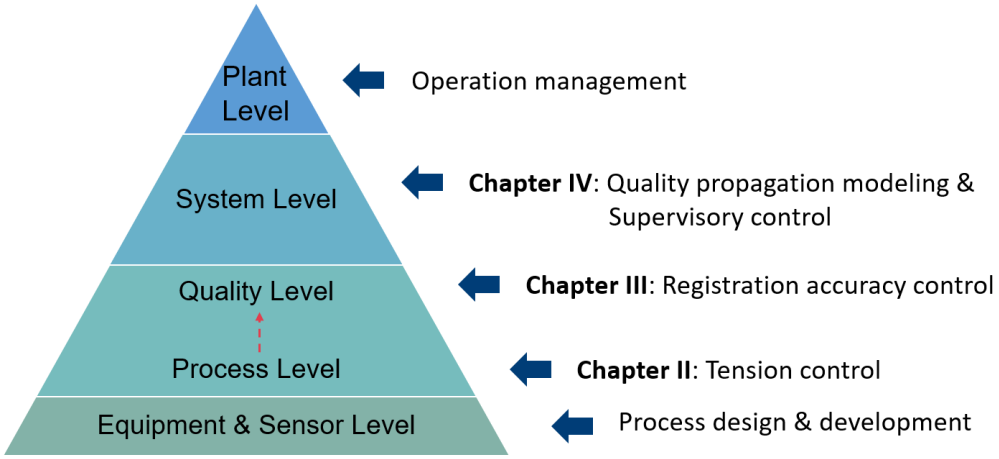

Figure 1.3: Framework of the dissertation.

In summary, this dissertation will make three main contributions to the field of R2R printing systems:

1. A robust tension control scheme is developed, enabling R2R printing to be applied to applications with tight tension margins.

2. A registration accuracy controller is designed to facilitate the fabrication of high-precision thin-film devices using R2R processes.

3. A data-driven supervisory controller is devised to coordinate process controllers and improve operational efficiency while reducing quality variations.

1.4 Thesis Outline

The rest of this thesis will describe the following topics in detail.

1.4.1 Chapter II: Tension Control

Studies have shown poor tension control can lead to cracks, deformation, and registration problems in the printed patterns [29, 30]. However, maintaining substrate tension at a desired stable level takes significant effort.

This chapter proposes a robust linear parameter-varying model predictive control (LPV-MPC) scheme to improve tension tracking performance in R2R systems. The controller is designed to handle model uncertainties and slowly-changing dynamics that can lead to performance degradation in traditional tension controllers. The proposed controller uses an incremental model to eliminate errors caused by the mismatch between the nominal model and the actual system. A tube-based MPC formulation, combined with scheduled parameters, enables adequate model updates and correction of time-varying dynamics. The operation of this control algorithm is illustrated through the simulation of an actual R2R system. The controller outperforms the

benchmarks in terms of fast transient response and offset-free tension tracking. It also demonstrates immunity from variations due to parametric uncertainties

1.4.2 Chapter III: Registration Control

For the production of most thin-film devices, it is necessary to stack multiple layers together. In traditional discrete manufacturing processes, low registration error can be achieved by aligning correction marks at a static position. However, aligning the patterns dynamically during movement in R2R processes can be challenging.

This chapter presents an algorithm for simultaneous control of registration accuracy and tension in R2R processes. In contrast to existing control algorithms that aim to balance both variables equally, the proposed algorithm aims to improve registration accuracy as the primary objective, while ensuring that tension remains within specified control limits. A primary controller is designed to reject fluctuations of registration errors during nominal operation, and a barrier functional evaluates the severity of tension constraints. A safety controller takes over the primary controller when tension is likely to violate the constraints to ensure system safety. The algorithm is validated on a simulation model, demonstrating improved registration accuracy and while maintaining stable tension control.

1.4.3 Chapter IV: Quality Propagation Modeling and Supervisory Control

R2R processes usually involve multiple operation stages and the final product quality is determined by a series of operations. Therefore, the determination of the optimal operation settings for the whole production system is important but challenging. Conventional approaches rely on pre-defined set points to guide processes, which do not allow for dynamic responses to unforeseen changes.

This chapter introduces a new framework that integrates deep learning techniques and Koopman operators to model quality propagation in R2R processes. By utilizing a transferred linear representation, the model captures the generic nonlinear quality evolution and enhances the

interpretability of the data-driven algorithm. A nonlinear programming problem is then formulated to determine optimal operation settings, which can dynamically respond to unforeseen changes and supervise the lower-level process controllers. A case study demonstrates that this methodology reduces variation in R2R processes. Additionally, this modeling and control framework requires minimal knowledge of the underlying system, making it adaptable to a wide range of processes. It can be combined with the methodologies presented in Chapters II and III to improve the coordination of manufacturing systems.

1.4.4 Chapter V: Conclusion

This chapter provides a comprehensive summary of the key findings and contributions of the dissertation. Additionally, the chapter suggests potential areas of investigation that could expand upon the current work, and outlines the importance of continued research in the field.

CHAPTER 2

Robust Constrained Tension Control for High Precision Roll-to-Roll Processes

2.1 Introduction

Tension control is critical for maintaining good product quality in most roll-to-roll (R2R) production systems. Substrate tension in different sections of the system can all be affected by local disturbances, such as ambient noises, non-uniform material properties, eccentricity of rollers, and changes in machine settings etc. In addition, the coupling between machines means that any presented tension fluctuation can be propagated to other sections of the production line, making the prediction of system behavior and compensation of the fluctuation harder than one would imagine. Hence, numerous studies have been conducted to design advanced tension controllers to address the issue of tension fluctuation in R2R systems. However, despite the progress made, the performance of these controllers falls short of the industry's requirements.

The overall objective of designing R2R motion controllers is to increase transport speed while maintaining tensions at the required level to avoid distortion or break of substrates. However, achieving this bi-objective task is difficult because of the great number of disturbance sources in the noisy manufacturing environment and, more importantly, the nonlinear and time-varying dynamics of R2R processes. Mechanics of R2R processes have been studied since the 1960s and are complemented in some recent works [20, 31, 32, 33, 34]. The never-ending improvements are essential because R2R is waiting to be applied in complicated scenarios requiring higher precision.

Early works modeling the lateral and longitudinal dynamics of R2R processes were reviewed in [31]. The R2R dynamics were summarized in differential equations and further utilized for deriving a proportional integral derivative (PID) controller. Following this approach, decentralized PI and PID controllers were developed to handle large-scale R2R systems with multiple spans. A PI controller designed with a tension observer was found in [35]. An adaptive PI control scheme was implemented in [36] to handle changing operating conditions and material properties. Due to the ease of implementation, decentralized PID controllers still serve as the mainstream control scheme in the current R2R industry [20].

Limitations of the PID-type controllers mainly come from their slow response and low control accuracy. With a state space representation of R2R processes being developed, multivariable controllers are designed to improve control performance. In [20], an optimal feedback gain-based decentralized controller was designed to outperform the PID-based controllers. However, the decentralized algorithm dismisses the inter-stage coupling in R2R systems. It is noticed that tension disturbances can propagate between adjacent manufacturing stages. A decentralized coordinated control strategy was proposed by [37] to reduce the propagation while enhancing the disturbance rejection performance. In [38, 39], active disturbance rejection controllers were designed to detect tension perturbances and provide significant anti-disturbance capability. It is well-recognized that model-based control algorithms may suffer from parametric uncertainties in real practice. Therefore, adaptive control and robust control schemes have been developed to better address the uncertainties. In [40], authors showed that an adaptive H_∞ controller designed with a neural-fuzzy gain approximator could accommodate parameter variations and improve the transient response of the system. An adaptive sliding mode controller was presented in [41] to compensate for the change in web elasticity caused by the heating/cooling sections of a R2R process. The limitation of adaptive controllers mainly lies in the fact that their stability is not guaranteed rigorously, and random process noises may degrade their performance. Alternatively, robust control schemes are used more often in R2R applications. 2-*DOF* gain-scheduled H_∞ controllers were presented in [42, 43]. The controllers included a feedforward mechanism to

decouple tensions and velocity, aside from the conventional considerations of only feedback to reject perturbations. H_∞ controllers with semi-centralized and decentralized structures were developed in [44, 45] to handle tension fluctuations under bounded model uncertainties. In [22], the researchers developed a robust decentralized coordinated controller by explicitly considering the variations in state and control matrices of the state space model.

The approaches mentioned above are primarily designed to improve the control performance in rejecting tension perturbations. In contrast, the study on the assurance of accurate tension tracking is relatively limited. High-precision tension tracking requires the actual substrate tension to closely follow its pre-designed set points. Keeping the substrate tension at a consistent level is critical, as drifting and fluctuations in tension can easily cause defects in semiconductor products [46]. In this work, we address three main challenges in high-precision tension control. Firstly, the complicated material processing operations (e.g. coating, drying) cause variations in substrate elasticity, leading to model uncertainties. Therefore, it is critical that a controller can handle discrepancies between the nominal model and the actual system, or saying, has good robustness against model mismatches. Secondly, R2R system dynamics are time-varying due to the continuous change in roller radius and inertia. A well-designed controller must correct for disturbances caused by the time-varying dynamics. Thirdly, the performance of the controller may degrade in the presence of constraints. Under complicated operating environments, violating physics-induced state and control constraints in the system risks the controller reliability and causes machine failures. We will demonstrate in the simulation study that these three challenges can all lead to failure in tracking the tension target.

Model predictive control (MPC) has been extensively applied to industrial applications [47]. It has great potential to resolve the above issues because of its verified performance in reference tracking tasks and ability to manage constraints. In [48], the author reviewed three different MPC formulations that achieved offset-free reference tracking under model mismatches. One offset-free MPC scheme was applied to R2R processes in [49]. However, these MPC formulations could not deal with time-varying disturbances. Min-max MPC and tube-based MPC

schemes are the most common MPC formulations to deal with disturbances. Min-max MPC seeks solutions that minimize the control loss for the worst case [50]. Solving a min-max MPC online is computationally expensive, and the solutions may be conservative. In contrast, tube-based MPC requires less online computation, which is more favorable in our case. Tube-based MPC needs one to define an uncertainty boundary so that the evolution of the uncertain system will stay within a sequence of tubes [51, 52]. In [53, 54], the tube-based MPC was generalized to linear time-varying systems. Most robust MPC schemes lump model uncertainties with disturbances and treat them together. In [55], the authors proposed an MPC scheme for linear time-invariant systems that coped with external disturbances separately from model uncertainties.

In this work, a robust linear parameter-varying model predictive control (LPV-MPC) scheme is designed and implemented to achieve high-precision tension tracking in R2R production lines. In [34, 22], a large disturbance set was introduced to bound the possible perturbations in R2R processes, resulting in conservative control performance. Following the idea of [55], our approach breaks down the perturbations into model mismatches and time-varying disturbances. Mismatches between the model and the true dynamics are essentially model uncertainties, which are handled by introducing an incremental model. Time-varying dynamics, as varying but bounded disturbances, are compensated by a tube-based MPC with scheduled parameters. A set of constraints on the rated motor torque is defined and formulated into the MPC design to account for the dynamical restrictions in R2R systems. Our method performs more progressively than the classical robust MPC frameworks when compensating for large disturbances. Specifically, we can achieve zero-offset tension tracking in the long run of a R2R process with reduced online computation. Simulation of an actual R2R deposition system for solid state lighting applications is carried out to demonstrate the control performance. It turns out that the proposed controller outperforms the benchmarks from the literature and shows good robustness to the parametric disturbances.

The rest of this chapter is organized as follows. Section 2.2 reviews the dynamic models from the literature and derives an augmented model in an incremental form. Section 2.3 describes the design of MPC schemes, including a standard formulation and the proposed robust formulation.

Section 2.4 introduces the setup of the simulation and the comparison studies. The short-term and long-term performance of the proposed controller in the simulated R2R system is demonstrated. Finally, section 2.5 concludes the work presented in this chapter and suggests future work.

2.2 Dynamic Models

A typical R2R process consists of a series of active rollers coupled with passive rollers in between. R2R processes can be decomposed into multiple operation stages: unwind stage, master speed stage, processing stages, and rewind stage. A schematic of a simplified R2R production line is shown in Figure 2.1.

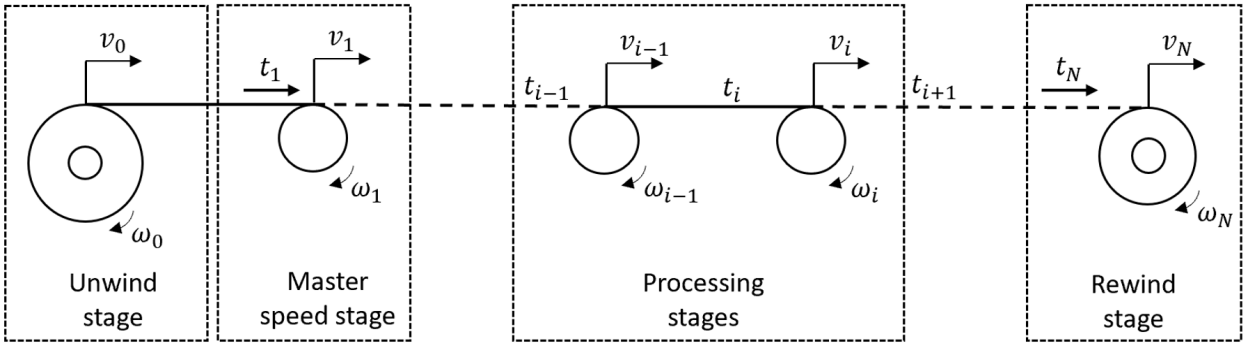

Figure 2.1: Schematic of a simplified R2R production line at steady state: only active rollers are depicted.

In Figure 2.1, v_i is the transport speed of substrate at the i^{th} stage, for $i = 0, 1, \ldots, N-1$, where N denotes the total number of active rollers. ω_i is the angular speed of the i^{th} active roller. t_i is the substrate tension between the $(i-1)^{th}$ and i^{th} rollers. Three major assumptions are made here to simplify the system:

1. Passive rollers directly affect tension dynamics at transient states due to acceleration/deceleration [20]. Their impact can be reflected in the mass of the system and frictional force at the steady state, and thus, they are ignored in the schematic.

2. At the steady state, tension is equivalent everywhere on the substrate span between two

adjacent rollers. Based on this assumption, an entire production line can be decomposed into multiple tension zones.

3. There is no slippery between rollers and substrates. Therefore, v_i and ω_i can be characterized by $v_i = \omega_i R_i$, where R_i is radius of the corresponding roller.

These assumptions are of great value in practice and are used to derive the dynamic models in the literature.

2.2.1 Nonlinear Model

The dynamics of each stage have been well studied in the literature. When modeling the tension and speed dynamics, one should pay attention to the key characteristics, tensions t_i, and speeds v_i. Control inputs are the motor torques applied on each active roller u_i, as discussed in the following content. A brief review of the dynamics is given below for the completeness of the presented work. More details can be found in [20].

Unwind stage: The unwind stage is where the material roll is stored. The mass of a material roll keeps decreasing during a process when the substrate is transported to downstream stages, causing the dynamics of a R2R process to change over time. Designing a controller that can adapt to such a change of dynamics will significantly improve the system performance. The dynamics of the unwind stage are given by:

$$\dot{t}_1 = \frac{AE}{L_1} v_1 - \frac{AE}{L_1} v_0 + \frac{t_0}{L_1} v_0 - \frac{t_1}{L_1} v_1 \tag{2.1}$$

$$\dot{v}_0 = \frac{R_0^2}{J_0} t_1 - \frac{b_{f0}}{J_0} v_0 - \frac{h_s}{2\pi J_0} \left(\frac{J_0}{R_0^2} - 2\pi \rho_s b_s R_0^2 \right) v_0^2 - \frac{n_0 R_0}{J_0} u_0 \tag{2.2}$$

where A, E, ρ_s, b_s, h_s are cross-sectional area, Young's modulus, density, width and thickness of the substrate, respectively; L_i is the length of the substrate span between the i^{th} roller and the $(i+1)^{th}$ roller; b_{fi} are friction coefficients; n_i are gear ratios; R_i and J_i are in-situ roller radius and inertia. Note that t_0 is tension in the material roll, while t_i are tensions on the downstream

substrates. We will use i to represent the index of the corresponding operating stage if not specified in the following content.

Master speed stage: Master speed roller usually refers to the active roller right before the first processing stage. It provides the reference speed for the entire production line. Its dynamics are derived as follows:

$$\dot{v}_1 = \frac{R_1^2}{J_1} t_2 - \frac{R_1^2}{J_1} t_1 - \frac{b_{f1}}{J_1} v_1 + \frac{R_1 n_1}{J_1} u_1 \tag{2.3}$$

Processing stage: There are different kinds of manufacturing processes, including pattern printing, heating, drying, etc., that can occur in the processing stage. The model is developed based on gravure printing processes. However, it can be easily extended to other applications. The dynamics are derived as follows:

$$\dot{t}_2 = \frac{AE}{L_2} v_2 - \frac{AE}{L_2} v_1 + \frac{t_1}{L_2} v_1 - \frac{t_2}{L_2} v_2 \tag{2.4}$$

$$\dot{v}_2 = \frac{R_2^2}{J_2} t_3 - \frac{R_2^2}{J_2} t_2 - \frac{b_{f2}}{J_2} v_2 + \frac{R_2 n_2}{J_2} u_2 \tag{2.5}$$

Rewind stage: The rewind roller is usually placed at the end of a R2R process, and used to collect the processed materials (product). In contrast to the unwind stage, the mass of the product roll keeps increasing during a process. The dynamics are given by:

$$\dot{t}_N = \frac{AE}{L_N} v_N - \frac{AE}{L_N} v_{N-1} + \frac{t_{N-1}}{L_N} v_{N-1} - \frac{t_N}{L_N} v_N \tag{2.6}$$

$$\dot{v}_N = -\frac{R_N^2}{J_N} t_N - \frac{b_{fN}}{J_N} v_N 0 + \frac{h_s}{2\pi J_N} \left(\frac{J_N}{R_N^2} - 2\pi \rho_s b_s R_N^2 \right) v_N^2 + \frac{n_N R_N}{J_N} u_N \tag{2.7}$$

Idlers: Idlers, or passive rollers, do not contribute to tension dynamics by assumption. Their impacts on the system can be introduced into J_i and b_{fi} terms in the previous equations.

2.2.2 Linearized Model

When applied to large-scale R2R systems, the nonlinear model can be represented in a

linear parameter-varying (LPV) form to achieve fast online computation. For state variables (t_i, v_i) and control inputs u_i, define $T_i = t_i - t_{ri}$, $V_i = v_i - v_{ri}$ and $U_i = u_i - u_{ri}$, where t_{ri}, v_{ri}, u_{ri} are the reference substrate tensions, transport speeds, and motor torques at steady state. In fact, t_{ri}, v_{ri}, u_{ri} are the pre-designed operating points that a R2R process should refer to. At time stamp k, define states $\boldsymbol{X}_k = [V_0, T_1, V_1, \ldots, T_N, V_N]_k^{\mathrm{T}}$, and control inputs $\boldsymbol{U}_k = [U_0, \ldots, U_N]_k^{\mathrm{T}}$. A discrete-time model can be derived as

$$\begin{aligned} \boldsymbol{X}_{k+1} &= A_{d,k}\boldsymbol{X}_k + B_{d,k}\boldsymbol{U}_k \\ \boldsymbol{Y}_k &= C_d\boldsymbol{X}_k \end{aligned} \tag{2.8}$$

where $A_{d,k} \in \mathbb{R}^{n_x \times n_x}$, $B_{d,k} \in \mathbb{R}^{n_x \times n_u}$, and $C_d \in \mathbb{R}^{n_y \times n_x}$ are the system matrix, input matrix and output matrix, respectively. For R2R systems, $A_{d,k}$ and $B_{d,k}$ are time-varying matrices due to the changing dynamics. In addition, it is assumed in our case that perfect observation of tension and speed measurements is available, thus C_d becomes an identity matrix.

Without loss of generality, we assume that a R2R process is run for T time steps. At any $k \in [0, T]$, the possible values of $A_{d,k}$ and $B_{d,k}$, for the given R2R process, form a polytope $\Omega := \mathrm{Co}\,\{[A_j, B_j], \forall j = 1, 2, \ldots, p\}$, where $\mathrm{Co}(\cdot)$ denotes the convex hull and $[A_j, B_j]$ are vertices of the polytope. Indeed, p specifies the number of operating regions of a R2R process. The selection of system matrices at k^{th} time step follows:

$$[A_{d,k}, B_{d,k}] = \sum_{j=1}^{p} \lambda_j [A_j, B_j] \tag{2.9}$$

where λ_i is a scheduling variable decided from R_0, J_0, R_N, J_N. Eq. (2.9) illustrates that $[A_j, B_j]$ acts as a basis for the time-varying system.

Remark 2.1. *The time-varying matrices $A_{d,k}$ and $B_{d,k}$ can be decomposed as $A_{d,k} = A_j + \Delta A_k$ and $B_{d,k} = B_j + \Delta B_k$, where A_j and B_j represent the nominal dynamics of a R2R process within a local neighborhood. ΔA_k and ΔB_k are unknown but bounded disturbances, including model mismatch, additive parametric uncertainty due to the changing dynamics, or a mixture of these. With proper transformation, the disturbances can be integrated into a term $\boldsymbol{W}_k =$*

$\Delta A_k \boldsymbol{X}_k + \Delta B_k \boldsymbol{U}_k \in \mathbb{W}$. *Therefore, static* A_d *and* B_d *matrices will be used in the following content for simpler representation, and a robust control algorithm is designed to deal with the bounded disturbance* $\boldsymbol{W}_k$.

Based on Remark 2.1, the following model is equivalent to model (2.8):

$$\begin{aligned} \boldsymbol{X}_{k+1} &= A_d \boldsymbol{X}_k + B_d \boldsymbol{U}_k + \boldsymbol{W}_k \\ \boldsymbol{Y}_k &= C_d \boldsymbol{X}_k \end{aligned} \tag{2.10}$$

Compensation for the disturbances in (2.10) is critical for high-precision R2R processes that require tight control margins of tension. The impact of the disturbances can be distinguished into two aspects: 1) model mismatch, as a constant disturbance, can cause an offset between the actual tension and its reference; and 2) time-varying parametric disturbance in roller radius and inertia can cause the system to be unstable. These two types of disturbances are separately treated in our work. In the next section, we derive an incremental model based on (2.10) to compensate for the possible constant disturbances.

2.2.3 Augmented Model in an Incremental Form

To realize offset-free tension tracking under model mismatch, model (2.10) is augmented into an incremental form by extending the states $\boldsymbol{X}_k$ into

$$\boldsymbol{X}_k^{\text{ext}} = [\Delta \boldsymbol{X}_k^{\mathrm{T}}, \boldsymbol{e}_k^{\mathrm{T}}, \boldsymbol{X}_{k-1}^{\mathrm{T}}, \boldsymbol{U}_{k-1}^{\mathrm{T}}] \tag{2.11}$$

Where $\Delta \boldsymbol{X}$ is the state increment and $\boldsymbol{e}_k$ is the error in tracking tension and speed set points. This incremental model is also known as the velocity-form model [48]. The state equations are defined as follows:

$$\Delta \boldsymbol{X}_k = A_d \Delta \boldsymbol{X}_{k-1} + B_d \Delta \boldsymbol{U}_{k-1} + \Delta \boldsymbol{W}_k \tag{2.12}$$

$$\boldsymbol{e}_k = C_d A_d \Delta \boldsymbol{X}_{k-1} + C_d B_d \Delta \boldsymbol{U}_{k-1} + \boldsymbol{e}_{k-1} + C_d \Delta \boldsymbol{W}_k \tag{2.13}$$

$$\boldsymbol{X}_k = \boldsymbol{X}_{k-1} + \Delta \boldsymbol{X}_k \tag{2.14}$$

$$\boldsymbol{U}_k = \boldsymbol{U}_{k-1} + \Delta \boldsymbol{U}_k \tag{2.15}$$

where $\Delta \boldsymbol{U}$ is the control increment.

Remark 2.2. *Since a linearized model from a nonlinear system is utilized, $\boldsymbol{X}_k$ is the state deviation by definition and $\Delta \boldsymbol{X}_k$ is the increment of $\boldsymbol{X}_k$ at each timestamp. In fact, $\Delta \boldsymbol{X}_k$ is the increment of the real system state $\boldsymbol{x}_k$ at the same time. By definition, $\Delta \boldsymbol{W}_k = \boldsymbol{W}_k - \boldsymbol{W}_{k-1}$, it is clear that the time-invariant part of $\boldsymbol{W}_k$ (from the model mismatch) will have no impact on the incremental model. However, the time-varying part of $\boldsymbol{W}_k$ (from the changing dynamics) in R2R processes invokes us to design a control algorithm that can robustly deal with the disturbances.*

Remark 2.3. *In the case where C_d is an identity matrix, Eq.* (2.14) *is actually the sum of Eqs.* (2.12) *and* (2.13)*. This means that $\boldsymbol{e}_k$ has the same physical meaning as X_k, which gives $\boldsymbol{e}_k = \Delta \boldsymbol{X}_k^{\mathrm{T}} + \boldsymbol{X}_{k-1}^{\mathrm{T}}$. Therefore, $\boldsymbol{X}_k^{\text{ext}}$ is degenerated to $\boldsymbol{X}_k^{\text{ext}} = [\Delta \boldsymbol{X}_k^{\mathrm{T}}, \boldsymbol{e}_k^{\mathrm{T}}, \boldsymbol{U}_{k-1}^{\mathrm{T}}]^{\mathrm{T}}$ and Eq.* (2.14) *can be relaxed.*

The advantage of using this incremental model is twofold. On the one hand, including the state increments is similar to adding an integral action to a proportional controller, which helps cancel out the steady state offset. On the other hand, the explicit expression of $\Delta \boldsymbol{X}$ and $\Delta \boldsymbol{U}$ enables the operators to enforce constraints on motor acceleration, which will be discussed in Section 2.3. To summarize, the augmented discrete-time state space model becomes:

$$\begin{aligned} \boldsymbol{X}_{k+1}^{\text{ext}} &= A_d^{\text{ext}} \boldsymbol{X}_k^{\text{ext}} + B_d^{\text{ext}} \Delta \boldsymbol{U}_k + B_w^{\text{ext}} \Delta \boldsymbol{W}_k \\ \boldsymbol{Y}_k^{\text{ext}} &= C_d^{\text{ext}} \boldsymbol{X}_k^{\text{ext}} \end{aligned} \tag{2.16}$$

where $A_d^{\text{ext}} = \begin{bmatrix} A_d & 0 & 0 \\ C_d A_d & \mathbb{I}_{n_x \times n_x} & 0 \\ 0 & 0 & \mathbb{I}_{n_u \times n_u} \end{bmatrix}$, $B_d^{\text{ext}} = \begin{bmatrix} B_d \\ C_d B_d \\ \mathbb{I}_{n_u \times n_u} \end{bmatrix}$, $C_d^{\text{ext}} = \begin{bmatrix} 0 & C_d & 0 \end{bmatrix}$, $B_w^{\text{ext}} = \begin{bmatrix} \mathbb{I}_{n_x \times n_x} & C_d & 0 \end{bmatrix}^T$, $\boldsymbol{Y}_k^{\text{T}}$ is the observation of the extended state. Note that the scheduling of A_d^{ext} and B_d^{ext} follows a similar expression to Eq. (2.9).

It has been demonstrated that the model (2.16) is derived by linearizing the nonlinear model around an operating point, followed by essentially a transformation of coordinate technique. It will be embedded into a robust LPV-MPC formulation to achieve high-precision tension tracking.

2.3 Control Design

The ultimate goal is to design a robust MPC controller that can 1) achieve accurate control of process characteristics (i.e., tension and speed); 2) enforce system constraints; and 3) demonstrate good performance when parametric uncertainties exist. To this end, we first introduce a standard MPC formulation and then put forward the full-scale MPC design that includes the incremental model and parameter scheduling.

2.3.1 Constrained Linear-quadratic (LQ) MPC

A standard constrained LQ-MPC is formulated based on the nominal counterpart of Eq. (2.10). In the following, $\tilde{\boldsymbol{X}}$ and $\tilde{\boldsymbol{U}}$ are used instead of $\boldsymbol{X}$ and $\boldsymbol{U}$ to represent the state and control inputs corresponding to a nominal model. Without loss of generality, assume that a R2R system is running at the k^{th} time stamp. A model predictive controller will predict the system's behavior for n future time steps. An optimal sequence of planned control inputs is decided by solving the following optimization problem:

$$
\begin{aligned}
\min_{u_k,\ldots,u_{k+n}} \quad & J_n = \sum_{i=k}^{k+n-1} \left(\tilde{\boldsymbol{X}}_i^{\mathrm{T}} Q \tilde{\boldsymbol{X}}_i + \tilde{\boldsymbol{U}}_i^{\mathrm{T}} R \tilde{\boldsymbol{U}}_i \right) + \tilde{\boldsymbol{X}}_{k+n}^{\mathrm{T}} P \tilde{\boldsymbol{X}}_{k+n} \\
\text{subject to} \quad & \tilde{\boldsymbol{X}}_{i+1} = A_d \tilde{\boldsymbol{X}}_i + B_d \tilde{\boldsymbol{U}}_i \\
& \tilde{\boldsymbol{X}}_k \text{ is given as the initial condition} \\
& \tilde{\boldsymbol{X}}_{i+1} \in \mathcal{X} \\
& \tilde{\boldsymbol{U}}_i \in \mathcal{U}
\end{aligned}
\tag{2.17}
$$

where J_n is the cost function, $R \in \mathbb{R}^{n_u \times n_u}$ is a positive definite weighting matrix, $Q \in \mathbb{R}^{n_x \times n_x}$, $P \in \mathbb{R}^{n_x \times n_x}$ are positive semidefinite weighting matrices, and $\mathcal{X}$ and $\mathcal{U}$ are compact admissible sets for states and control inputs, respectively. One can obtain a planned control sequence $\tilde{\boldsymbol{U}}^* = \left[\tilde{\boldsymbol{U}}_k, \tilde{\boldsymbol{U}}_{k+1}, \ldots, \tilde{\boldsymbol{U}}_{k+n-1}\right]^{\mathrm{T}}$ by solving the quadratic programming problem (2.17). The first move in this stacked control sequence is selected to be the optimal inputs to the system at time stamp k. Therefore, the control law follows:

$$
\begin{aligned}
\tilde{\boldsymbol{U}}_{MPC} &= \begin{bmatrix} \mathbb{I}_{n_u \times n_u} & 0 & \ldots & 0 \end{bmatrix} \tilde{\boldsymbol{U}}^* \\
\tilde{\boldsymbol{u}}_k &= \boldsymbol{u}_r + \tilde{\boldsymbol{U}}_{MPC}
\end{aligned}
\tag{2.18}
$$

Where $\boldsymbol{u}_r$ are the reference control inputs at steady state and $\tilde{\boldsymbol{u}}_k$ are the control inputs that are applied to the actual R2R system.

In formulation (2.17), Q and R penalize states and control inputs, whereas P is the terminal penalty for regulating the final state of the system. If the pair (A_d, B_d) is stabilizable, a symmetric matrix P_∞ can be calculated to replace P for the terminal penalty. P_∞ helps one find the optimal feedback gain that stabilizes the system. Expression of P_∞ can be obtained by solving the discrete algebraic Riccati equation (DARE) [56]:

$$
P_\infty = Q + A_d^{\mathrm{T}} P_\infty A_d - A_d^{\mathrm{T}} P_\infty B_d \left(R + B_d^{\mathrm{T}} P_\infty B_d \right)^{-1} B_d^{\mathrm{T}} P_\infty A_d \tag{2.19}
$$

Remark 2.4. *Using P_∞ as the terminal cost means that the MPC law in Eq.* (2.18) *will converge*

to the control law given by an infinite horizon Linear Quadratic Regulator (LQR), when no constraints are violated.

Two types of constraints are introduced to this formulation. $\tilde{\boldsymbol{X}}_i \in \mathcal{X}$ indicates that substrate tension and transport speed, as the states of the dynamical system, should not exceed the boundaries that operators demand. Similarly, $\tilde{\boldsymbol{U}}_i \in \mathcal{U}$ sets hard constraints on the motor torque.

The third constraint type that needs to be considered is the changing rate of the motor torque, saying $\Delta \boldsymbol{U}_i$. In sheet metal rolling processes (e.g., [57]), the rollers are designed with large inertia, and they cannot instantly respond to control commands. Therefore, high-frequency control commands will be filtered for those rollers during operations. Regulating the control rates beforehand becomes an essential step in such scenarios. However, constraints on control rates are not introduced to (2.17) because they are not explicitly monitored. In the following section, applying the incremental model will enable this action.

2.3.2 Robust LPV-MPC

The predicted state evolution obtained by the standard MPC (2.17) may differ from the real system behavior because it does not have the disturbance information. To counter the disturbances in R2R processes, we present a robust LPV-MPC formulation such that the system states are guaranteed to evolve within a safe region under bounded disturbances. This design follows that of a tube-based MPC. A tube is a small range of states surrounding the nominal set points. Based on invariant set theory [58], a tube-based MPC develops tightened constraint sets to guarantee constraint fulfillment under every admissible disturbance. Since tube-based MPC has been widely discussed in the literature, one can refer to [51, 52] for detailed information. In our approach, the tube-based MPC formulation is combined with the incremental model to mitigate the conservatism of this robust control method.

The development of the proposed LPV-MPC outlined in the following consists of three steps: 1) tighten the system constraints so that the system is stabilized under bounded disturbances; 2) integrate the incremental model to the MPC formulation; and 3) schedule the system matrices

based on the measurement of roller radius.

The tightened constraints are first computed for the incremental system (2.16), then transformed to the equivalent ones for system (2.10). Assume that a time-varying disturbance $\boldsymbol{W}_k \in \mathbb{W}$ is bounded but unknown, then a MPC can only use nominal states (undisturbed) to predict the system behavior. The nominal model of (2.16) is:

$$\tilde{\boldsymbol{X}}_{k+1}^{\text{ext}} = A_d^{\text{ext}} \tilde{\boldsymbol{X}}_k^{\text{ext}} + B_d^{\text{ext}} \Delta \tilde{\boldsymbol{U}}_k \tag{2.20}$$

where $\tilde{\boldsymbol{X}}_k^{\text{ext}}$ is the nominal state. $\Delta \tilde{\boldsymbol{U}}_k$ is the nominal control increment. The difference between the nominal and the real state is defined as

$$\boldsymbol{d}_k = \boldsymbol{X}_k^{\text{ext}} - \tilde{\boldsymbol{X}}_k^{\text{ext}} \tag{2.21}$$

The task is to eliminate the offset $\boldsymbol{d}_k$ between the prediction by MPC and the real system response. Therefore, the actual control increment applied to the system should be:

$$\Delta \boldsymbol{U}_k = \Delta \tilde{\boldsymbol{U}}_k + K_p \boldsymbol{d}_k \tag{2.22}$$

where $K_p \boldsymbol{d}_k$ is called a state feedback term. Assume that there exists a priori gain K_p such that $(A_d^{\text{ext}} - B_d^{\text{ext}} K_p)$ is Schur, then the evolution of $\boldsymbol{d}_k$ is bounded and given by

$$\boldsymbol{d}_{k+1} = \left(A_d^{\text{ext}} - B_d^{\text{ext}} K_p\right) \boldsymbol{d}_k + B_w^{\text{ext}} \Delta \boldsymbol{W}_k \tag{2.23}$$

At time instance k, a robust positive invariant set that contains all possible $\boldsymbol{d}_k$, together with the disturbances $\boldsymbol{W}_{k-1}$, can be computed. The evolution of $\mathbb{D}_k$ is determined as follows [55]

$$(\boldsymbol{d}_k, \boldsymbol{W}_{k-1}) \in \mathbb{D}_k = \begin{bmatrix} B_w^{\text{ext}} \\ \mathbb{I}_{n_x \times n_x} \end{bmatrix} \mathbb{W}$$

$$(\boldsymbol{d}_{k+i}, \boldsymbol{W}_{k+i-1}) \in \mathbb{D}_{k+i} = \mathbb{D}_{k+i-1} \oplus \left(\begin{bmatrix} A_d^{\text{ext}} - B_d^{\text{ext}} K_p & -B_w^{\text{ext}} \\ 0 & 0 \end{bmatrix} \right)^i \begin{bmatrix} B_w^{\text{ext}} \\ \mathbb{I}_{n_x \times n_x} \end{bmatrix} \mathbb{W}, \quad i = 1, 2, \dots \tag{2.24}$$

Where $\oplus$ defines the Minkowski sum of two sets $\mathbb{X}$ and $\mathbb{Y}$ with $\mathbb{X} \oplus \mathbb{Y} = \{x+y | x \in \mathbb{X}, y \in \mathbb{Y}\}$. The term $\left(\begin{bmatrix} A_d^{\text{ext}} - B_d^{\text{ext}} K_p & -B_w^{\text{ext}} \\ 0 & 0 \end{bmatrix} \right)^i \begin{bmatrix} B_w^{\text{ext}} \\ \mathbb{I}_{n_x \times n_x} \end{bmatrix} \mathbb{W}$ vanishes as it propagates over time, and $\mathbb{D}_{k+i}$ will finally converge to the minimal robust positive invariant set $\mathbb{D}_\infty$. It is possible to approximate $\mathbb{D}_\infty$ within finite time, as shown in [58]. The following proposition states that control law (2.22) keeps the real disturbed state $\boldsymbol{X}_k^{\text{ext}}$ close to the nominal state $\tilde{\boldsymbol{X}}_k^{\text{ext}}$.

Proposition 2.1. *[52] Suppose $\mathbb{D}_\infty$ is disturbance invariant for system* (2.16)*. If $(\boldsymbol{d}_k, \boldsymbol{W}_\infty)$ and control law* (2.22) *is applied, then for all $\boldsymbol{W}_{k+i} \in \mathbb{W}$, it holds that $(\boldsymbol{X}_{k+1}^{\text{ext}}, \boldsymbol{W}_{k+i-1}) \in (\tilde{\boldsymbol{X}}_{k+i}^{\text{ext}}, 0) \oplus \mathbb{D}_\infty$, for $i \geq 0$.*

Note that $\mathbb{D}_\infty$ is the minimal robust positive invariant set that acts on the constraints for the extended states $\tilde{\boldsymbol{X}}_k^{\text{ext}}$. An equivalent invariant set for $\mathcal{X}$ and $\mathcal{U}$ needs to be derived, such that one can give direct constraint commands on motor torques in real practice. The conversion is derived based on the following proposition.

Proposition 2.2. *In view of Remark 3, the conversion between the models* (2.10) *and* (2.16) *gives:*

$$\begin{bmatrix} \Delta \boldsymbol{X}_k \\ \boldsymbol{e}_k \\ \boldsymbol{U}_{k-1} \end{bmatrix} = \underbrace{\begin{bmatrix} A_d - \mathbb{I}_{n_x \times n_x} & B_d \\ A_d & B_d \\ 0 & \mathbb{I}_{n_u \times n_u} \end{bmatrix}}_{\Sigma_1} \begin{bmatrix} \boldsymbol{X}_{k-1} \\ \boldsymbol{U}_{k-1} \end{bmatrix} + \underbrace{\begin{bmatrix} \mathbb{I}_{n_x \times n_x} \\ \mathbb{I}_{n_u \times n_u} \\ 0 \end{bmatrix}}_{\Sigma_2} \boldsymbol{W}_{k-1} \tag{2.25}$$

Usually, Σ_1 is a non-square matrix in R2R systems. Assume that $\text{rank}\,(\Sigma_1) = n_x + n_u$,

then denote the left inverse of Σ_1 as Σ_1^{-1}, and the following equations hold:

$$\begin{bmatrix} \tilde{\boldsymbol{X}}_k \\ \tilde{\boldsymbol{U}}_{k-1} \end{bmatrix} = \begin{bmatrix} A_d & B_d \\ 0 & \mathbb{I}_{n_u \times n_u} \end{bmatrix} \Sigma_1^{-1} \tilde{\boldsymbol{X}}_k^{\text{ext}} \tag{2.26}$$

$$\begin{bmatrix} \boldsymbol{X}_k \\ \boldsymbol{U}_{k-1} \end{bmatrix} = \begin{bmatrix} A_d & B_d \\ 0 & \mathbb{I}_{n_u \times n_u} \end{bmatrix} \Sigma_1^{-1} \boldsymbol{X}_k^{\text{ext}} + \left(\begin{bmatrix} \mathbb{I}_{n_x \times n_x} \\ 0 \end{bmatrix} - \begin{bmatrix} A_d & B_d \\ 0 & \mathbb{I}_{n_u \times n_u} \end{bmatrix} \Sigma_1^{-1} \Sigma_2 \right) \boldsymbol{W}_{k-1} \tag{2.27}$$

Proof. The proof follows similar steps as shown in [55], but specific modifications are made according to the incremental model that is defined in (2.16). From (2.10), one can obtain the following:

$$\begin{bmatrix} \boldsymbol{X}_k \\ \boldsymbol{U}_{k-1} \end{bmatrix} = \begin{bmatrix} A_d & B_d \\ 0 & \mathbb{I}_{n_u \times n_u} \end{bmatrix} \begin{bmatrix} \boldsymbol{X}_{k-1} \\ \boldsymbol{U}_{k-1} \end{bmatrix} + \begin{bmatrix} \mathbb{I}_{n_x \times n_x} \\ 0 \end{bmatrix} \boldsymbol{W}_{k-1} \tag{2.28}$$

By (2.25), we have $\begin{bmatrix} \boldsymbol{X}_{k-1} \\ \boldsymbol{U}_{k-1} \end{bmatrix} = \Sigma_1^{-1}(\boldsymbol{X}_k^{\text{ext}} - \Sigma_2 \boldsymbol{W}_{k-1})$, which is then plugged into Eq. (2.28) to obtain Eq. (2.27). Similar procedures can be taken to derive Eq. (2.26). □

We denote $C_X = \begin{bmatrix} A_d & B_d \\ 0 & \mathbb{I}_{n_u \times n_u} \end{bmatrix} \Sigma_1^{-1}$ and $C_W = \left(\begin{bmatrix} \mathbb{I}_{n_x \times n_x} \\ 0 \end{bmatrix} - \begin{bmatrix} A_d & B_d \\ 0 & \mathbb{I}_{n_u \times n_u} \end{bmatrix} \Sigma_1^{-1} \Sigma_2 \right)$. From Eqs. (2.26)-(2.27), the state and control input of model (2.10) can be written in terms of the state of the incremental model (2.16):

$$\begin{bmatrix} \boldsymbol{X}_k - \tilde{\boldsymbol{X}}_k \\ \boldsymbol{U}_{k-1} - \tilde{\boldsymbol{U}}_{k-1} \end{bmatrix} = \begin{bmatrix} C_X & C_W \end{bmatrix} \begin{bmatrix} \boldsymbol{X}_k^{\text{ext}} - \tilde{\boldsymbol{X}}_k^{\text{ext}} \\ \boldsymbol{W}_{k-1} \end{bmatrix} \tag{2.29}$$

Combining with (2.24), the tightened constraints on states and control inputs can be expressed as:

$$\begin{bmatrix} \tilde{\boldsymbol{X}}_k \\ \tilde{\boldsymbol{U}}_{k-1} \end{bmatrix} \in (\mathcal{X} \times \mathcal{U}) \ominus \begin{bmatrix} C_X & C_W \end{bmatrix} \mathbb{D}_\infty \tag{2.30}$$

where $\ominus$ is the Pontryagin difference of two sets $\mathbb{X}$ and $\mathbb{Y}$ defined by $\mathbb{X} \ominus \mathbb{Y} = \{x | x + y \in \mathbb{X}, \forall y \in \mathbb{Y}\}$.

Applying control law (2.22) and the tightened constraints (2.30) enables the controller to predict the system behavior using a nominal model while robustly fulfilling the constraints for any disturbance $\boldsymbol{W}_k \in \mathbb{W}$. Now, we consider the selection of the disturbance bounds $\mathbb{W}$. One can choose a large $\mathbb{W}$ so that it contains disturbances from model mismatch and time-varying dynamics. However, a large $\mathbb{W}$ will lead to conservative control performance. We alternatively choose a $\mathbb{W}$ so that it only covers a specific range of time-varying disturbances, while the model mismatch is handled by the incremental model.

Introducing the incremental model and the tightened constraints, the formulation of the MPC problem with a prediction horizon of n becomes:

$$
\begin{aligned}
\min_{\Delta \boldsymbol{U}_k, \ldots, \Delta \boldsymbol{U}_{k+n}} \quad & J_n = \sum_{i=k}^{k+n-1} \left(\left(\tilde{\boldsymbol{X}}_i^{\text{ext}} \right)^{\mathrm{T}} Q^{\text{ext}} \tilde{\boldsymbol{X}}_i^{\text{ext}} + \Delta \tilde{\boldsymbol{U}}_i^{\mathrm{T}} R^{\text{ext}} \Delta \tilde{\boldsymbol{U}}_i \right) + \left(\tilde{\boldsymbol{X}}_{k+n}^{\text{ext}} \right)^{\mathrm{T}} P^{\text{ext}} \tilde{\boldsymbol{X}}_{k+n}^{\text{ext}} \\
\text{subject to} \quad & \tilde{\boldsymbol{X}}_{i+1}^{\text{ext}} = A_d^{\text{ext}} \tilde{\boldsymbol{X}}_i^{\text{ext}} + B_d^{\text{ext}} \Delta \tilde{\boldsymbol{U}}_i \\
& \Delta \tilde{\boldsymbol{X}}_i = \tilde{\boldsymbol{X}}_i - \tilde{\boldsymbol{X}}_{i-1} \\
& \Delta \tilde{\boldsymbol{U}}_i = \tilde{\boldsymbol{U}}_i - \tilde{\boldsymbol{U}}_{i-1} \\
& \begin{bmatrix} \tilde{\boldsymbol{X}}_{i+1} \\ \tilde{\boldsymbol{U}}_i \end{bmatrix} \in (\mathcal{X} \times \mathcal{U}) \ominus \begin{bmatrix} C_X & C_W \end{bmatrix} \mathbb{D}_\infty
\end{aligned}
\tag{2.31}
$$

where Q^{ext}, R^{ext} and P^{ext} are penalty matrices for states, control inputs and terminal states, respectively. Considering that this MPC aims to eliminate the tension tracking error, only $\boldsymbol{e}_k$ needs to be penalized in $\tilde{\boldsymbol{X}}_k^{\text{ext}}$. Therefore, Q^{ext} is designed in the following form

$$
Q^{\text{ext}} = \begin{bmatrix} 0 & 0 & 0 \\ 0 & Q_e & 0 \\ 0 & 0 & 0 \end{bmatrix} \tag{2.32}
$$

where Q_e is a positive definite penalty matrix for $\boldsymbol{e}_k$. Based on Q^{ext} and R^{ext}, the terminal penalty P^{ext} can be obtained to stabilize the nominal system, as shown in [49].

Controller (2.22) with (2.31) can robustly stabilize a R2R system within a specific time window based on the selection of the disturbance bound. To update the system model, one needs to monitor the in-situ radius of the unwind and rewind rollers, which can be achieved by adding reflective laser sensors next to the rollers. When a sensor-free condition is required, the radius of a material roll can be estimated through integral:

$$\dot{R}_0(t) \approx -\frac{h_s v_0(t)}{2\pi R_0(t)} \tag{2.33}$$

$$J_0(t) = J_0(0) - \frac{\pi}{2} b_s \rho_s \left(R_0^4(0) - R_0^4(t)\right) \tag{2.34}$$

The radius and inertia of the unwind roll $R_N(t)$, $J_N(t)$ can be estimated similarly. Based on Eqs. (2.33)-(2.34) one can decide the best fit of the system using scheduled system matrices in (2.9). In our implementation, a Kronecker delta function is used to define the scheduling parameter λ_j. Assume the system is working within operating region i, which gives:

$$\lambda_j = \begin{cases} 0, & j \neq i \\ 1, & j = i \end{cases} \tag{2.35}$$

Then A_d^{ext}, B_d^{ext} and the tightened constraints need to be updated accordingly. Note that Eq. (2.35) reveals a simple switching control strategy where variations in A_d^{ext}, B_d^{ext} are considered as disturbances.

Eqs. (2.31)-(2.35) give the full-scale formulation of the robust LPV-MPC method. The proposed LPV-MPC can be reduced into a quadratic programming (QP) problem and solved using the gradient projection method [59].

A solution to the corresponding QP is precisely the sequence of optimal control increments at the kth time step, denoted as $\Delta\tilde{\boldsymbol{U}}^*(\boldsymbol{X}_k^{\text{ext}}) = \left[\Delta\tilde{\boldsymbol{U}}_k^*, \Delta\tilde{\boldsymbol{U}}_{k+1}^*, \ldots, \Delta\tilde{\boldsymbol{U}}_{k+n}^*\right]$. The robust control law

is given by

$$\Delta \boldsymbol{U}_{MPC} = \Delta \tilde{\boldsymbol{U}}_k^* \tag{2.36}$$

Since $\Delta \boldsymbol{U}_{MPC}$ results from an incremental model, the actual control inputs that should be applied to the system follow an incremental summation

$$\boldsymbol{u}_k = \boldsymbol{u}_r + \boldsymbol{U}_{k-1} + \Delta \boldsymbol{U}_{MPC} + K_p(\boldsymbol{X}_k^{\text{ext}} - \tilde{\boldsymbol{X}}_k^{\text{ext}}) \tag{2.37}$$

Note that the four terms at the right-hand side can be distinguished into three parts: $\boldsymbol{u}_r$ is the control input that maintains the system at steady state; $\boldsymbol{U}_{k-1} + \Delta \boldsymbol{U}_{MPC}$ is the nominal control obtained by solving (2.31); $K_p(\boldsymbol{X}_k^{\text{ext}} - \tilde{\boldsymbol{X}}_k^{\text{ext}})$ is a state feedback term compensating for the error between predicted and real system states. By expression (2.37), one will notice that $\boldsymbol{X}_k^{\text{ext}}$ is the state from the real dynamic system, which can be noisy. A state observer in company with the proposed control algorithm is critical to ensure the control performance under potential process and measurement noises. A Kalman filter based on the augmented state space model in Eq. (2.16) serves as the state observer in our implementation. The Kalman filter updates the estimation of $\boldsymbol{X}_k^{\text{ext}}$ following:

$$\hat{\boldsymbol{X}}_{k|k}^{\text{ext}} = \hat{\boldsymbol{X}}_{k|k-1}^{\text{ext}} + K_f \left(\boldsymbol{Y}_k^{\text{ext}} - C_d^{\text{ext}} \hat{\boldsymbol{X}}_{k|k-1}^{\text{ext}} \right) \tag{2.38}$$

where $\hat{\boldsymbol{X}}_{k|k}^{\text{ext}}$ is the estimation of the $\boldsymbol{X}_k^{\text{ext}}$ given sensor measurements, $\hat{\boldsymbol{X}}_{k|k-1}^{\text{ext}}$ is the estimation of the state from model (2.16). K_f is the Kalman gain decided based on A_d^{ext} and B_d^{ext}, which are computed from the polytopic representation (2.9). For detailed implementation of the LPV Kalman filter, one can refer to [60]. Therefore, the control law (2.37) becomes

$$\boldsymbol{u}_k = \boldsymbol{u}_r + \boldsymbol{U}_{k-1} + \Delta \boldsymbol{U}_{MPC} + K_p(\hat{\boldsymbol{X}}_{k|k}^{\text{ext}} - \tilde{\boldsymbol{X}}_k^{\text{ext}}) \tag{2.39}$$

The following lemma defines the choice of K_p.

Lemma 2.1. *[61] Consider the augmented system* (2.16) *and the switching law* (2.35)*, if there*

exist matrices $Y, G > 0$*, such that*

$$\begin{bmatrix} G & \left(A_j^{ext} G + B_j^{\text{ext}} Y\right)^{\text{T}} \\ A_j^{\text{ext}} G + B_j^{ext} Y & G \end{bmatrix} > 0, \quad \forall j \in [i, i+1], i \in [1, p-1] \tag{2.40}$$

Where $[A_j^{ext}, B_j^{ext}]$ *are vertices derived from* $[A_j, B_j]$ *in Eq.* (2.9)*.*

Then the control gain $K_p = -YG^{-1}$ guarantees the stability of the error system

$$\left(\hat{\boldsymbol{X}}_{k+1|k+1}^{\text{ext}} - \tilde{\boldsymbol{X}}_{k+1}^{\text{ext}}\right) = \left(A_j^{\text{ext}} - B_j^{\text{ext}} K_p\right) \left(\hat{\boldsymbol{X}}_{k|k}^{\text{ext}} - \tilde{\boldsymbol{X}}_{k}^{\text{ext}}\right) + B_w^{\text{ext}} \Delta \boldsymbol{W}_k \tag{2.41}$$

Note that we enforce the inequality (2.40) to be valid for any pairs of adjacent operating regions. Based on Lemma 2.1, the robust stability of the augmented system is proved as follows.

Theorem 2.1. *Consider the augmented system* (2.16) *with bounded disturbance* $\boldsymbol{W}_k \in \mathbb{W}$*. Denote* $\hat{\boldsymbol{d}}_k = \hat{\boldsymbol{X}}_{k|k}^{\text{ext}} - \tilde{\boldsymbol{X}}_k^{\text{ext}}$*. Assume that the initial state at time stamp* k *:* $\left(\hat{\boldsymbol{d}}_k, \boldsymbol{W}_{k-1}\right) \in \mathbb{D}_\infty$*, with the MPC control law* (2.36)*, the Kalman filter gain* K_f*, and the choice of control gain* (2.40)*, the robust stability of the system is guaranteed.*

Proof. Lyapunov function of the error system (2.41) is defined as $V(\hat{\boldsymbol{d}}_k) = \hat{\boldsymbol{d}}_k^T G^{-1} \hat{\boldsymbol{d}}_k$. Plug in $K_p = -YG^{-1}$ and by Schur complements, inequality (2.40) gives

$$\left(A_j^{\text{ext}} G - B_j^{\text{ext}} K_p G\right)^{\text{T}} G^{-1} \left(A_j^{\text{ext}} G + B_j^{\text{ext}} K_p G\right) < G \tag{2.42}$$

Multiply G^{-1} on both sides gives $\left(A_j^{\text{ext}} - B_j^{\text{ext}} K_p\right)^{\text{T}} G^{-1} \left(A_j^{\text{ext}} - B_j^{\text{ext}} K_p\right) < G^{-1}$. Therefore, $V(\hat{\boldsymbol{d}}_{k+1}) - V(\hat{\boldsymbol{d}}_k) = V\left(\left(A_j^{\text{ext}} - B_j^{\text{ext}} K_p\right) \hat{\boldsymbol{d}}_k\right) - V(\hat{\boldsymbol{d}}_k) < 0$. The stability of (2.41) is proved. Rewrite (2.41) into the polytopic form:

$$\hat{\boldsymbol{d}}_{k+1} = \left(A_d^{\text{ext}} - B_d^{\text{ext}} K_p\right) \hat{\boldsymbol{d}}_k = \sum_{j=1}^{p} \lambda_j \left(A_j^{\text{ext}} - B_j^{\text{ext}} K_p\right) \hat{\boldsymbol{d}}_k \tag{2.43}$$

Since we enforce (2.40) for all adjacent pairs of vertices in Ω, stability is guaranteed for all points

within the corresponding adjacent operating regions. Solving formulation (2.31) gives the nominal control law that stabilizes the nominal system, ensuring the nominal state converges to the set point. Based on proposition (2.1), K_p guarantees the actual states of system (2.16) with disturbances are limited within a tube whose center is the nominal state. This provides that the actual state converges to a bounded set that surrounds the set points, and robust local stability is proved. □

In real practice, obtaining $\mathbb{D}_\infty$ for high-dimensional systems is computationally expensive. Therefore, we compute the tubes only at the subsystems where the time-varying disturbances are severe. One can refer to [62] to find a rigorous design of a decentralized version of K_p. The implementation procedure of the proposed LPV-MPC is summarized as follows. The algorithm is run for T time steps with a model update scheduled every τ steps.

Algorithm 1 Pseudo code of the proposed LPV-MPC.

Require: Process parameters; Designed matrices Q,R; Admissible sets $\mathcal{X}$,$\mathcal{U}$; Disturbance bound $\mathbb{W}$

1: Solve $A_d^{\text{ext}}, B_d^{\text{ext}}, C_d^{\text{ext}}, Q^{\text{ext}}, R^{\text{ext}}, P^{\text{ext}}, \boldsymbol{u}_r$
2: Solve $K_p, C_X, C_W, \mathbb{D}_\infty$
3: Solve reduced constraints $(\mathcal{X} \times \mathcal{U}) \ominus [C_X \quad C_W]\mathbb{D}_\infty$
4: $\boldsymbol{U}_0 \leftarrow \mathbf{0}$
5: **while** $k < T$ **do**
6: **if** $R_0 =$ scheduled R_j **then**
7: Update $A_d^{\text{ext}}, B_d^{\text{ext}}$ and parameters in lines 1, 2, 3
8: **end if**
9: Solve MPC to get $\Delta \boldsymbol{U}_{MPC}, \tilde{\boldsymbol{X}}_k^{\text{ext}}$
10: Solve Kalman filter to get $K_f, \hat{\boldsymbol{X}}_{k|k}^{\text{ext}}$
11: $\boldsymbol{u}_k \leftarrow \boldsymbol{u}_r + \boldsymbol{U}_{k-1} + \Delta \boldsymbol{U}_{MPC} + K_p(\hat{\boldsymbol{X}}_{k|k}^{\text{ext}} - \tilde{\boldsymbol{X}}_k^{\text{ext}})$
12: $\boldsymbol{U}_k \leftarrow \boldsymbol{U}_{k-1} + \Delta \boldsymbol{U}_{MPC}$
13: **end while**

2.4 Case Study

A simulation study is conducted to demonstrate the effectiveness of the proposed LPV-MPC. The parameters used for building the simulation are identified from a high-precision laboratory R2R setup, as shown in Figure 2.2.

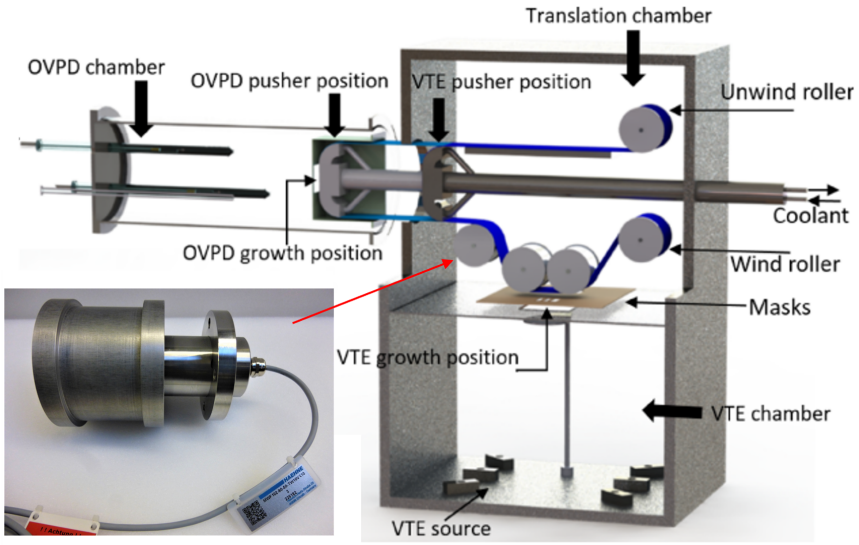

Figure 2.2: Cross-sectional schematic of a R2R deposition system. A tension sensor is used to replace one of the passive rollers.

The setup includes two active rollers: an unwind roller and a rewind roller. The R2R process installed within a vacuum chamber is used for patterning organic light emitting devices. Unlike the gravure printing systems discussed in Section 2.2, this prototype R2R equipment is designed to perform vapor phase deposition of materials. Therefore, there are no active rollers comprised in the processing stages. More details about its operational modes are found in [5]. A complete run-through of the deposition process is performed to collect unwind speed v_0, rewind speed v_1, tension t_1, unwind torque u_0 and rewind torque u_1. The dataset is then fed into a white-box model (2.44) to identify system parameters.

$$\begin{bmatrix} \dot{v}_0 \\ \dot{t}_1 \\ \dot{v}_1 \end{bmatrix} = \begin{bmatrix} a_{11} & \frac{R_0^2}{J_0} & 0 \\ \frac{t_0 - AE}{L_1} & -\frac{v_{r1}}{L_1} & \frac{AE - t_{r1}}{L_1} \\ 0 & -\frac{R_1^2}{J_1} & a_{33} \end{bmatrix} \begin{bmatrix} v_0 \\ t_1 \\ v_1 \end{bmatrix} + \begin{bmatrix} -\frac{n_0 R_0}{J_0} & 0 \\ 0 & 0 \\ 0 & \frac{n_1 R_1}{J_1} \end{bmatrix} \begin{bmatrix} u_0 \\ u_1 \end{bmatrix} \tag{2.44}$$

Where $a_{11} = -\frac{h_s v_{r0}}{\pi J_0}\left(\frac{J_0}{R_0^2} - 2\pi\rho_s b_s R_0^2\right)$ and $a_{33} = \frac{h_s v_{r1}}{\pi J_1}\left(\frac{J_1}{R_1^2} - 2\pi\rho_s b_s R_1^2\right)$. Measured process characteristics and the corresponding predictions from the simulated model are plotted in Figure 2.3. It can be observed that the whole system is in a static condition at the beginning, and the process proceeds to start from 12 s. The PLC first commands impulse speed signals to the motors

so that the substrate is tightened. An overshoot in tension can be noticed during this tightening operation. Then the tension is reduced to $33\ \mathrm{N}$ to follow the target value as the substrate moves at a steady speed of $1\ \mathrm{cm/s}$. One can observe from Figure 2.3 that predicting the transient speed dynamics is relatively difficult. This is because our model primarily focuses on describing the tension-speed relationship and is not integrated with an explicit representation to discern the dynamics within an AC servo motor. Despite the limitations, model (2.44) can precisely capture the tension dynamics of the R2R system.

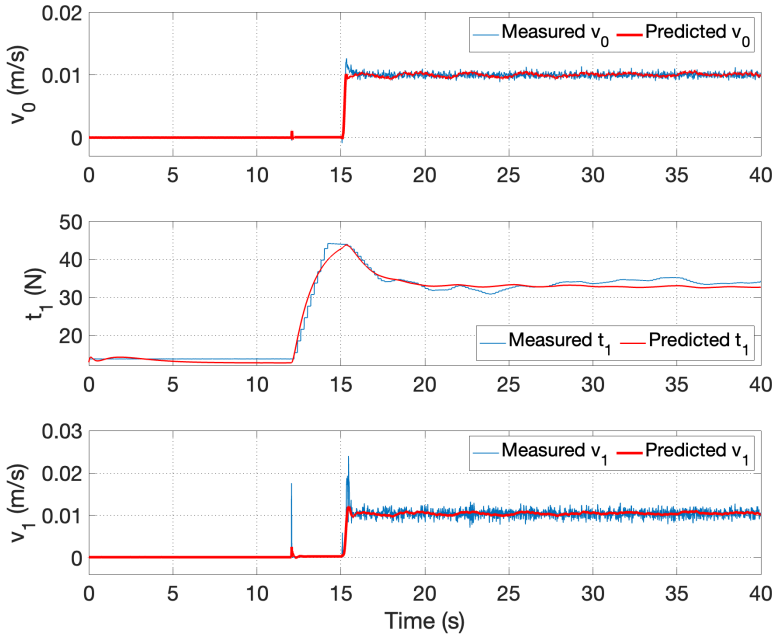

Figure 2.3: Substrate tension is designed to be $33\ \mathrm{N}$, and transport speed is $1\ \mathrm{cm/s}$. The substrate is first tightened at $12\ \mathrm{s}$ and then relaxed to the target tension value. The substrate starts to move at $15\ \mathrm{s}$.

2.4.1 Simulation Setup

The experimental setup consists of only two active rollers and one tension section, which represents a single-span R2R system. However, it's worth noting that the proposed controller can be applied to multi-span R2R systems. To demonstrate its performance more comprehensively,

the identified parameters were extended to a five-active-roller, four-span R2R system, as shown in Figure 2.4.

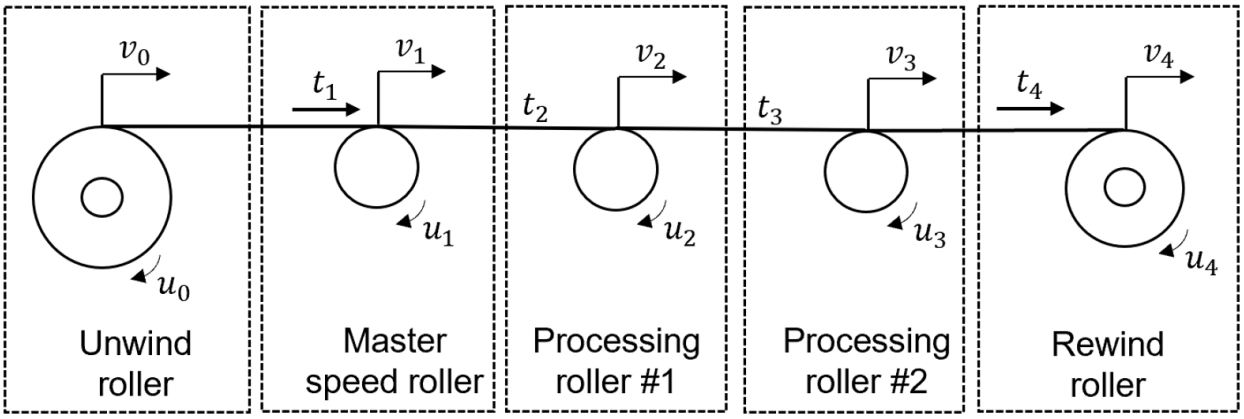

Figure 2.4: A R2R system with five active rollers.

It is assumed that the normal operation condition requires the transport speed to be $1\ \mathrm{cm/s}$ (same as the high-precision R2R setup in Figure 2.2). Substrate tensions in the four substrate spans are designed to be $t_{r1} = 28\ \mathrm{N}, t_{r2} = 30\ \mathrm{N}, t_{r3} = 36\ \mathrm{N}, t_{r4} = 38\ \mathrm{N}$, for easier visualization. As for the constraints, the rated motor torque is constrained between $-1.3\ \mathrm{Nm}$ and $1.3\ \mathrm{Nm}$, and torque increment is constrained between $-5\ \mathrm{Nm/s}$ and $5\ \mathrm{Nm/s}$. In addition, tensions are constrained within $\pm 10\%$ from their set point values. Other nominal values used in the simulation include $\rho_s = 700\ \mathrm{kg/m^3}, b_s = 0.12\ \mathrm{m}, h_s = 1 \times 10^{-4}\ \mathrm{m}, E = 200\ \mathrm{MPa}, R_0 = 0.19\ \mathrm{m}, R_1 = R_2 = R_3 = R_4 = 0.05\ \mathrm{m}, J_0 = 0.150\ \mathrm{kg \cdot m^2}, J_1 = J_2 = J_3 = J_4 = 0.091\ \mathrm{kg \cdot m^2}, b_{f0} = b_{f1} = b_{f2} = b_{f3} = 5 \times 10^{-3}, b_{f4} = 4.5 \times 10^{-3}, L_1 = L_2 = L_3 = L_4 = 0.89\ \mathrm{m}, n_0 = 6, n_4 = 2, n_1 = n_2 = n_3 = 1$. Inertia and radius of the passive rollers are $J_p = 0.091\ \mathrm{kg \cdot m^2}$ and $R_p = 0.05\ \mathrm{m}$. The system is separated into five stages where nine variables need to be controlled. That includes $\boldsymbol{X}_k = [V_0, T_1, V_1, T_2, V_2, T_3, V_3, T_4, V_4]_k^{\mathrm{T}}$, and accordingly, $\boldsymbol{U}_k = [U_0, U_1, U_2, U_3, U_4]_k^{\mathrm{T}}$.

The system dynamics is simulated by using the continuous-time nonlinear models (2.1)-(2.7) solved by the ode45 function in MATLAB, with the sampling time being $T_s = 10\ \mathrm{ms}$. The proposed robust LPV-MPC controller generates control inputs every $100\ \mathrm{ms}$. A standard zero-order hold is applied on the control inputs in the following $100\ \mathrm{ms}$ time interval. To balance the

trade-off between computational efficiency and closed-loop performance, the prediction horizon is decided to be $n = 5$ in our use case. A block diagram in Figure 2.5 illustrates the implementation strategy of the robust MPC. A decentralized PI (DPI) controller and an H_∞ tension controller are implemented for benchmark comparison. It is assumed that the PI controllers and H_∞ controller are computationally efficient. Therefore, they can respond to the system dynamics in real time by generating control inputs every 10 ms.

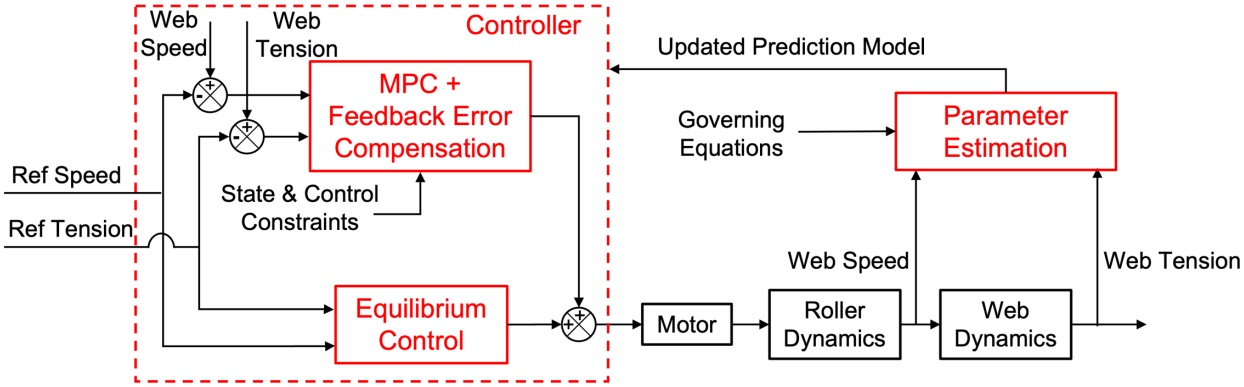

Figure 2.5: Control diagram with the proposed robust LPV-MPC.

To comprehensively test the proposed MPC, the simulation covers three different scenarios:

1. *Change of set points*: Local tension and speed responses of the R2R system are investigated when their corresponding set points are changed.

2. *Robustness to a model mismatch*: The same reference trajectories as Case 1 are used. However, random parametric errors in Young's Modulus and roller inertia are introduced as constant disturbances.

3. *Robustness to time-varying dynamics*: The R2R system is run for a longer time window, where roller radius and inertia change continuously.

2.4.2 Computation of the Tightened Constraint Set

The time-varying disturbances in R2R processes primarily arise from the change in the wind and unwind roller radius and inertia during substrate deployment. Therefore, the tightened

constraint sets are computed based on disturbances that are related to R_0, J_0, R_4, J_4. In fact, the disturbances affect four states, including v_0, t_1, t_4, v_4. The system matrices are updated every $1500\,\mathrm{s}$, and a disturbance bound of $|\boldsymbol{W}_k| \leq \begin{bmatrix} 0.0004 & 0.0168 & 0.1065 & 0.0007 \end{bmatrix}^{\mathrm{T}}$ is introduced to v_0, t_1, t_4, v_4 within the $[0, 1500]$ time window. Following Eq. (2.30), the constraint sets on motor torques u_0 and u_4 are tightened to be $-1.2981 \leq u_0 \leq 1.2981$ and $-1.2475 \leq u_4 \leq 1.2475$, as shown in Figure 2.6. For R2R systems that are operated under a higher velocity, updates on system parameters need to be at an increased rate, and disturbance bounds should be computed accordingly. It turns out that the rewind roller experiences more severe disturbances than the unwind roller in the simulated scenario. This is because the radius R_4 changes rapidly at the beginning of the process.

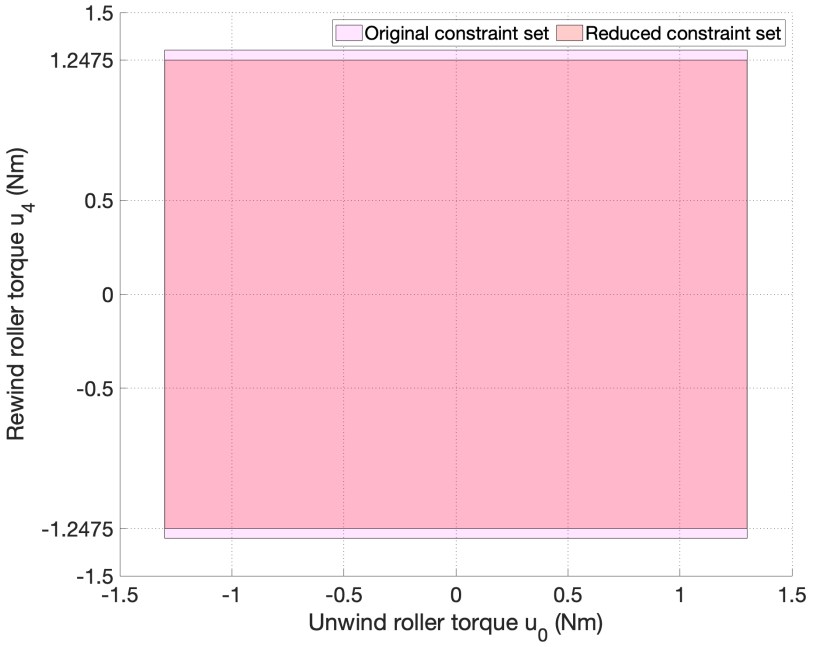

Figure 2.6: Tightened constraint sets on u_0 and u_4.

2.4.3 Change of Set Points

In the simulation, the reference speed increases by $1\ \mathrm{cm/s}$ at $5\,\mathrm{s}$ and decreases back to normal at $20\,\mathrm{s}$. The reference tension at t_{r2} increases by $3\,\mathrm{N}$ at $30\,\mathrm{s}$ and decreases back to normal

at 45 s. Comparison is conducted between a conventional DPI controller, an H_∞ controller and the proposed LPV-MPC. The robust LPV-MPC can explicitly consider the pre-defined constraints when generating control inputs. To enforce the constraints to the benchmarks, a set of saturation conditions are added to filter the control inputs generated by the DPI controller and H_∞ controller. Simulation results are illustrated in Figure 2.7 through Figure 2.10.

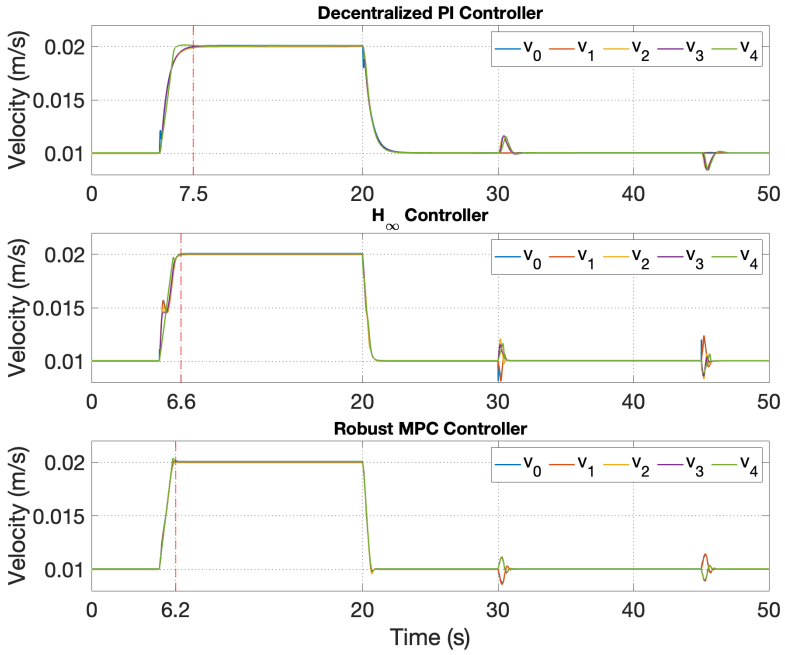

Figure 2.7: Speed responses under change of set points.

It is showcased in Figure 2.7 that the MPC features a faster response to speed change where the speed response is stabilized within 1.2 s, in contrast to the 2.5 s from the DPI controller and 1.6 s from the H_∞ controller. Figure 2.8 shows that the H_∞ controller achieves the fastest response to the commanded tension change. Both benchmarks undergo noticeable process fluctuations during the test. At around 5 s, minor fluctuations happen in the speed responses of the two benchmarks, which further cause severe swings in the tension responses. Additionally, change of set point command in the DPI and H_∞ system will lead to unexpected speed and tension fluctuations at all stages. Such unsatisfying performance is due to two reasons. Firstly, the benchmark algorithms cannot treat the constraints well. The motors do not properly execute the

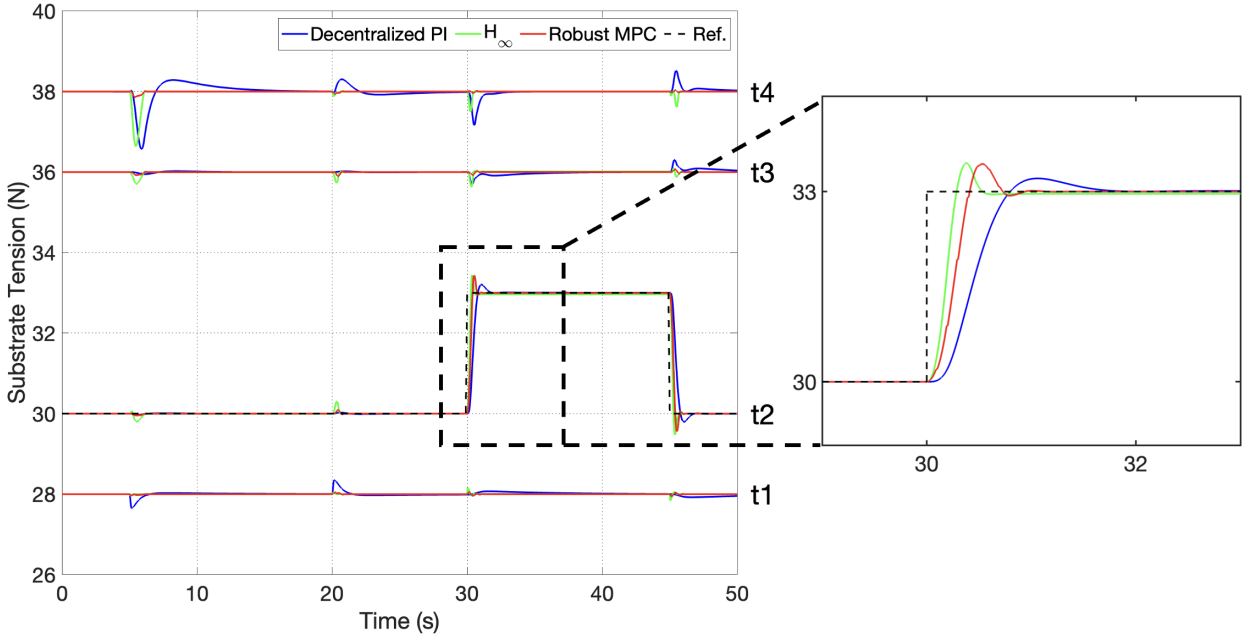

Figure 2.8: Tension responses under change of set points. DPI and H_∞ controller experienced large tension variation due to control input saturation.

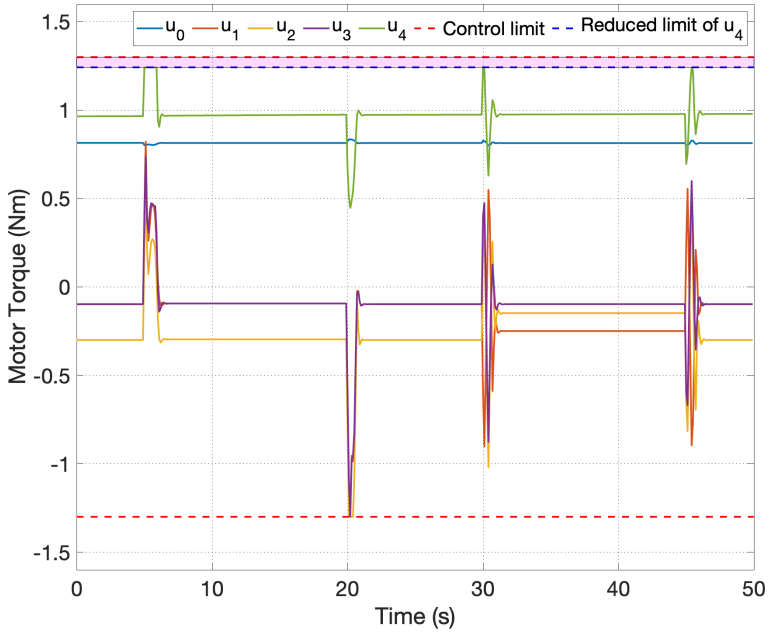

Figure 2.9: Constrained control inputs under change of set points by the MPC. The shaded area indicates the reduced control constraint of u_4.

control inputs computed by the controller due to the saturation conditions. Secondly, the DPI and H_∞ controllers cannot fully eliminate the strong coupling between stages. The proposed MPC algorithm can actively consider the process constraints and plan for the optimal control behavior for all stages. In Figure 2.9, the shaded area illustrates the reduction in the control limit for u_4 for the robust MPC. It is observed that the control inputs from the MPC are well-bounded within limits. Our MPC algorithm effectively reduces the risk of losing performance during operations.

We introduced a 5% Gaussian process noise to the system to demonstrate the MPC performance in a noisy environment in manufacturing facilities. The Kalman filter is used to observe the actual system state from the noisy signals. Figure 2.10 demonstrates that our proposed MPC can track the set points closely despite process noises.

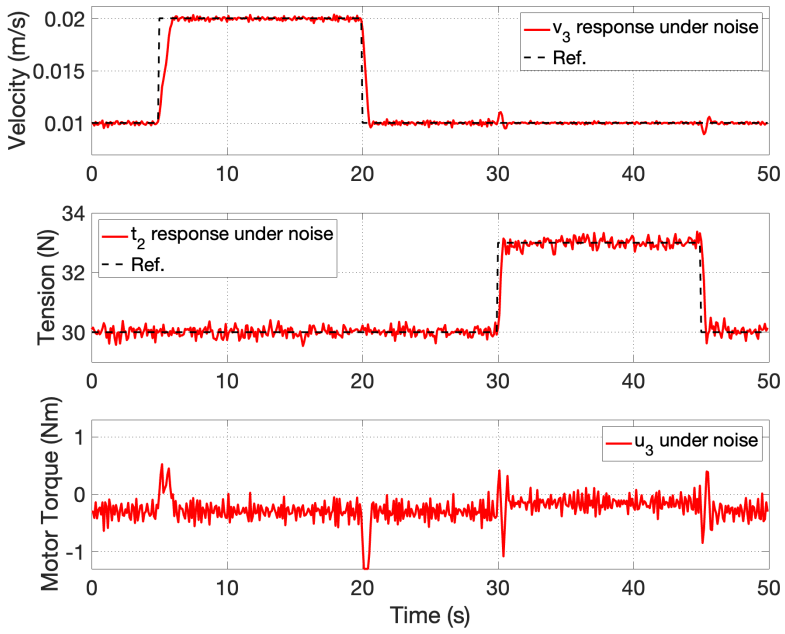

Figure 2.10: System responses and control inputs at stage 2 when 5% process noise is introduced to the system.

2.4.4 Robustness to Model Uncertainty

The robust MPC (2.31) shows fast responses to the change of set points while enforcing

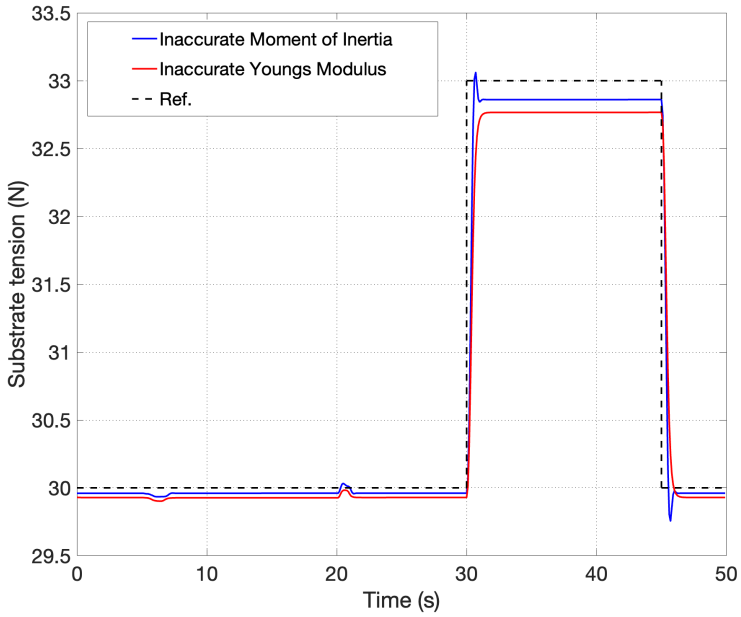

Figure 2.11: Tension response at stage 2 when a standard MPC formulation is applied, and model mismatches exist.

the constraints. An important question that remains to be answered is whether similar performance can be achieved when model mismatches exist. Figure 2.11 shows a case where random errors are introduced to the system parameters in a standard MPC formulation using (2.17). Offsets between the tension reference and actual system responses can be noticed.

A roller's moment of inertia can be easily over or under-estimated in a R2R process. Young's modulus of a substrate is also a varying property because of the change in the strength of the printed material. We consider scenarios where random errors of $\pm 20\%$ in roller inertia, J_i, and $\pm 30\%$ in Young's Modulus, E, exist in the system identification phase. The exact change of set points conditions is used as in Case 1. Simulation results from Figure 2.12 and Figure 2.13 show that the proposed MPC controller can achieve zero-offset tracking of tension and speed references in the presence of parametric uncertainties. The parametric uncertainties will mainly lead to errors in predicting the system response, thus causing offsets in tracking references. The incremental model built in the proposed MPC framework helps monitor the accumulation of such offset errors and compensate for them in real time. Therefore, the proposed MPC has better robustness to model

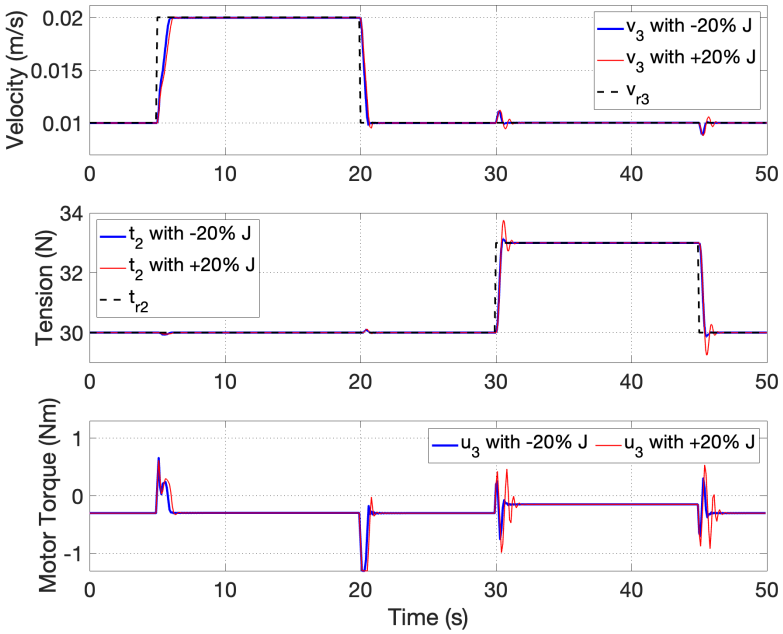

Figure 2.12: System responses and control inputs at stage 2 when rollers' moment of inertia incorporates $\pm 20\%$ random errors.

uncertainties than the standard MPC controller.

2.4.5 Robustness to Time-varying Dynamics

The performance of controllers in the long run is always of interest in R2R processes, but it is rarely studied in the literature. In this case study, we conducted simulations for a duration of 6000 s. The results of the simulation demonstrate that the system undergoes significant changes in dynamics during this period, which can lead to a degradation in the performance of conventional tension controllers. After the long run, R_0 reduces from 0.190 m to 0.184 m; R_4 increases from 0.050 m to 0.067 m; J_0 reduces from 0.150 kg$\cdot$m^2 to 0.132 kg$\cdot$m^2; J_4 increases from 0.091 kg$\cdot$m^2 to 0.094 kg $\cdot$ m^2. The blue curves in Figure 2.14 reveal the drift when a standard MPC controller cannot adapt to the changing dynamics.

We implemented a linear time-varying robust MPC algorithm proposed by P. Bumroongsri [53] as a benchmark. From the green curves, we deduce that the state feedback mechanism

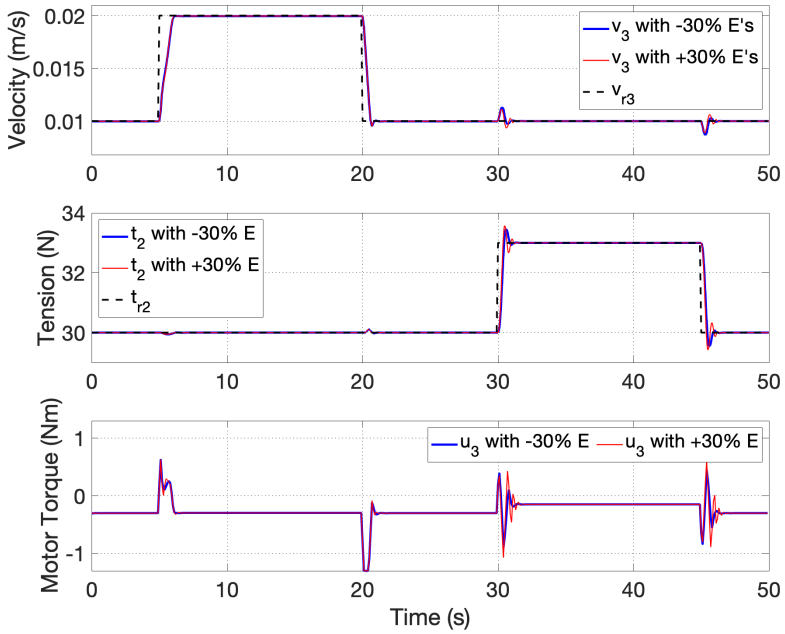

Figure 2.13: System responses and control inputs at stage 2 when Young's modulus of substrates incorporate $\pm 30\%$ random errors.

designed in the conventional robust MPC framework greatly reduces tracking errors. However, minor drifting phenomena still exist because we schedule a model update every $1500\,\mathrm{s}$, less frequently than required in [53]. Without frequent model updates, the benchmark algorithm will have wrong estimations of the reference control input $\boldsymbol{u}_r$, which is among the root causes of the drifting. With the help of the incremental model and the state feedback control, our controller takes incremental steps to approach an appropriate control input that eliminates the tracking error. Hence, the proposed LPV-MPC performs better than the conventional robust MPCs in R2R applications. It shows good robustness to time-varying disturbances and strong capability in tracking piecewise constant tension references.

2.5 Conclusion of the Chapter

The chapter presents a robust LPV-MPC strategy for accurate tension tracking in high-precision R2R processes [49, 63]. Simulation studies demonstrate that the proposed controller

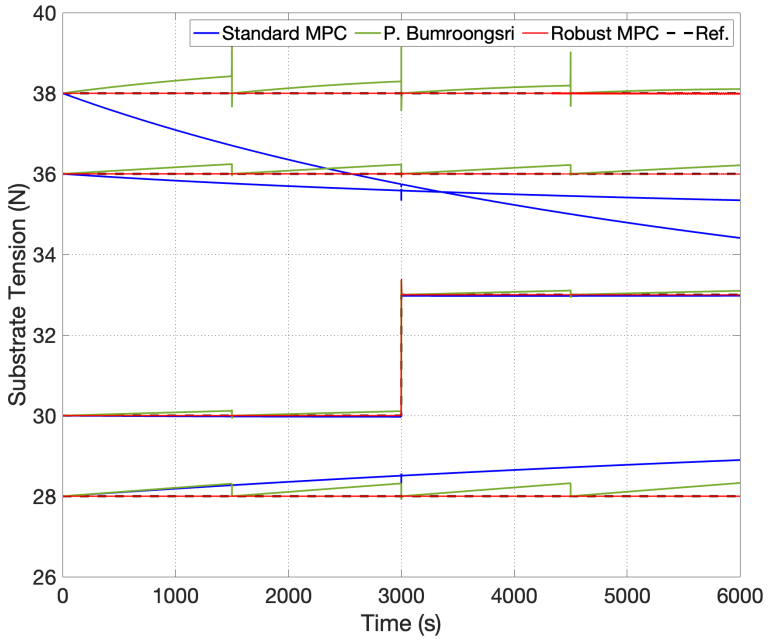

Figure 2.14: The tension drift happens when a standard MPC is employed. The test is run at the same setpoint as in Case 1, with a change of setpoint commanded at 3000 s.

achieves good performance while enforcing essential system constraints. This tension controller can improve the reliability of a wide range of R2R systems, thereby establishing a solid foundation for future research. The following conclusions are drawn based on the analytical work and simulation case studies:

1. System feasibility-oriented constraints should be taken into account when designing controllers. Failing to meet the constraints will lead to control input saturation and cause the controller performance to degrade. The proposed controller is designed based on a discrete-time linearized model of R2R systems. The controller can achieve fast responses when a change of setpoint is commanded. Constraints can be well enforced during operations.

2. Discrepancies between the nominal model and the actual system can degrade the performance of a standard MPC. This incremental implementation of the MPC is less vulnerable to model uncertainties. It can stabilize the system and achieve offset-free tension tracking.

3. The proposed controller can compensate for the time-varying disturbances caused by the

changing dynamics in R2R processes. The disturbance bound within a certain time window is computed. Parameter scheduling is applied in the controller design and proved to be helpful in long-term runs.

There are several limitations of the work presented in this chapter that need to be considered. Firstly, the proposed method focuses on improving the controller's tracking performance rather than disturbance rejection performance. This means that it may not perform as well as benchmark methods when dealing with fast impulse-like disturbances. However, the strong tracking capability of the proposed method enables the controller to closely follow the set point from higher-level commands. To further enhance the overall control performance, it may be preferable to integrate the proposed controller with a supervisory controller, which will be presented in Chapter 4.

Secondly, the proposed method requires offline computation of the constraint sets, as mentioned in Section 2.4.2. In this work, the computation was simplified to only focus on the unwinding and rewinding parts of an R2R production line. However, readers may want to explore the possibility of applying this method to higher-dimensional systems. It may be possible to approximate the actual constraint set to enable faster computation, as described in [64].

Finally, this chapter conducted a simulation study to demonstrate the proof-of-concept of the proposed method. To fully validate its performance and applicability, future work should consider extending the proposed control scheme to large-scale R2R systems and conducting physical experiments.

Scholarly Contribution of the Chapter

Zhiyi Chen, Boning Qu, Baoyang Jiang, Stephen R Forrest, and Jun Ni. "Robust constrained tension control for high-precision roll-to-roll processes." ISA Transactions, 136:651-662, 2023.

Zhiyi Chen, Baoyang Jiang, and Jun Ni. "High precision tracking of roll-to-roll

manufacturing processes." International Manufacturing Science and Engineering Conference. ASME, 2020.

Boning Qu, **Zhiyi Chen**, Lucas Lahann, and Stephen R Forrest. "Cost estimates of roll-to-roll production of organic light emitting devices for lighting." ACS Photonics, 2023.

.

CHAPTER 3

Control Barrier Functionals for Safety-critical Control of Registration Accuracy in Roll-to-Roll Printing Systems

In the previous chapter, a process control algorithm is developed to achieve accurate tension control in various R2R processes, including coating, printing, laminating, and slitting. The implementation of tension control in these processes offers numerous benefits, such as improved production efficiency, enhanced process stability, and reduced material waste. However, for the fabrication of flexible thin-film devices, tension control alone is not sufficient to meet the stringent requirements. Another crucial aspect that poses challenges to R2R processes is registration accuracy. Precise registration is essential for aligning multiple layers on a moving substrate and ensuring high-quality printed patterns. Registration errors can result in misaligned patterns, disconnected printing, and device malfunction. Overcoming these challenges is critical for the successful adoption of high-speed R2R printing processes in flexible electronics fabrication. In light of this, this chapter will focus on addressing the issue of registration accuracy, paving the way for wider adoption of R2R processes in the production of thin-film devices.

3.1 Introduction

The manufacturing of thin-film devices plays a vital role in various industries, ranging

from electronics to renewable energy. Currently, the predominant approach for producing these devices is the sheet-to-sheet (S2S) method, which offers high precision during the fabrication process. However, as the demand for high-volume production increases, there is a growing interest in adopting roll-to-roll (R2R) methods due to their potential for high-speed and continuous manufacturing. While R2R processes have shown promise in terms of scalability and efficiency, one critical aspect that requires improvement is registration accuracy. Registration accuracy refers to the precise alignment of multiple layers in the printing process, ensuring the desired pattern is consistently reproduced. R2R methods face challenges in attaining the same level of registration accuracy compared to S2S methods. Overcoming this hurdle is crucial to enable the successful transition from S2S to R2R manufacturing for thin-film devices.

Registration errors in R2R processes can be influenced by several factors inherent to the system dynamics. These factors include variations in substrate tension, fluctuations in transport velocity, substrate strain arising from material properties or process conditions, mis-synchronization of printing or processing equipment, inaccuracies in guiding and positioning systems, and thermal expansion or contraction of materials, among others [65]. It is important to note that registration error measures the misalignment between a given layer and previously printed layers that are "in the past" in terms of the printing sequence. Consequently, modeling and control of registration errors necessitate the consideration of the inherent time delays associated with the process.

In the context of registration accuracy in Roll-to-Roll (R2R) processes, moving direction (MD in short, or machine direction in some literature) registration has received more attention compared to lateral direction registration. This focus is primarily due to the significant impact of MD registration on the functionality and performance of the final product, as well as the challenges associated with designing effective control strategies for MD registration in dynamic R2R processes.

Over the past decades, researchers have dedicated significant efforts to developing mathematical models that aim to understand and quantify the generation of MD registration errors.

Yoshida *et al.* proposed a model that utilized substrate strain variation and line moving speed to estimate MD registration errors [66, 67]. Based on this model, nonlinear control laws were designed to compensate for registration errors in real-time. The algorithm was thoroughly validated through simulations and experiments, demonstrating its reliability. Building upon Yoshida's work, Liu *et al.* and Kang *et al.* refined the MD registration model and employed perturbation methods to derive a linearized model that facilitated the design of registration controllers [68, 69]. In another study by Seshadri *et al.*, a comprehensive model was proposed that incorporated the dynamics of a compensator roller, enabling the extension of the model to a wider range of operating conditions [65]. These physics-based models provided valuable insights and advantages in the design of registration controllers. However, they often focused on specific process fluctuations while neglecting minor disturbances that could also affect registration accuracy. To complement this limitation, Lee *et al.* studied thermal effects on registration characteristics in [70]. Furthermore, a data-driven modeling algorithm was introduced in a recent work by Shah *et al.* in [71], which aimed to better accommodate unconsidered issues by leveraging data-driven techniques.

With an understanding of the factors contributing to registration errors in R2R processes and the development of mathematical models to quantify them, researchers have developed control algorithms to compensate for registration inaccuracies. Notably, nonlinear control schemes based on Lyapunov stability analysis were proposed in [67, 72] to mitigate registration errors. However, these algorithms were designed based on the analysis of single-span systems, which might not provide the optimal performance when multiple printing stages were involved. A decentralized control scheme was proposed in [73] to handle multi-span systems. It is important to note that registration errors can be influenced not only by random process fluctuations, but also by the actions of tension and registration controllers themselves. This is attributed to the interconnected nature of R2R printing systems, where compensating for local process fluctuations can inadvertently introduce disturbances to other stages. Therefore, controllers were designed to decouple the behavior of different printing sections in [74, 75]. Since the interstage couplings in R2R systems were complicated, Liu *et al.* proposed an active disturbance rejection controller

to estimate and eliminate the coupling in real time [76]. Another approach to achieve effective decoupling of subsystems is to design model predictive controllers based on data-driven models of the system, as demonstrated in [71]. Despite the recent advancements in registration control algorithms, the performance of R2R printing processes still falls short of standards in the semiconductor industry, as reviewed in [77]. Therefore, there is ongoing research that aims to improve the registration accuracy of large-scale multistage R2R printing systems.

Extensive research, as demonstrated in [46], showed that variations in substrate tension significantly contribute to registration errors in R2R processes. Consequently, most existing registration control schemes aim to address both registration and tension fluctuations simultaneously. However, the significance of safety as a prerequisite for control performance is often overlooked in these controllers. While the primary objective in R2R printing sections is to achieve high registration accuracy, control limits on tension variations are typically imposed to mitigate the risk of system failures, such as substrate breakage. Therefore, when designing registration controllers, it is imperative to consider the constraints imposed by tension fluctuations. In light of these considerations, the control objective should be revised to prioritize the minimization of registration errors while constraining substrate tension within acceptable control limits. This refined focus enables the development of more effective and robust registration control schemes in R2R processes.

Several control schemes are proposed in the literature to handle constraints. The two commonly used approaches are Model Predictive Control (MPC) and Reference Governors. However, these control schemes have limited applications in registration control. MPC (as proposed in Chapter 2) is not well-suited for controlling time-delay systems due to the high computational complexity associated with solving the optimization problem, particularly when long time delays are present. On the other hand, reference governors have been shown to handle time delays in [78, 79]. However, their applicability is limited to linear time-delay systems. In recent years, safety functional-based approaches have emerged to address safety concerns in nonlinear time-delay systems [80, 81]. Building upon this idea, Control Barrier Functionals

(CBFals) are developed to guide the design of safety control synthesis [82, 83]. The CBFal approach offers a promising approach for addressing safety issues in registration control, making it a preferable choice over MPC and reference governors in this specific domain.

In this chapter, a comprehensive control framework is developed to address the safety-critical control of registration accuracy and tension in R2R printing systems. The primary objective is to achieve high registration accuracy, which is accomplished by designing a dedicated primary controller. The primary controller is responsible for compensating for registration errors and ensuring system stability during normal operation. However, to ensure the safety of the R2R printing system, an additional safety controller is introduced as an add-on scheme to the primary controller. The safety controller plays a critical role in formally guaranteeing that the tension variations induced by the control actions of the primary controller remain within specified control limits. The proposed framework is validated through a numerical study, demonstrating its ability to enhance registration accuracy while mitigating the risk of tension-related system failures.

The remainder of this chapter is structured as follows. Section 3.2 presents the mathematical model of registration errors. Section 3.3 discusses the design of the registration controller, encompassing the primary controller and the safety controllers. Section 3.4 validates the control algorithms through a numerical case study of a three-roller printing system. Finally, Section 3.5 concludes the chapter and outlines potential future directions.

3.2 Modeling of Registration Errors

The schematic in Figure 3.1 illustrates the R2R printing system to be studied in this work. The notation used in this work is consistent with the model presented in Chapter 2, providing a clear and unified representation for the analysis of the system.

The R2R printing system consists of multiple printing sections where the substrate is unwound from a roller, passes through the printing process, and is collected onto a rewind roller. The objective is to ensure that each printed layer is precisely stacked on top of the previous layer.

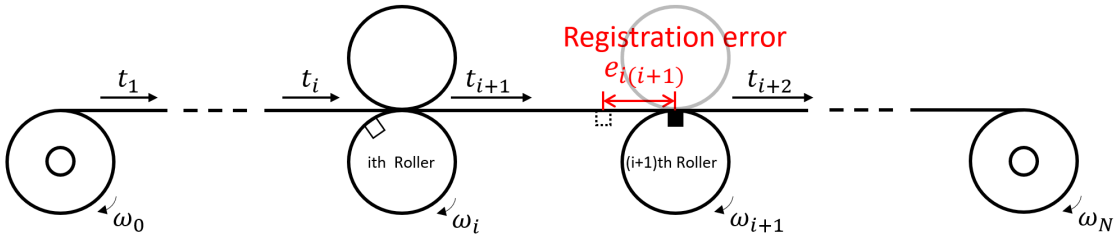

Figure 3.1: Illustration of registration error in a R2R printing system.

In our study, we define the registration error as the misalignment between two adjacent layers. In Figure 3.1, ω_i represents the rotation speed of the i^{th} roller, and t_i denotes the substrate tension between the $(i-1)^{th}$ and i^{th} rollers. We focus on the registration error $e_{i(i+1)}$ between the i^{th} and $(i+1)^{th}$ printing rollers as a key parameter for control purposes.

In Chapter 2, motor torques are defined as the control inputs for the system. This choice is made because the torque mode of a motor allows for faster and more accurate responses in force control. However, it is a common practice to use the speed mode of a motor to conduct registration control. Motor speed, denoted as ω_i, is considered as the control input in this work. By adjusting the motor speed, the position of the printed pattern can be rapidly adjusted to address misalignments between layers. It is assumed that there is no slippage during the printing process, so the substrate moving speed, denoted as v_i, follows the relationship $v_i = \omega_i R_i$, where R_i represents the radius of the i^{th} roller.

Studies have demonstrated that registration errors in R2R printing systems are influenced by substrate strain and variations in substrate speed [65, 67, 69]. To estimate registration errors in real-time, mathematical models are developed in the literature. Although there are differences among these models, one particular model is utilized in the latter part of this work to showcase the effectiveness of the proposed method. Experimental validation has provided evidence supporting the accuracy of the following equations in estimating registration errors [67, 84]:

$$\dot{e}_{i(i+1)} = \frac{v_{ri}}{\left(1 + \frac{t_i(t-\tau)}{AE}\right)} - \frac{v_{r(i+1)}}{\left(1 + \frac{t_{i+1}(t)}{AE}\right)} \tag{3.1}$$

$$\dot{t}_{i+1} = \frac{AE}{L_{i+1}} v_{i+1} - \frac{AE}{L_{i+1}} v_i - \frac{t_{i+1}}{L_{i+1}} v_{i+1} + \frac{t_i}{L_{i+1}} v_i \tag{3.2}$$

where v_{ri} is the reference speed of the i^{th} roller, t is the time index, A is the cross-sectional area of the substrate, E is the Young's modulus, L_{i+1} is the span length of the substrate between i^{th} and $(i+1)^{th}$ roller. In addition, τ is the time delay between the printing of two adjacent layers, which is determined by $\tau = L_{i+1}/v_{ri}$.

Eqs. (3.1) and (3.2) describe a nonlinear model that quantifies the relationship between registration error, substrate tension and speed. In this model, the state variable is defined as $(e_{i(i+1)}, t_{i+1})$, and v_{i+1} is the control input. The nonlinear model can be linearized by defining $E_{i(i+1)} = e_{i(i+1)} - 0$, $T_i = t_i - t_{ri}$, and $V_i = v_i - v_{ri}$, where t_{ri} and v_{ri} are tension and speed references. Further assume that $t_i \ll AE, i = 1, 2, \cdots, N$ (which implies the substrate strain is very small), the nonlinear model can be simplified as follows [69]:

$$\dot{E}_{i(i+1)} = \frac{1}{AE} \left(v_{ri} T_i(t-\tau) - v_{r(i+1)} T_{i+1}(t) \right) \tag{3.3}$$

$$\dot{T}_{i+1} = \frac{1}{L_{i+1}} \left(v_{r(i)} T_i(t) - v_{r(i+1)} T_{i+1}(t) \right) + \frac{AE}{L_{i+1}} (V_{i+1}(t) - V_i(t)) \tag{3.4}$$

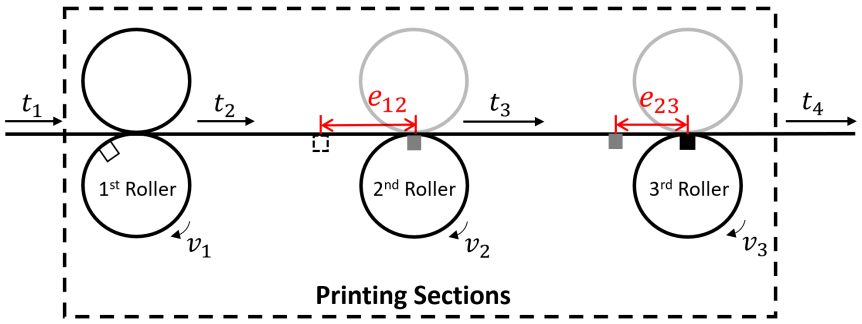

Figure 3.2: A R2R system with three printing sections.

Now consider a R2R system with three printing sections, as shown in Figure 3.2. Three key assumptions are made here to formulate the control problem: 1) Substrate tensions are well

regulated by tension controllers at the entrance and exit of the printing sections, i.e., t_1 and t_4 are constants; 2) Speed of the 1^{st} printing roller is considered as the reference speed, i.e., v_1 is not considered as a control input; and 3) The printing rollers have the same radius and each section shares the same time delay. These assumptions allow us to refine the design space of the registration control problem.

One can obtain a nonlinear vectorized state space representation of Eqs. (3.1) and (3.2) by defining the state vector $\boldsymbol{x}(t) = [e_{12}(t), e_{23}(t), t_2(t), t_3(t)]^{\mathrm{T}}$ and control inputs $\boldsymbol{u}(t) = [v_2(t), v_3(t)]^{\mathrm{T}}$, which then follows:

$$\begin{aligned} \dot{\boldsymbol{x}}(t) &= f\left(\boldsymbol{x}(t), \boldsymbol{x}(t-\tau)\right) + g\left(\boldsymbol{x}(t), \boldsymbol{x}(t-\tau)\right)\boldsymbol{u}(t) \\ \boldsymbol{y}(t) &= h(\boldsymbol{x}(t)) \end{aligned} \tag{3.5}$$

where $f : \mathbb{R}^{n_x \times n_x} \to \mathbb{R}^{n_x}$, $g : \mathbb{R}^{n_x \times n_x} \to \mathbb{R}^{n_x \times n_u}$ and $h : \mathbb{R}^{n_x} \to \mathbb{R}^{n_x}$ are Lipschitz continuous functions. Note that Eq. (3.5) defines a nonlinear affine control system where delay appears in the state.

Alternatively, a linear state space model can be constructed for the R2R printing system utilizing Eqs. (3.3) and (3.4). Let $\boldsymbol{X}(t) = [E_{12}(t), E_{23}(t), T_2(t), T_3(t)]^{\mathrm{T}}$ represent the state vector, and $\boldsymbol{U}(t) = [V_2(t), V_3(t)]^{\mathrm{T}}$ denote the control inputs, the linear retarded state space model can be expressed as follows:

$$\begin{aligned} \dot{\boldsymbol{X}}(t) &= A_0\boldsymbol{X}(t) + A_1\boldsymbol{X}(t-\tau) + B\boldsymbol{U}(t) \\ \boldsymbol{Y}(t) &= C\boldsymbol{X}(t) \end{aligned} \tag{3.6}$$

where $A_0 \in \mathbb{R}^{n_x \times n_x}$, $A_1 \in \mathbb{R}^{n_x \times n_x}$, $B \in \mathbb{R}^{n_x \times n_u}$, and $C \in \mathbb{R}^{n_y \times n_x}$ are the system matrix, retarded system matrix, input matrix and output matrix, respectively. Expressions of these matrices can be found in [71]. Eq. (3.6) is a simplified version of Eq. (3.5) that represents a linear affine control system.

3.3 Control Design

The overarching objective is to develop a registration controller that addresses two key aspects: 1) mitigating registration errors induced by disturbances, and 2) maintaining tension fluctuations within predefined control limits to ensure system safety. To achieve this, the controller design is divided into two steps. Firstly, a primary controller is designed to stabilize the time delay system and eliminate registration errors during normal operation. Subsequently, a safety controller is introduced as an add-on scheme to the primary controller. The safety controller is responsible for taking over the control when events occur that may jeopardize the safety of the system.

The following notations will be used in the remaining sections.

1. $\mathcal{B}$ (Banach space) is the space of continuous functions mapping from $[-\tau, 0]$ to $\mathbb{R}^{n_x}$, where the norm is defined to be $\|\phi\| = \max_{s\in[-\tau,0]} \|\phi(s)\|_2$, $\forall \phi \in \mathcal{B}$.

2. $\boldsymbol{x}_t : [-\tau, 0] \to \mathbb{R}^{n_x}$ represents the history of the state over $[t-\tau, t]$ with $\boldsymbol{x}_t(s) = \boldsymbol{x}(t+s), s \in [-\tau, 0]$.

3. $\boldsymbol{X}_t : [-\tau, 0] \to \mathbb{R}^{n_x}$ represents the history of the linearized state over $[t-\tau, t]$ with $\boldsymbol{X}_t(s) = \boldsymbol{X}(t+s), s \in [-\tau, 0]$.

3.3.1 Primary Controller

In this section, a primary controller is designed based on the linear representation (3.6) of a R2R printing system. For instance, consider a controller of the form $\boldsymbol{U}(t) = -K_p\boldsymbol{X}(t)$. To establish the asymptotic stability of system (3.6), a quadratic Lyapunov-Krasovsky functional can be constructed with the form:

$$V(\boldsymbol{X}_t) = \boldsymbol{X}^{\mathrm{T}}(t)P\boldsymbol{X}(t) + \int_{t-\tau}^{t} \boldsymbol{X}^{\mathrm{T}}(s)Q\boldsymbol{X}(s)\,ds \tag{3.7}$$

where $P \in \mathbb{R}^{n_x\times n_x}$ and $Q \in \mathbb{R}^{n_x\times n_x}$ are positive-definite matrices.

Definition 3.1. *[85] The system* (3.6) *is uniformly stable with the Lyapunov functional* (3.7)*, if there exist K_p and a constant $\lambda > 0$, such that $V(\boldsymbol{X}_t)$ is positive definite and its derivative along* (3.6) *is non-positive for all $\boldsymbol{X}_t \in \mathcal{B}$ as:*

$$\begin{aligned}\frac{dV(\boldsymbol{X}_t)}{dt} &= 2\boldsymbol{X}^T(t)P\dot{\boldsymbol{X}}(t) + \boldsymbol{X}^T(t)Q\boldsymbol{X}(t) - \boldsymbol{X}^T(t-\tau)Q\boldsymbol{X}(t-\tau) \\ &= 2\boldsymbol{X}^T(t)P\left[(A_0 - BK_p)\boldsymbol{X}(t) + A_1\boldsymbol{X}(t-\tau)\right] \\ &\quad + \boldsymbol{X}^T(t)Q\boldsymbol{X}(t) - \boldsymbol{X}^T(t-\tau)Q\boldsymbol{X}(t-\tau) \\ &\leq -\lambda|\boldsymbol{X}(t)|^2\end{aligned} \tag{3.8}$$

The above Lyapunov functional yields an equivalent linear matrix inequality [86]:

$$\begin{bmatrix}(A_0 - BK_p)^{\mathrm{T}}P + P(A_0 - BK_p) + Q & PA_1 \\ A_1^{\mathrm{T}}P & Q\end{bmatrix} < 0, \tag{3.9}$$

which implies that the choice of control gain K_p needs to satisfy the following criteria to guarantee the stability of system (3.6):

1. $(A_0 - BK_p)$ is Hurwitz, meaning every eigenvalue of the matrix has a negative real part.
2. $(A_0 - BK_p) \pm A_1$ is Hurwitz.
3. $(A_0 - BK_p)^{-1}A_1$ is a Schur matrix, meaning all eigenvalues of the matrix have a magnitude less than one.

Seshadri *et al.* reached a similar conclusion in [87], and used the matrix perturbation theory to design K_p. Here, we propose an algebraic Riccati equation (ARE) based method, which can be solved using numerical methods efficiently, to compute a candidate control gain that satisfies the above criteria. Compared to the methods from the literature, this modified ARE approach can be easily extended to R2R systems that yield models with high dimensions.

Theorem 3.1. *If there exist $Q > 0$ and $Q_1 > 0$, such that the following modified ARE has a*

symmetric positive definite solution P:

$$A_0^T P + P A_0 - P B B^T P + P A_1 Q^{-1} A_1^T P + C^T C + Q + Q_1 = 0 \tag{3.10}$$

Then the feedback control law

$$\boldsymbol{U}(t) = -K_p \boldsymbol{X}(t), \quad K_p = B^T P \tag{3.11}$$

can stabilize the time-delay system (3.6) *regardless of the time delay τ.*

Proof. By Schur complement theory, the linear matrix inequality (3.9) is equivalent to

$$\begin{aligned} &Q > 0, \\ &(A_0 - B K_p)^{\mathrm{T}} P + P(A_0 - B K_p) + Q + P A_1 Q A_1^{\mathrm{T}} P < 0 \end{aligned} \tag{3.12}$$

Substituting the control law (3.11) into (3.10), and minus $PBB^{\mathrm{T}}P$ on both sides of the equation, one can obtain

$$A_0^{\mathrm{T}} P + P A_0 - P B K_p + P A_1 Q^{-1} A_1^{\mathrm{T}} P + Q - P B K_p = -C^{\mathrm{T}} C - Q_1 - P B B^{\mathrm{T}} P \tag{3.13}$$

Since $Q_1 > 0$ by definition, the right-hand side of (3.13) is clearly negative, which implies the second inequality of (3.12). Thus the proof is complete. □

Since a linearized retarded model is used for designing the primary controller, the actual control input that should be applied to the R2R system is:

$$\boldsymbol{u}_{\text{primary}}(t) = \boldsymbol{u}_r + \boldsymbol{U}(t) \tag{3.14}$$

where $\boldsymbol{u}_r$ is the reference control input that maintains the system at a steady state. Note that speed mode is used to control registration accuracy in this case, therefore, $\boldsymbol{u}_r$ corresponds to the pre-defined reference motor speeds.

The deterministic control law (3.14) is designed to stabilize a R2R printing system and eliminate registration errors. One can refer to [88] to find a robust control algorithm that counters parametric uncertainties in the R2R process. The primary controller is responsible for most of the control actions during the operation. However, it does not explicitly consider the safety constraints of the underlying system. A safety controller is proposed in the following section, which evaluates the safety of the system and takes over the control when necessary.

3.3.2 Safety Controller using CBFal

Unlike the previous section, where the primary controller is built upon a linearized model, we will now design the safety controller using the nonlinear affine control model in Eq. (3.5). This provides a more accurate evaluation of system safety and ensures reliable control performance.

During the operation of a R2R printing system, it is crucial to establish control boundaries for the process parameters to ensure proper system operation. In this work, particular attention is given to maintaining tensions within a predefined control limit, denoted as $t_i \in [t_{lb}, t_{ub}]$. This ensures that the tension values of the printing sections remain within the specified range, promoting system stability and preventing potential issues associated with excessive or insufficient tension. The following definition provides a mathematical characterization of the safety concept in dynamical systems without time delays.

Definition 3.2. ***Safety of delay-free systems [82].*** *Consider a dynamic system described by the ordinary differential equation $\dot{\boldsymbol{x}}(t) = f(\boldsymbol{x}(t))$, where $f(\cdot)$ is a locally Lipschitz continuous function. The system is said to be safe w.r.t. set $S \subset \mathbb{R}^{n_x}$, if S is forward invariant s.t. $\boldsymbol{x}(0) \in S \Rightarrow \boldsymbol{x}(t) \in S$, $\forall t \geq 0$.*

This definition states that a delay-free system is considered safe if the initial state $\boldsymbol{x}(0)$ belonging to the set S guarantees that the subsequent evolution of the system remains within S. It is important to note that Definition 3.2 is defined for an autonomous system without considering the role of controllers. In practical applications, controllers need to be designed to ensure the safety

of the system. Now, let us consider extending this definition of safety to time delay systems. We will focus on a general time delay system described using the Hale-Krasovsky notation:

$$\dot{\boldsymbol{x}}(t) = \mathcal{F}(\boldsymbol{x}_t) \tag{3.15}$$

where $\mathcal{F}$ is a locally Lipschitz continuous functional. Under such configurations, Eq. (3.15) has a unique solution, given any state history $\boldsymbol{x}_0 \in \mathcal{B}$. Then the safety of system (3.15) can be extended from definition 3.2 as:

Definition 3.3. ***Safety of time-delay systems [82].*** *System* (3.15) *is said to be safe w.r.t set $\mathcal{S} \subset \mathcal{B}$, if $\mathcal{S}$ is forward invariant s.t. $\boldsymbol{x}_0 \in \mathcal{S} \Rightarrow \boldsymbol{x}_t \in \mathcal{S}$, $\forall t \geq 0$.*

It can be noticed that constructing the forward invariant set $\mathcal{S}$ is critical to ensure the system safety. The following theorem addresses the construction of the forward invariant set and the so-called safety functional.

Theorem 3.2. *[80] Given that the set $\mathcal{S}$ is a 0-superlevel set of a continuously differentiable functional $\mathcal{H}$ satisfying*

$$\mathcal{S} = \{\boldsymbol{x}_t \in \mathcal{B} : \mathcal{H}(\boldsymbol{x}_t) \geq 0\} \tag{3.16}$$

Then $\mathcal{H}$ is a safety functional if it satisfies

$$\dot{\mathcal{H}}(\boldsymbol{x}_t) \geq -\alpha(\mathcal{H}(\boldsymbol{x}_t)) \tag{3.17}$$

where $\alpha : [0, a] \to [0, \infty]$ is a Class $\mathcal{K}$ function[1]*. Note that $\dot{\mathcal{H}}(\cdot)$ is the time derivative of $\mathcal{H}$ along* (3.15)*.*

The aforementioned theorem still defines safety for autonomous time delay systems. The focus of this work is to ensure safety for a controlled R2R printing system with time delays. We now introduce the concept of control barrier functional, which is built upon the safety functionals

[1] A continuous function α belongs to Class $\mathcal{K}$ function if it is strictly increasing and $\alpha(0) = 0$.

to optimize the control of safety-critical systems. In general, Eq. (3.15) can be extended to the following form to consider the role of controllers:

$$\dot{\boldsymbol{x}}(t) = \mathcal{F}(\boldsymbol{x}_t) + \mathcal{G}(\boldsymbol{x}_t)\boldsymbol{u}(t) \tag{3.18}$$

where $\mathcal{F} : \mathcal{B} \to \mathbb{R}^{n_x}$ and $\mathcal{G} : \mathcal{B} \to \mathbb{R}^{n_x \times n_u}$ are locally Lipschitz continuous functionals. Without loss of generality, the nonlinear model (3.5) can be equivalently written in the form of Eq. (3.18) when perfect observation is available for the underlying R2R system (i.e., h is an identity function in (3.5)). For system (3.18), the control purpose is to design a controller to drive the system under the safety region. To do this, the control barrier functionals are defined in the following statement:

Definition 3.4. *[82] Given the forward invariant set $\mathcal{S}$ defined by Eq.* (3.16)*, a continuously differentiable functional $\mathcal{H}$ is a CBFal for system* (3.18) *if it satisfies*

$$\sup_{\boldsymbol{U} \in \mathbb{R}^{n_u}} \dot{\mathcal{H}}(\boldsymbol{x}_t, \boldsymbol{u}) \geq -\alpha(\mathcal{H}(\boldsymbol{x}_t)) \tag{3.19}$$

where $\alpha : [0, a] \to [0, \infty]$ is a Class $\mathcal{K}$ function. $\dot{\mathcal{H}}(\cdot)$ is the time derivative of $\mathcal{H}$ following:

$$\dot{\mathcal{H}}(\boldsymbol{x}_t, \boldsymbol{u}) = \mathcal{L}_{\mathcal{F}}\mathcal{H}(\boldsymbol{x}_t) + \mathcal{L}_{\mathcal{G}}\mathcal{H}(\boldsymbol{x}_t)\boldsymbol{u} \tag{3.20}$$

where the functionals $\mathcal{L}_{\mathcal{F}}\mathcal{H}$ and $\mathcal{L}_{\mathcal{G}}\mathcal{H}$ are derivative of $\mathcal{H}$ along $\mathcal{F}$ and $\mathcal{G}$, respectively.

The inequality (3.19) represents a safety constraint that must be satisfied by the system. It guides operators in designing the safety controller for the R2R printing system. At each time instance, the inequality (3.19) is evaluated. If the inequality is satisfied, it indicates that the primary controller is capable of keeping the system states within the safety set. However, if the inequality is violated, it implies that the safety constraints are at risk of being breached, and adjustments need to be made to the primary controller to restore safe operation. To implement this concept, a switching controller can be designed for the R2R printing system. The registration accuracy controller is

denoted as $\boldsymbol{u}_{\text{reg}}$, which is defined as follows:

$$\boldsymbol{u}_{\text{reg}} = \begin{cases} \boldsymbol{u}_{\text{primary}} & \text{if (3.19) is satisfied} \\ \boldsymbol{u}_{\text{safety}} & \text{otherwise} \end{cases} \tag{3.21}$$

The safety controller $\boldsymbol{u}_{\text{safety}}$ can be obtained by formulating a constrained optimization problem. The objective is to find an alternative control input that closely resembles the primary controller, ensuring the asymptotic stability of the registration system, while simultaneously enforcing the safety constraints. The following optimization problem seeks to strike a balance between achieving accurate registration and maintaining system safety.

$$\begin{aligned} \min_{\boldsymbol{u}_{\text{safety}} \in \mathbb{R}^{n_u}} \quad & J_n = \|\boldsymbol{u}_{\text{safety}} - \boldsymbol{u}_{\text{primary}}\|_2^2 \\ \text{subject to} \quad & \dot{\mathcal{H}}(\boldsymbol{x}_t, \boldsymbol{u}_{\text{safety}}) \geq -\alpha(\mathcal{H}(\boldsymbol{x}_t)) \end{aligned} \tag{3.22}$$

The optimization problem can be efficiently solved by using quadratic programming. Alternatively, an explicit solution can be found offline by Karush-Kuhn-Tucker conditions [82]. Combined with Eq. (3.11), the explicit solution of (3.22) provides the control synthesis as follows:

$$\boldsymbol{u}_{\text{reg}} = \begin{cases} \boldsymbol{u}_r - K_p \boldsymbol{X}(t) & \text{if } \phi(\boldsymbol{x}_t) \geq 0 \\ \boldsymbol{u}_r - K_p \boldsymbol{X}(t) - \frac{\phi(\boldsymbol{x}_t)\phi_0^{\mathrm{T}}(\boldsymbol{x}_t)}{\phi_0(\boldsymbol{x}_t)\phi_0^{\mathrm{T}}(\boldsymbol{x}_t)} & \text{otherwise} \end{cases} \tag{3.23}$$

where

$$\begin{aligned} \phi_0(\boldsymbol{x}_t) &= \mathcal{L}_{\mathcal{G}}\mathcal{H}(\boldsymbol{x}_t) \\ \phi(\boldsymbol{x}_t) &= \mathcal{L}_{\mathcal{F}}\mathcal{H}(\boldsymbol{x}_t) + \mathcal{L}_{\mathcal{G}}\mathcal{H}(\boldsymbol{x}_t)(-K_p \boldsymbol{x}(t)) + \alpha(\mathcal{H}(\boldsymbol{x}_t)) \end{aligned} \tag{3.24}$$

Even though Eq. (3.23) employs Eq. (3.11) as the primary controller, users can substitute it with the original registration controllers installed in their systems. This highlights the advantage of the safety controller as an add-on scheme, as it can be readily implemented on existing production systems without the need for complex modifications to the overall control logic.

3.4 Case Study

A simulation study is conducted to evaluate the performance of the proposed controller in a R2R system with three printing rollers, as depicted in Figure 3.2. Most simulation parameters are chosen to be consistent with those used in Chapter 2. It is assumed that the configuration and characteristics of all printing sections are identical. The specific values for the key parameters can be found in Table 3.1.

Table 3.1: Simulation Setup

Symbol	**Parameter**	**Value**
A	Cross-sectional Area	1.2×10^{-5} (m^2)
E	Young's Modulus	200 (MPa)
R	Roller Radius	0.05 (m)
L	Span Length	0.2 (m)
v_r	Speed Reference	0.01 $(\mathrm{m/s})$
t_r	Tension Reference	30 (N)
t_{lb}	Tension lower bound	29 (N)
t_{ub}	Tension upper bound	31 (N)

The system dynamics are simulated using the nonlinear models (3.1) and (3.2), which are solved using the dde23 function in MATLAB. The simulation duration is set to $100\,\mathrm{s}$, and a sampling time of $T_s = 10\,\mathrm{ms}$ is chosen. It is important to note that unlike the LPV-MPC discussed in the previous chapter, the proposed primary and safety controllers require less online computation. As a result, the controllers are capable of generating control inputs almost in real time, allowing for efficient and timely control of the system.

3.4.1 Open-loop Response of the Printing System

In this simulation, the R2R printing system is initially operating at steady state. At $t = 10\,\mathrm{s}$, a step disturbance is introduced by increasing the motor speed ω_2 by 1%, resulting in a local line speed increment of $1 \times 10^{-4}\ \mathrm{m/s}$ in the second printing section. The motor speed then returns to its normal value at $t = 20\,\mathrm{s}$. The responses of the system to this disturbance are depicted in

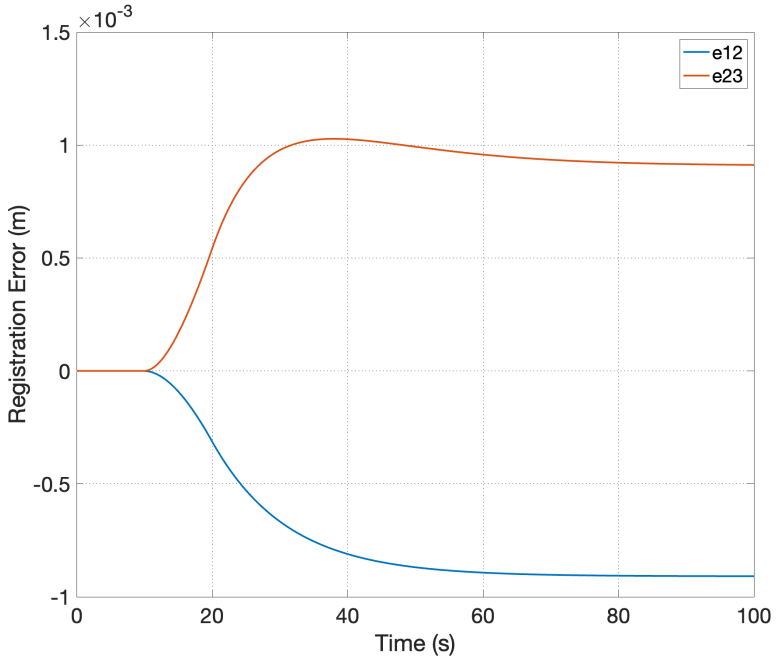

Figure 3.3: Disturbance in motor speed ω_2 causes registration errors in both printing sections II and III. The registration errors cannot be eliminated when no control is applied.

Figures 3.3 and 3.4.

In Figure 3.3, it can be observed that the step disturbance in the motor speed ω_2 leads to the generation of registration errors in the printing sections. Specifically, e_{12} exhibits a negative registration error, indicating that the second printed layer falls behind the desired position due to the speed variation. On the other hand, e_{23} shows a positive registration error, indicating that the third layer is ahead of the desired position. Figure 3.4 illustrates the variations in tension (t_2 and t_3) caused by the speed variation. It can be seen that t_2 experiences a 46% increase, while t_3 undergoes a 26% decrease. These tension variations are a direct consequence of the disturbance in motor speed. However, it is worth noting that the tension variations subside once the disturbed motor speed returns to its normal value. These observations from the case study highlight the importance of designing a registration controller with two primary objectives: 1) Active compensation of registration errors back to zero when process disturbances occur; and 2) Prevention of large tension variations to avoid substrate distortion and breakage.

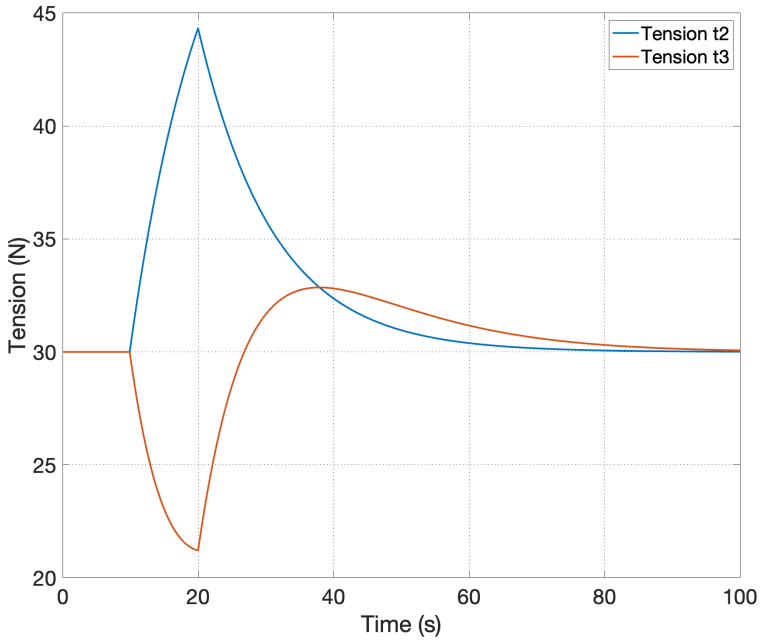

Figure 3.4: Disturbance in motor speed ω_2 causes significant tension variations in both printing sections II and III.

3.4.2 Closed-loop Response of the Printing System

In this part of the study, we simulate the case where only the primary controller is deployed to the system. Subsequently, we implement a safety controller as an add-on scheme to assist the registration control. By comparing the results of these two simulations, we can assess the effectiveness of the safety controller in improving the system performance and ensuring its safety.

3.4.2.1 Implementation Details

In both scenarios, the printing system starts from the steady state. At $t = 10\,\mathrm{s}$, a registration error $e_{12} = 100\,\mu\mathrm{m}$ is applied between the first and second printing units. To compensate for the registration error, a primary controller is designed according to the modified ARE (3.10) and the control law (3.11). Recall that $\boldsymbol{x}(t) = [e_{12}(t), e_{23}(t), t_2(t), t_3(t)]^{\mathrm{T}}$ and $\boldsymbol{X}(t) = \boldsymbol{x}(t) - [0, 0, t_{r2}, t_{r3}]^{\mathrm{T}} = [E_{12}(t), E_{23}(t), T_2(t), T_3(t)]^{\mathrm{T}}$. The corresponding control gain is determined to be:

$$K_p = \begin{bmatrix} -89.4690 & 44.6687 & 0.0028 & -0.0014 \\ -44.6687 & -89.4690 & 0.0014 & 0.0028 \end{bmatrix}$$

In addition, the tension control limits are considered in the design of the safety controller. The following candidate control barrier functional is used:

$$\mathcal{H}(\boldsymbol{x}_t) = -(\boldsymbol{x}(t) - x_{min})^{\mathrm{T}} Q_w (\boldsymbol{x}(t) - x_{max}) \tag{3.25}$$

where x_{min} and x_{max} are the modified control limits and Q_w is a positive-semidefinite weighting matrix. Note that different from the cases demonstrated in [82] (where the CBFals only enforced constraints on one state variable), Eq. (3.25) is a CBFal computed following a vectorized fashion. In our case, $\mathcal{H}(\boldsymbol{x}_t)$ is in a quadratic form and takes the sum of penalties that are applied to multiple state variables. Therefore, x_{min}, x_{max} and Q_w need to be designed carefully to restore the actual constraints, i.e., every single state x_i belongs to its own admissible set $[x_{i,lb}, x_{i,ub}]$. Since there are no safety constraints for registration errors, Q_w is decided to be:

$$Q_w = \begin{bmatrix} 0 & 0 & 0 & 0 \\ 0 & 0 & 0 & 0 \\ 0 & 0 & 1 & 0 \\ 0 & 0 & 0 & 1 \end{bmatrix}$$

To enforce the tension constraints (± 1 N from the nominal value 30 N), the modified control limits are decided to be:

$$x_{min} = \begin{bmatrix} 0 \\ 0 \\ 30 - \sqrt{2}/2 \\ 30 - \sqrt{2}/2 \end{bmatrix}, \quad x_{max} = \begin{bmatrix} 0 \\ 0 \\ 30 + \sqrt{2}/2 \\ 30 + \sqrt{2}/2 \end{bmatrix}$$

To keep $\boldsymbol{x}(t)$ evolving within the control limits, the condition in (3.19) needs to be satisfied.

Therefore, we need to compute the time derivative of $\mathcal{H}$ along (3.5), which follows:

$$\begin{aligned}\dot{\mathcal{H}}(\boldsymbol{x}_t) &= \left[-2\boldsymbol{x}^{\mathrm{T}}(t)Q_w + (x_{max}^{\mathrm{T}} + x_{min}^{\mathrm{T}})Q_w\right]\dot{\boldsymbol{x}}(t) \\ &= \underbrace{\left[-2\boldsymbol{x}^{\mathrm{T}}(t)Q_w + (x_{max}^{\mathrm{T}} + x_{min}^{\mathrm{T}})Q_w\right] f(\boldsymbol{x}(t), \boldsymbol{x}(t-\tau))}_{\mathcal{L}_{\mathcal{F}}\mathcal{H}(\boldsymbol{X}_t)} \\ &\quad + \underbrace{\left[-2\boldsymbol{x}^{\mathrm{T}}(t)Q_w + (x_{max}^{\mathrm{T}} + x_{min}^{\mathrm{T}})Q_w\right] g(\boldsymbol{x}(t), \boldsymbol{x}(t-\tau))}_{\mathcal{L}_{\mathcal{G}}\mathcal{H}(\boldsymbol{X}_t)}\boldsymbol{u}(t)\end{aligned} \tag{3.26}$$

Then follow the definition in Eq. (3.24), one can obtain

$$\begin{aligned}\phi_0(\boldsymbol{x}_t) &= \left[-2\boldsymbol{x}^{\mathrm{T}}(t)Q_w + (x_{max}^{\mathrm{T}} + x_{min}^{\mathrm{T}})Q_w\right] g(\boldsymbol{x}(t), \boldsymbol{x}(t-\tau)) \\ \phi(\boldsymbol{x}_t) &= \left[-2\boldsymbol{x}^{\mathrm{T}}(t)Q_w + (x_{max}^{\mathrm{T}} + x_{min}^{\mathrm{T}})Q_w\right] f(\boldsymbol{x}(t), \boldsymbol{x}(t-\tau)) \\ &\quad - \left[2\boldsymbol{x}^{\mathrm{T}}(t)Q_w + (x_{max}^{\mathrm{T}} + x_{min}^{\mathrm{T}})Q_w\right] g(\boldsymbol{x}(t), \boldsymbol{x}(t-\tau))\left(\boldsymbol{u}_r - K_p\boldsymbol{X}(t)\right) \\ &\quad - \alpha\left((\boldsymbol{x}(t) - x_{min})Q_w(\boldsymbol{x}(t) - x_{max})^{\mathrm{T}}\right)\end{aligned} \tag{3.27}$$

where $\alpha(r) = r$ is the chosen Class $\mathcal{K}$ function.

3.4.2.2 Control Performance

At this stage, the control synthesis outlined in Eq. (3.23) is prepared for deployment. The simulation results are presented in Figures 3.5 through 3.8. By examining the red curves in Figure 3.5, it is observed that the primary controller effectively eliminates the introduced registration error within 40 s. During this period, a registration error e_{23} is observed at the third printing unit, as shown in Figure 3.6, resulting from the control actions taken to compensate for the upstream errors. As anticipated, the primary controller successfully eliminates e_{23} within a finite time. In addition to the registration errors, the actions of the primary controller can be observed to cause tension variations, as shown in Figures 3.7 and 3.8. Given that the safe tension limit for this system is $\pm 1\mathrm{N}$ (approximately $\pm 3.3\%$), it becomes evident that the induced tension variations pose a risk to system safety. Consequently, the safety controller is activated in this scenario.

In Figures 3.5 through 3.8, the blue curves represent the system responses when the

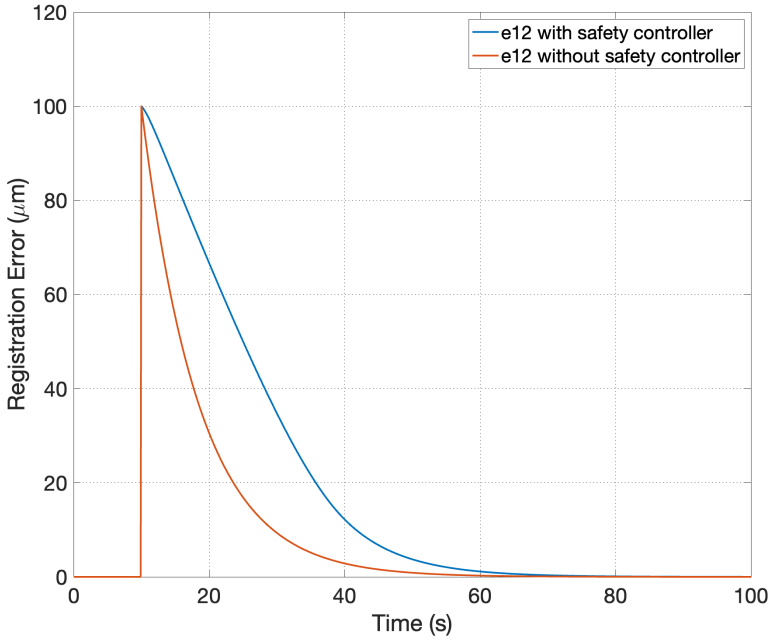

Figure 3.5: Registration error e_{12} is eliminated by the controllers when an initial registration error occurs at 10 s.

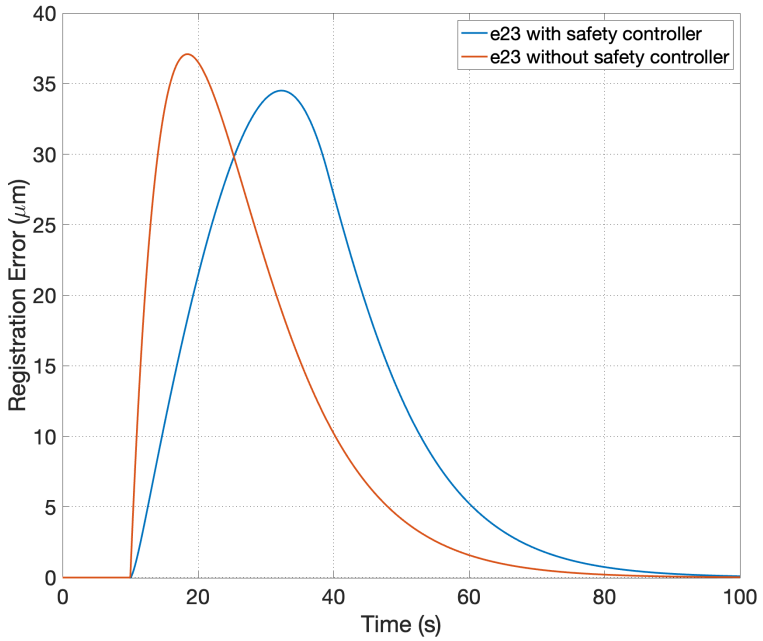

Figure 3.6: Registration error e_{23} occurs due to the control actions.

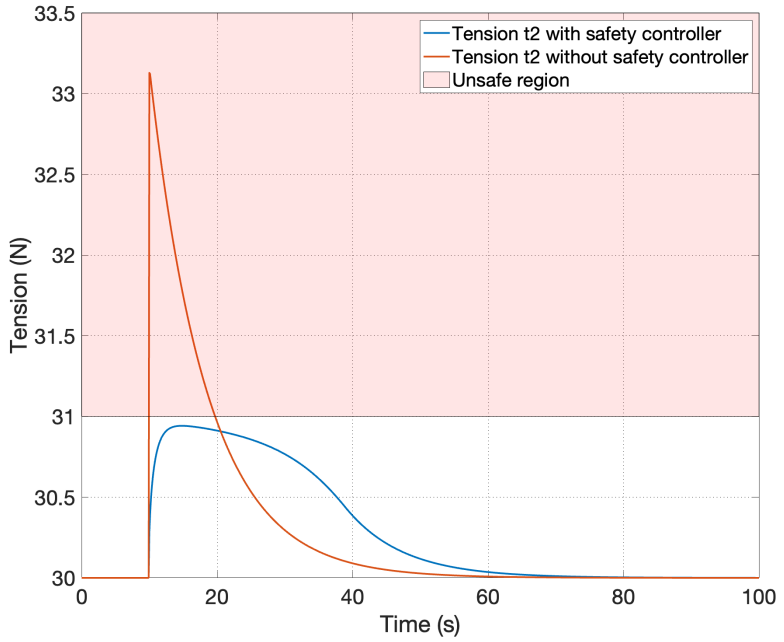

Figure 3.7: Variation in t_2 is effectively reduced by the safety controller.

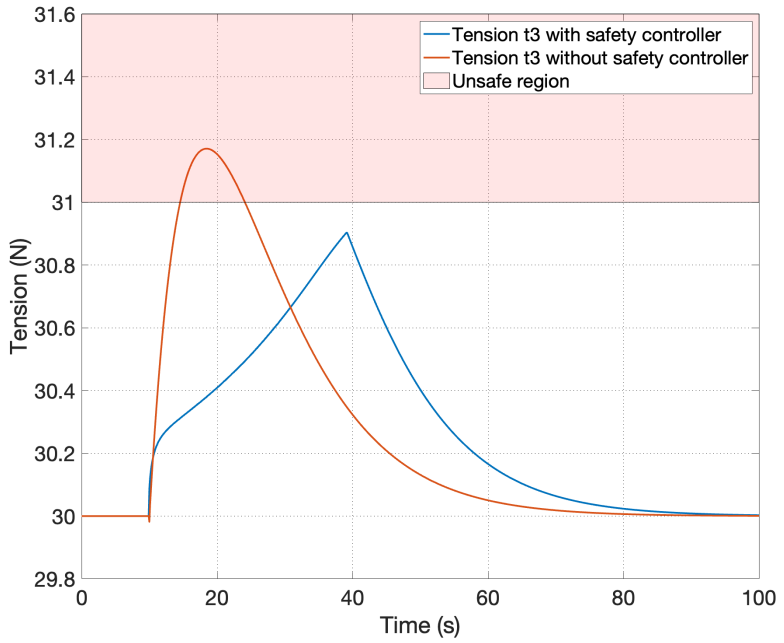

Figure 3.8: Response of tension t_3 is bounded within the safe region.

safety controller is introduced. It can be observed that the safety controller compensates for the registration errors in a less aggressive manner, resulting in a slower rate of reduction in the registration errors. However, it is remarkable that the tension variations are effectively constrained within the specified control limits. When compared to the case where only the primary controller is implemented, the introduction of the safety controller ensures the safe operation of the system without altering its stability properties. In fact, the proposed safety control synthesis can be combined with the controllers proposed in [73]-[76] to enhance their performance in safety-critical environments, featuring the practical significance of this research in improving the operation of real-world R2R printing systems.

Figure 3.9 shows the safety region defined by the candidate control barrier functional in Eq. (3.25). The quadratic functional shapes an ellipse that represents a subset of the required control limits. This indicates that the choice of the quadratic barrier functional provides a conservative safety set, suggesting that a barrier functional that generates a larger invariant set may provide better control performance for the R2R printing system. The system responses shown in the plot demonstrate that the tension deviates from its steady state when a disturbance is introduced. However, with the implementation of the safety controller, the tension responses are effectively constrained to the boundaries of the safety set, preventing system failure caused by excessive tension variations.

3.4.2.3 Choice of the Weight Matrix and Control Limits

In this particular case study, special attention is given to the design of the weighting matrix Q_w and the modified control limits. The control limits $x_{min} = [0, 0, -1, -1]^{\mathrm{T}}$ and $x_{max} = [0, 0, 1, 1]^{\mathrm{T}}$ are specifically designed to align with the direct controller limits. Furthermore, the weighting matrix Q_w is chosen to be diagonal, taking the form $\mathrm{diag}([0, 0, q_3, 1])$, where $q_3 \in [1, 2, 5, 100]$ is selected to assign different safety weights to tension t_2. A larger value of q_3 indicates that the safety of t_2 is more critical, while the safety of t_3 is relatively less important.

The impact of these design choices on the safety performance is demonstrated in Figure

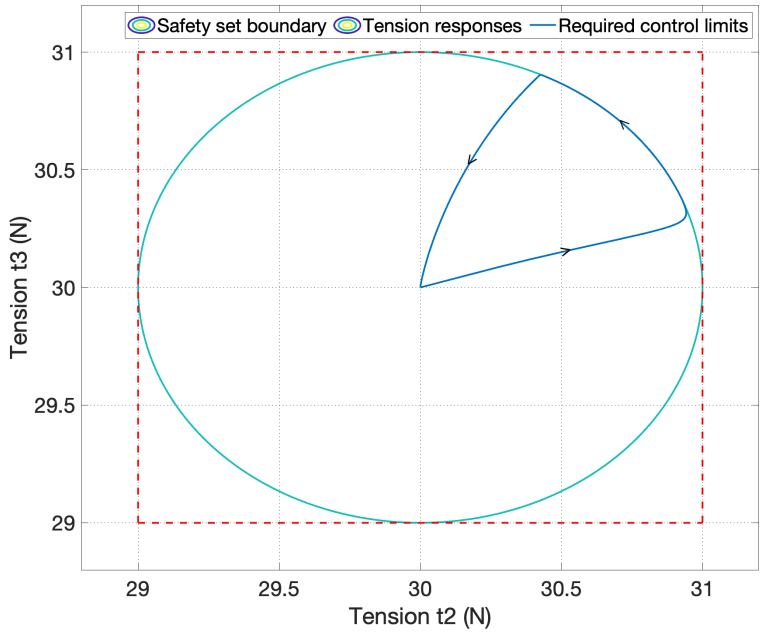

Figure 3.9: Comparison between the required control limits, safety set defined by Eq. (3.25) and the actual system responses.

3.10. It can be observed that different selections of these factors can significantly influence the safety performance of the system. Since $\mathcal{H}(\boldsymbol{X}_t)$ in Eq. (3.25) is evaluated as the sum of safety factors from all state variables, applying the original control limits to x_{min} and x_{max} may not precisely constrain the tension responses within the desired boundaries. However, by assigning a higher weighting factor to t_2, it can be effectively pushed back into the safe region.

Both the current case study and the previous one indicate that operators have two options to enforce strict control limits: 1) Design x_{min} and x_{max} based on worst-case scenarios, as demonstrated in the previous case study; and 2) Assign higher weights to the safety-critical stages of the system, as exemplified in this study. Actually, one can also consider replacing the quadratic design of Eq. (3.25) with higher-order norms. These options provide flexibility for operators to ensure the rigorous enforcement of control limits based on the specific requirements of the system.

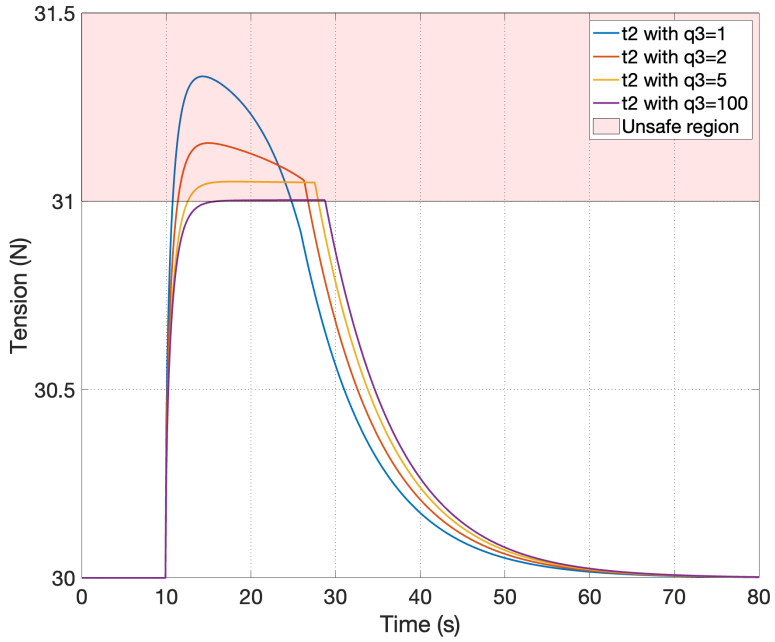

Figure 3.10: Safety performance when different safety weights are chosen.

3.5 Conclusion of the Chapter

In this chapter, we addressed the registration control problem in a R2R printing system, focusing on improving registration accuracy and system safety. We proposed a control synthesis framework that combines a primary controller and a safety controller.

To address the registration control problem, we proposed a control synthesis framework that combines a primary controller and a safety controller. A modified algebraic Riccati equation is designed based on the linearized time delay model of the R2R system. Then a control barrier functional is constructed to ensure the system safety. Simulation results demonstrate the effectiveness of the proposed control approach. We observed that the primary controller successfully eliminated registration errors, while the safety controller constrained tension variations within prescribed limits. The proposed approach can be readily implemented in practical systems without the need for online computation, making it suitable for real-time control applications.

One limitation of the proposed algorithm is the requirement for an accurate registration model, which is challenging to obtain due to the complex behavior of R2R printing systems.

Modeling specific components, such as dancers, adds further difficulty. Efforts should be focused on developing advanced models that accurately characterize the registration dynamics. In addition, incorporating model uncertainty into the controller design would enhance its robustness in the presence of varying operating conditions and disturbances.

Another limitation lies in the convergence rate of the primary controller. As this study provides a proof-of-concept for the proposed registration control framework, the convergence rates of registration errors are not fine-tuned to their optimal level. In real applications, one should consider optimizing the controller's response time to achieve faster convergence.

Future research can explore experimental validation and application of the proposed control approach in industrial-scale R2R printing systems, considering model uncertainties and noise factors. This would provide valuable insights into practical implementation and performance evaluation.

Scholarly Contribution of the Chapter

Zhiyi Chen, Orosz Gabor, and Jun Ni. "Control barrier functionals for safety-critical control of registration accuracy in roll-to-roll printing systems." (manuscript to be submitted to ACC 2024)

CHAPTER 4

Deep Koopman-based Modeling and Control of Quality Propagation in Multistage Roll-to-Roll Systems

In the previous chapters, two control schemes were developed for R2R processes based on the first principle models found in literature. However, for R2R systems used in real production, their operation settings are often too complex for even experienced engineers to fully comprehend. This highlights the need for a universal modeling scheme that can capture the dynamics of R2R processes with minimal understanding of the underlying physics. In this chapter, a deep learning-based modeling method will be presented for analyzing quality propagations in R2R systems. Since R2R systems involve multiple operation stages, they are considered a specific type of multistage manufacturing system (MMS).

Modeling of multistage manufacturing systems has attracted increased attention from both academia and industry in the past decade. We will introduce a novel framework that models the dynamics of generic multistage manufacturing systems. Through two case studies of R2R systems, we will demonstrate how this framework can replace physical or hybrid model approaches that are commonly used in benchmark studies. Furthermore, we will show how this modeling algorithm benefits the design of supervisory controllers to improve the performance of R2R systems.

4.1 Introduction

The control of quality variations is critical for ensuring the consistency of product quality in modern manufacturing industry. Traditional quality control schemes (e.g., statistical process control or SPC) monitor a process using control charts and alert the operators once an anomaly is detected [89, 90]. Such techniques rely on the observations from quality inspections. However, many processes are difficult to monitor directly with full observability. In R2R systems, substrates usually need to be processed in environments with high temperature, low pressure and strong vibration, making it hard to obtain comprehensive quality measurements in real time. Operators usually make inspections only at specific stations, leading to difficulties in quantifying the in-process product quality beyond those stations [91]. Recent advancements in sensing and automation technology have shown that improved data collection and in-situ analytics can enable novel virtual metrology platforms that generate accurate quality predictions [92].

The emergence of quality prediction models can bring substantial enhancement to production systems, including R2R systems. Such models are developed offline using historical data and then used to guide online operations. Engineers can identify defective products based on model predictions and plan corrective actions in response. Moreover, follow-up studies such as root cause analysis and predictive control can be conducted using the model to further improve the production process.

Quality prediction using physics-based models is appealing due to the models' interpretability. As seen in Chapter 3, the retarded ODEs are developed based on R2R dynamics and used to compute registration errors in an online manner. However, accurately modeling the dynamics of most R2R operations that involve fluid-related treatments can be challenging and costly. Simple physics-based models may not capture the complexity of R2R systems, and model inaccuracies due to unknown parameters, uncertain assumptions, and environmental noise can degrade the performance of first-principle models [93]. Similar challenges arise in modeling other high-complexity manufacturing systems. As an alternative, researchers have explored data-driven methods to fill these gaps. For example, Bai *et al.* compared different feature engineering

techniques and used a support vector machine (SVM) to predict quality indices using features extracted from nineteen sensor measurements [94]. However, such conventional machine learning approaches require expert knowledge to conduct feature engineering, rendering them impractical for tasks with high-dimensional and nonintuitive data.

In recent years, variants of deep neural network (DNN) architectures have emerged as effective approximators equipped to deal with complex manufacturing systems with high-dimensional data. Yuan *et al.* proposed an augmented long short-term memory (LSTM) network to learn the quality-relevant hidden dynamics from long-term sequential data [95]. When both time-sequential and time-invariant data were involved, Ren *et al.* combined LSTM with an improved Wide-and-Deep model to capture the key quality information [96]. Li *et al.* further made use of image data and devised a convolutional neural network (CNN) to pre-process and classify the images taken from an additive manufacturing process [97]. A thorough review of DNN for manufacturing applications can be found in [98]. These approaches effectively delegated feature engineering to DNNs and sidestepped the need for human expertise-based feature design. However, a key drawback of DNN models is that they offer poor interpretability. More importantly, these studies are all limited to single-stage processes. Although these schemes can potentially be applied to model a single stage in a R2R system, they will fail to capture interstage correlations.

Most R2R production lines are multistage manufacturing systems (MMSs) that involve multiple stations to fabricate products. Generally, the modeling of MMSs is more challenging than single-stage systems due to confounding interstage couplings. In MMSs, product quality at each stage is a function of the previous steps, the current operation, and stage-specific noise factors. Conventional data-driven methods aggregate information from all stages together to build an end-to-end model that does not reveal the coupling between stages. As a result, the consequential predictions may be overwhelmingly opaque for operators to interpret. In such cases, isolating root causes for a quality disruption can itself become a bottleneck, leading to significant delays in introducing corrections [99]. Therefore, methods that can capture the interstage dynamics while enabling straightforward interpretation are required.

Filz *et al.* suggested that monitoring the state of intermediate products could provide valuable insights into the interstage behavior in MMS [100]. They proposed using clustering methods to categorize different classes of intermediate products. Arif *et al.* combined multiple principal component analysis (PCA) modules with decision trees for binary classification of products [101]. Notably, both approaches do not involve direct prediction of product quality. Liu *et al.* developed an algorithm that learned the prediction model through three steps: Quality embedding, Temporal-interactive learning, and Decoding (QTD) [102]. Zhang *et al.* proposed a path enhanced bidirectional graph attention network (PGAT) to learn the long-distance machine dependencies [103]. Wang *et al.* introduced a multi-task joint learning approach and designed a loss function to automatically learn the importance of different operation stages and quality indices, leading to improved prediction performance [104]. Such approaches were developed to enable quantitative prediction of quality while paying more attention to learn the interaction between stages. However, how to leverage those frameworks for supporting operational decisions remains an open question. In contrast, Bayesian methods in [105] and [106] could describe the uncertainty associated with different operations and aid in diagnosing root causes. Nevertheless, these methods often require prior knowledge of the distributions of process variables, making them less practical in complicated MMSs. Zhao *et al.* combined LSTM and genetic algorithm to enhance quality control for a multistage boring process [107]. Yet, the model cannot provide in-process quality estimations for intermediate products, leading to less flexibility in conducting process improvements.

Stream-of-variation (SoV) analysis is the mainstream methodology widely implemented for modeling MMSs (see [99, 108] for comprehensive reviews). SoV uses state space representations to capture the propagation of quality variations and predict stage-by-stage product quality in MMSs in order to aid variation reduction. However, the use of SoV requires linear dynamics, and therefore these techniques have been mostly limited to machining and assembly processes.

Despite these shortcomings, SoV analysis has demonstrated the benefits of modeling quality propagation; namely, it provides better visibility of a process and greatly helps with

implementing predictive control schemes [109]. Following this idea, Shui *et al.* proposed a hybrid approach that integrated data-driven methods into SoV to model R2R systems [92]. Nevertheless, the proposed hybrid model relied on manual feature selection, which still presented a challenge for large-scale systems. In [110], Jiang *et al.* designed a directed graph to represent the topology of multistage machining processes, then used neural networks (NNs) to encode the quality evolution between different stations. The method involves training multiple distinct NNs, which may lead to cumulative prediction errors. Yan *et al.* designed a multi-task stacked DNN to predict all sensing outputs jointly, and used a two-layer neural network to model the quality propagation between stages [111]. This work explores an interesting direction that uses deep learning techniques to link all variables in a complex MMS. However, the method yields a model with nonlinear transitions between stages, making it difficult to adapt the existing SoV-based algorithms (e.g. process control [109], system design [112] and tolerance allocation [113]) to improve the production system.

The use of SoV modeling offers advantages not only in analyzing the correlation between stages in MMSs, but also in the design of control algorithms that help reduce quality variations. For instance, in [109], an SoV model was constructed for analyzing the flow of dimensional errors in a multistage machining system, followed by the development of a stochastic control law that adjusted flexible tooling elements to compensate for quality variations. Similarly, Djurdjanovic *et al.* considered uncertainties in the knowledge of noise characteristics and designed a robust control method to ensure good product quality under strong process noise, outperforming traditional stochastic process control algorithms [114]. In [115], Abellan-Nebot *et al.* explained how active control for variation reduction in computer numerical controlled (CNC) machining centers could be achieved. Specifically, SoV models assisted in the identification of the source of variations, and then an algorithm that adjusted tool paths could be designed to compensate for dimensional errors. These examples demonstrate that modeling quality propagation in MMSs can lead to improved product quality through active compensation for quality variations. However, conventional SoV-based control algorithms are mostly applied to linear systems. In the later part, we will illustrate how a deep Koopman model can be used to design a feedforward error compensator for nonlinear

MMSs.

In this chapter, we first propose a novel framework for modeling quality propagation in MMSs that possesses three key properties: (1) it can automatically process sensor data, making it scalable for large-scale manufacturing systems; (2) it can handle nonlinear systems; and (3) it offers interpretability through linear latent dynamics modeling, allowing for informed decision-making to improve the MMS. Specifically, the linear dynamics in (3) is enabled by a stochastic deep Koopman (SDK) framework that models the complex behavior of MMSs in a transformed linear latent space and predicts product quality on a per-stage basis. Then based on this Koopman framework, we develop an optimal controller that can dynamically adjust process parameters in response to unexpected changes in nonlinear MMSs to effectively reduce quality variations. When being applied to R2R systems, this optimal controller functions as a supervisory controller that optimizes set points for lower-level controllers that are designed in Chapter 2 and Chapter 3.

An overview of the modeling methodology is illustrated in Figure 4.1. We implement a variational autoencoder (VAE) for each stage to translate process data into a set of quality indicators, serving as a latent expression of the crucial quality information. The evolution of the quality indicators along a production line is then captured by Koopman transition models. The novel combination of VAEs and Koopman operators maps a nonlinear MMS onto a Hilbert space (e.g. the latent space) where the state evolution is approximately linear. The latent model is indeed a new variant of the conventional linear SoV models, while the overall framework can be considered a generalized SoV model that is applicable to nonlinear systems. Therefore, following the approach that designs a feedforward error compensation scheme in [109], a set point optimizer can be designed based on our quality propagation model. However, unlike the compensator in [109], which involves a linear control law, the proposed optimizer presents a nonlinear optimization problem due to the nonlinearity of the MMS.

The main novelties of the work presented in this chapter are as follows.

1. The proposed method stacks all stages of an MMS into a single modeling scheme, enabling a uniform representation of the underlying evolution of product quality.

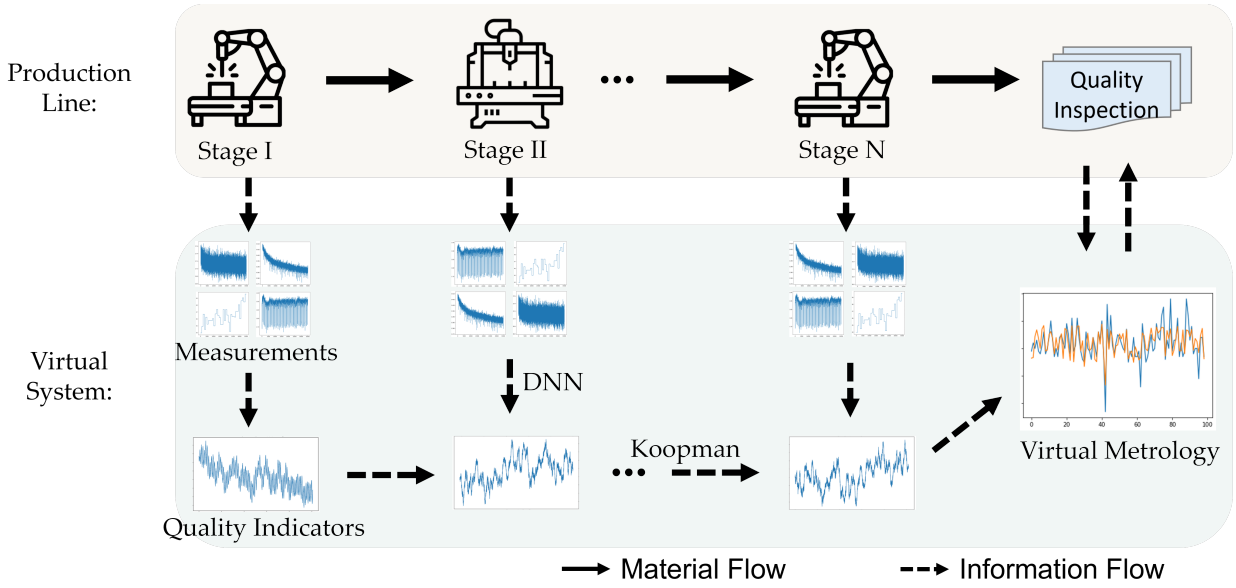

Figure 4.1: Overview of the proposed Deep Koopman framework.

2. To approximate the nonlinear quality evolution in MMSs, we devised Koopman operators to enforce linear propagation of quality indicators in the latent space. This provides better process visibility and interpretability to facilitate locating the root causes of potential quality variations. In contrast to established SoV techniques, our method captures the stream-of-quality [116] in a more generalized way.

3. Building upon the modeling framework, this work designs a nonlinear supervisory control that dynamically adjusts the optimal set point for an MMS once an in-process quality prediction is made.

4. We demonstrate through experimental results that the proposed method is a fast and cost-effective way to model and control multistage R2R systems.

This chapter is organized as follows. Section 4.2 describes the overall problem statement. Section 4.3 then presents preliminary background on the Koopman operator, followed by the overall deep Koopman methodology and the controller design in Section 4.4. The proposed method is then tested on two R2R case studies in Section 4.5. Finally, Section 4.6 provides concluding remarks and future work.

4.2 Problem Statement

We first present the mathematical formulation of the tasks that need to be addressed. In the following sections, it is assumed that minimal physical knowledge is available for the system of interest, without making any assumptions specific to R2R systems.

4.2.1 Part I: Modeling

Consider an archetypal N-stage production line with $N \geqslant 2$. Each stage is denoted by S_k, $k = 1, 2, \ldots, N$, and has m_k machines. Each machine at the k^{th} stage is denoted by $M_{k,i}$, $i = 1, 2, \ldots, m_k$. Let $p_{k,i}$ be the number of process measurements taken from machine $M_{k,i}$, and the total number of process measurements from stage S_k is $p_k = \sum_i p_{k,i}$. The process measurements include material properties, environmental and human factors (which may be considered a shared variable for multiple machines within a stage), and process parameters (which are specific to each machine). We aggregate all process measurements from stage S_k into a single measurement vector of dimension p_k. Then, Each process measurement is denoted by $x_{k,i}$, $i = 1, 2, \ldots, p_k$. Similarly, the quality indices at S_k are denoted by $y_{k,i}$, $i = 1, 2, \ldots, q_k$, where q_k is the total number of quality indices at stage S_k.

The quality prediction task is to find mappings g_k so that

$$\tilde{Y}_k = g_k(X_1, \ldots, X_k), \qquad k \geq 1 \tag{4.1}$$

where $\tilde{Y}_k = [\tilde{y}_{k,1}, \ldots, \tilde{y}_{k,q_k}]^{\mathrm{T}}$ are the estimated quality indices and $X_k = [x_{k,1}, \ldots, x_{k,p_k}]^{\mathrm{T}}$ are the process measurements specific to each product. The structure of Eq. (4.1) indicates that quality Y_k is causally affected by X_1 through X_k. Information that is unavailable to 1^{st} through k^{th} stages should not be brought into the prediction model.

To accomplish this task, a conventional SoV-based model can be constructed as follows:

$$\tilde{Y}_i = A_i \tilde{Y}_{i-1} + B_i X_i, \qquad i = 1, 2, \ldots, k \tag{4.2}$$

$$\tilde{Y}_k = \sum_{i=1}^{k} \left(\Gamma_i X_i \right) \tag{4.3}$$

where A_i, B_i and Γ_i are transformation matrices. Eq. (4.2) indicates that a linearized mapping between Y and X is used to model a generic nonlinear system. When modeling R2R systems using Eq. (4.2), as demonstrated in [12], one needs to design the state variables X_i based on physical knowledge (i.e., including $x_{k,i}^2$ or $x_{k,i}^3$ terms). Therefore, a lack of physical knowledge may lead to a degradation of model performance.

4.2.2 Part II: Supervisory Control

From Equation (4.1), it is seen that the final product quality $\tilde{Y}_N$ is jointly determined by the process settings X_1 through X_N. In the event of a quality disruption, an active control law must determine adjustments ΔX_i for $i \in [1, N]$ so that the adjusted process parameters $X_i = X_{\text{nom},i} + \Delta X_i$, where $X_{\text{nom},i}$ represents the nominal process parameter, will minimize the quality variations. Substituting into Equation (4.1), the control law must ultimately optimize the following objective function:

$$\min_{\Delta X_i} \quad \|\Delta Y_N\|_2^2 = \|Y_{\text{nom},N} - g_N \left(X_{\text{nom},1} + \Delta X_1, \ldots, X_{\text{nom},N} + \Delta X_N \right) \|_2^2 \tag{4.4}$$

where ΔY_N and $Y_{\text{nom},N}$ are the quality variation and the nominal product quality at the final stage, respectively. It should be noted that the control law presented in this chapter aims to adjust process set points directly, rather than through control inputs $\boldsymbol{U}$ as in Chapters 2 and 3. Therefore, it functions as a supervisory controller.

There are mainly two ways to design a supervisory controller: feedback and feedforward. The feedback quality control scheme, as illustrated in Figure 4.2, is more commonly applied in

MMSs. In this scheme, one observes quality variations in y_N and manipulates process variables x_1 and x_2 to avoid variations in future products.

On the other hand, the feedforward quality control scheme, as illustrated in Figure 4.3, utilizes the prediction model to assess the quality variations caused by disturbances in x_1 before an actual disruption is observed. The controller can then plan for adjustments in the following operations at stages S_2 through S_N to compensate for the foreseen variations. This scheme is different from the feedback control scheme in that it uses a prediction model to anticipate potential disturbances before they occur, making it a more proactive approach. This chapter is primarily focused on the design and implementation of a feedforward control scheme.

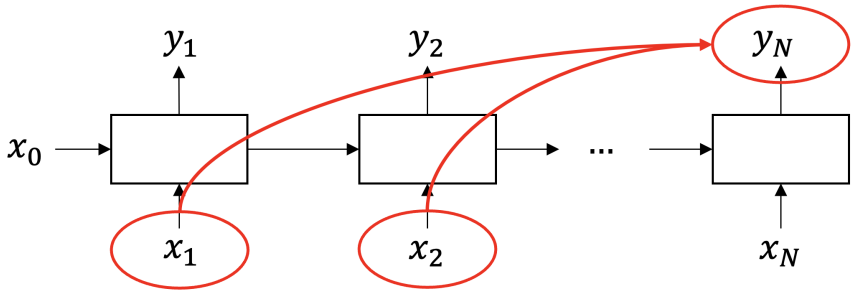

Figure 4.2: Feedback quality control schemes react to quality disruptions after they happened.

4.3 Preliminary: Koopman Operator Theory

The linearization of a nonlinear dynamic system, i.e., $x_{t+1} = F(x_t)$ with $x \in \mathbb{R}^n$

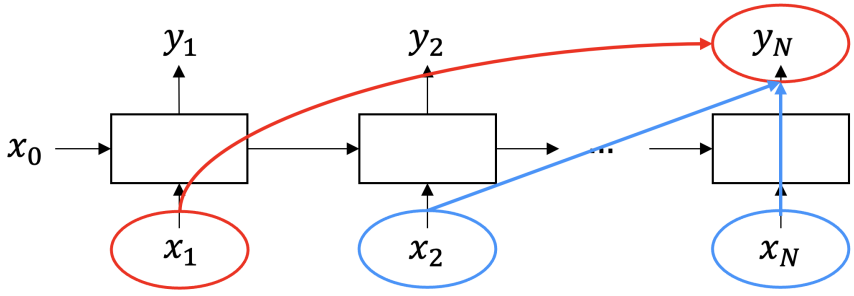

Figure 4.3: Feedforward quality control schemes anticipate quality disruptions and plan for adjustments in advance.

and $t \in \mathbb{N}_0$, is a common practice, but conventional linearized models provide reduced-order approximations with local behavior. In 1931, B.O. Koopman proposed an alternative, global linearization method that maps the original state of a nonlinear system onto an infinite dimensional Hilbert space via possible measurements $\gamma(x_t)$ [117]. The Koopman operator $\mathcal{K}$ then linearly advances the system dynamics in the invariant subspace as

$$\gamma(x_{t+1}) = \gamma \circ F(x_t) = \mathcal{K}\gamma(x_t). \tag{4.5}$$

In practice, a finite-dimensional approximation of the infinite-dimensional $\mathcal{K}$ is sought, for example, by numerical methods such as the dynamic mode decomposition (DMD) and extended DMD [118, 119]. Recently, Lusch *et al.* used autoencoders (AEs) to identify the Koopman eigenfunctions and achieved high accuracy in predicting the behavior of nonlinear fluid flow [120]. The eigenfunctions $\phi(x)$ are designed deliberately, satisfying:

$$\phi(x_{t+1}) = \mathcal{K}(\lambda)\phi(x_t) = \lambda\phi(x_t) \tag{4.6}$$

where λ represents the corresponding eigenvalues. From this eigenspace, $\mathcal{K}$ can be approximated by a block-diagonal Koopman matrix. Balakrishnan *et al.* further improved the performance of the deep Koopman model by integrating it with a generative adversarial network and enforcing a stochastic latent embedding [121]. While most existing works utilize Koopman models to predict the evolution of time series systems, we will instead use Koopman operators to propagate quality characteristics over stages in an MMS.

4.4 Proposed Method

We will first present the proposed deep Koopman framework for MMSs through a base model that uses a deterministic expression of the quality indicators in the latent space. Then, an augmentation that enforces a stochastic expression in the latent space will be introduced. We will

demonstrate through a case study that the stochastic model outperforms the deterministic model due to its robust capability in handling noise.

Figure 4.4 illustrates the base model of the proposed framework, consisting of three modules for each stage: the encoding module, the Koopman transition module, and the prediction module. At the k^{th} stage, the model takes process measurements X_k as the inputs, and the encoding model extracts the temporal quality indicators. Combining with the quality information propagated by a Koopman transition model $\mathcal{K}_{k-1}$ from the upstream stage, the latent quality indicators H_k are computed. A multilayer perceptron (MLP) network is designed to serve as the prediction model that predicts the quality indices using the quality indicators. Note that the quality propagation starts from S_1 and terminates at S_N.

In contrast to Eq. (4.2), the proposed method brings two benefits: 1) quality propagation is modeled using critical parameters instead of raw process data; and 2) a linear embedding is captured for a nonlinear system instead of applying simple linearization.

4.4.1 Encoding Module by AE

In general, the evolution of quality information in MMSs is nonlinear. We intend to find a suitable invariant subspace where this nonlinear propagation can be approximated well by a linear embedding. Based on Koopman's theory, the linear approximation should converge to the original propagation system as we increase the dimension of the linearly embedded space. This contrasts significantly with standard feature engineering techniques present in machine learning, which typically aim to reduce dimensionality with techniques such as principal component analysis (PCA). We note that the selection of this subspace is not unique. Since AE allows one to construct flexible mappings from X_k, we use it to identify the best invariant subspace where quality indicators simultaneously serve as the eigenfunctions in Eq. (4.6).

The encoding module for the k^{th} stage takes process measurements as inputs and returns

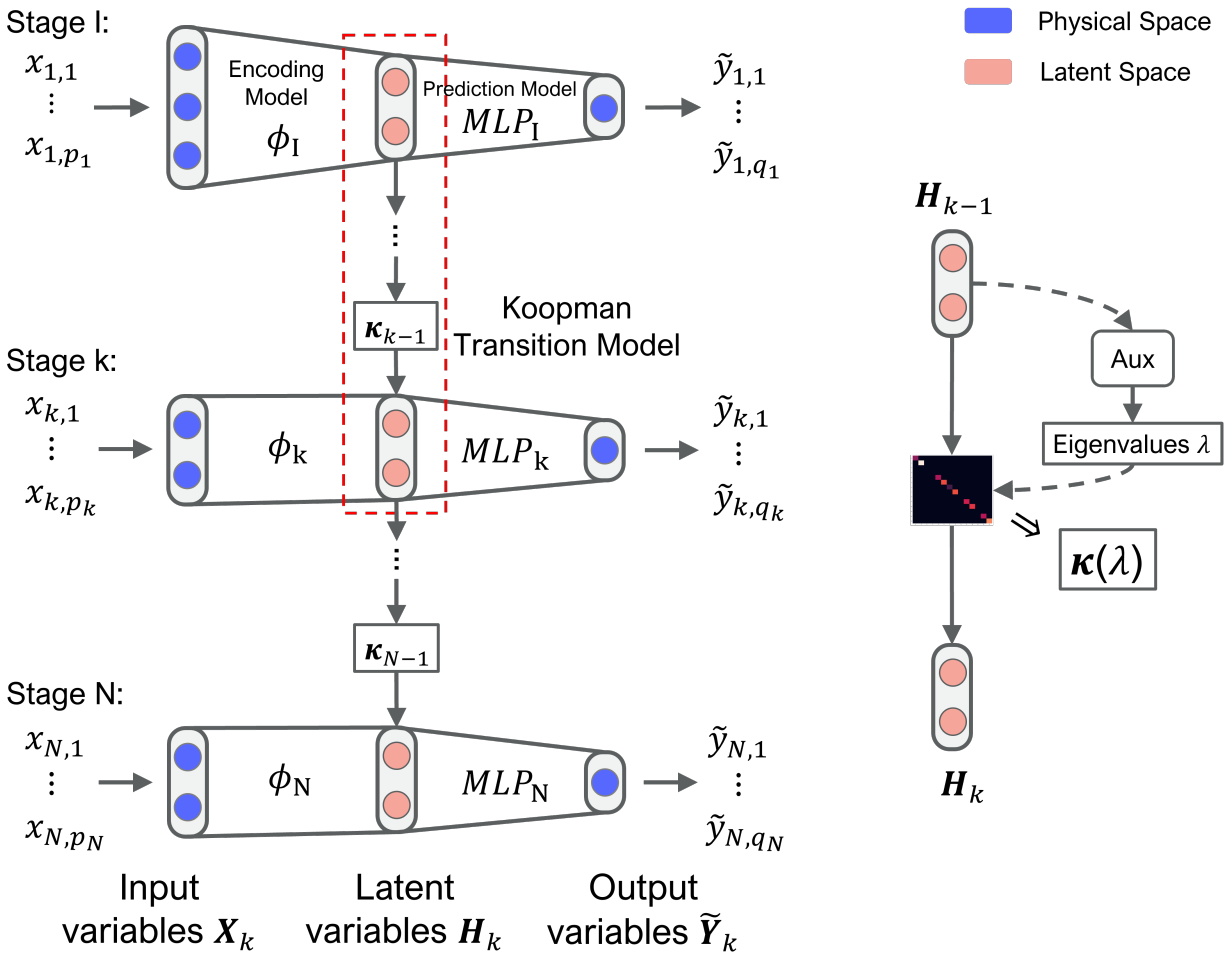

Figure 4.4: In the base framework, the quality indicators are propagated in a deterministic latent space. The Koopman transition models are constructed from eigenvalues that are parameterized by auxiliary networks.

the temporal quality indicators, as given by:

$$\hat{H}_k = \phi_k(X_k) \tag{4.7}$$

where $\hat{H}_k \in \mathbb{R}^{d_{h,k}}$ and $d_{h,k}$ indicates the dimension. Normally, the AE consists of an encoder ϕ_k and a decoder ψ_k. In [120], the authors used the encoder to derive the latent variables and the decoder to map from the latent space to reconstruct the original state space inversely. Therefore, it follows

$$\tilde{X}_k = \psi_k \circ \phi_k(X_k) \tag{4.8}$$

where $\tilde{X}_k$ are the reconstructed states. However, only the encoder plays a functional part in our framework following Eq. (4.7). The decoder ($\psi_k : H_k \rightarrow X_k$) is used for computing a regularization term, called reconstruction loss, to train ϕ_k:

$$\mathcal{L}_{recon,k} = \frac{1}{n}\sum_{i=1}^{n} \|(X_k - \tilde{X}_k)_i\|_2^2 \tag{4.9}$$

where n is the total number of data points. Note that ψ_k is omitted in Figure 4.4.

4.4.2 Koopman Transition Module

In MMSs, the product quality at stage S_k is determined by the local process characteristics and the quality inherited from stage S_{k-1}. Therefore, the general expression of the quality indicators follows

$$H_k = f_k(X_k, H_{k-1}) \tag{4.10}$$

where $H_k \in \mathbb{R}^{d_{h,k}}$, f_k combines an encoding model and a propagation model. This recursive expression indicates that H_k summarizes all the process measurements prior to S_k. Our goal here is to identify the universal linear embedding for a nonlinear system and clearly observe the quality propagation in the latent space. Therefore, we seek Koopman operators that induce the linear aggregation of quality indicators following:

$$H_k = \hat{H}_k + \mathcal{K}_{k-1} H_{k-1} \tag{4.11}$$

In practice, $\mathcal{K}_{k-1}$ can be approximated by a Koopman matrix $\mathbf{K}_{k-1}$. There are several ways to set up the Koopman matrix, including dense matrices [121], or Jordan blocks [120], etc. In the view of Eq. (4.6), we choose to use a diagonal Koopman matrix that consists of the eigenvalues corresponding to the Koopman eigenfunctions identified by AEs. $\mathbf{K}_{k-1}$ constrains a decoupled propagation between the quality indicators from adjacent stages. The method of constructing the matrix is inspired by [120], as shown in Figure 4.4. An auxiliary network is used to parameterize

the eigenvalues λ. The eigenvalues are then aggregated and reshaped to form the diagonal Koopman matrix. It follows $\mathbf{K}_{k-1} = diag(\lambda) \in \mathbb{R}^{d_{h,k-1} \times d_{h,k}}$.

Unlike conventional Koopman approaches where $\mathbf{K}_{k-1}$ is a static matrix, $\mathbf{K}_{k-1}$ is allowed to vary according to different X_k and H_k in our design. The advantage of this design is: (1) the quality indicators are decoupled from each other, which provides a clear view of the quality evolution; and (2) it allows input-dependent quality propagation, in contrast to the static propagation model in [111], meaning the proposed method can adapt to a wide range of operating conditions without sacrificing accuracy. Even though the input-dependent $\mathbf{K}_{k-1}$ yields only a piecewise (not globally) linear latent system, it allows one to account for nonlinear systems with continuous spectrum using a low-dimension network [120].

4.4.3 Prediction Module

After sequential propagations, a two-layer MLP network is used to predict the quality indices Y_k using H_k. To this end, we have introduced all the essential modules to predict the quality indices as in Eq. (4.1). For the deterministic model, it follows:

$$\tilde{Y_k} = MLP_k(H_k) \tag{4.12}$$

where H_k is updated following a linear transition rule as defined in (4.11). Substituting (4.11) into (4.12) yields:

$$\tilde{Y_k} = MLP_k\left(\sum_{i=1}^{k}\left(\Big(\prod_{j=i}^{k}\mathbf{K}_j\Big)\phi_i(X_i)\right)\right) \tag{4.13}$$

where $\mathbf{K}_k = I$ for the current stage S_k. The expression between $\tilde{Y_k}$ and X_k represents a nonlinear system. However, the cumulative product of $\mathbf{K}_k$ in (4.13) yields a linear system in the latent space. Our method first selects the most valuable parameters to find the Koopman embedding, which is then combined with MLP to capture the nonlinearity in a linear manner. Pseudocode of the prediction process can be found as follows.

Algorithm 2 Prediction of quality indices.

Require: Process data $X_1, \ldots, X_N$, Quality data $Y_1, \ldots, Y_N$

while $k < N$ **do**
  Compute local latent variable $\hat{H}_k = \phi_k(X_k)$
  if $k = 1$ **then**
    Compute $H_k = \hat{H}_k$
  else
    Compute cumulated latent variable $H_k = \hat{H}_k + K_{k-1}H_{k-1}$
  end if
  Predict $\tilde{Y}_k = MLP_k(H_k)$
  Compare $\tilde{Y}_k$ with Y_k when desired
end while

4.4.4 Two-step Training and Loss Functions

Many traditional machine learning algorithms require feature engineering before building prediction models, whereas deep learning models enable combining these two tasks together. In [102, 103], process data are converted into a unified feature space using feedforward neural networks. However, training a DNN with a complicated structure can be unstable. For example, the diffusion of gradients may happen when backpropagating errors to early stages of an MMS. In practice, we propose a two-step training for our framework. This can be useful when global optimality is difficult to obtain.

1. *Step 1 (pre-training)*: This step requires the encoding module and prediction module to be trained separately. An AE is trained for each stage to minimize (4.9), allowing for unsupervised feature learning. This will guide the encoder modules to find optimal local latent embeddings that best reconstruct the original data. Then, starting from stage 1, the Koopman transition modules are trained together with their consequent prediction modules. These modules can be trained jointly, with the temporal quality indicators and the propagated quality indicators being inputs, and the ground truth quality measurements being outputs. Figure 4.5 shows the training process at stage II. The loss function follows:

$$\mathcal{L}_{pred,k} = \frac{1}{n}\sum_{i=1}^{n} \|(Y_k - \tilde{Y}_k)_i\|_2^2 \tag{4.14}$$

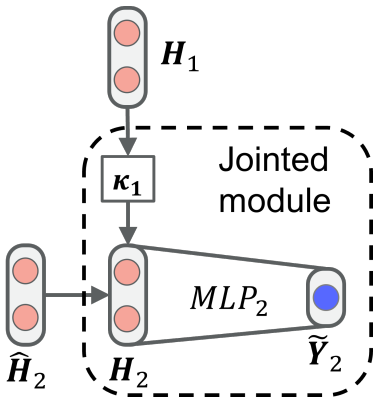

Figure 4.5: Pre-training of the prediction module at stage II.

The performance of the pre-trained model is usually limited because it cannot guarantee that the extracted quality indicators are universally optimized for all stages. Therefore, a fine-tuning step is required.

2. *Step 2 (fine-tuning)*: All modules are connected to form a complete network model. The loss function consists of the penalty for prediction errors and other regularization terms. The proposed deep Koopman model must enable quality predictions not only at the final stages, but also at the intermediate stages, and likewise for reconstructing raw data from latent variables. Therefore, we define the full loss function as:

$$\mathcal{L}_{total} = \sum_{i=1}^{N} \left(\rho_i \mathcal{L}_{pred,i} + \theta_i \mathcal{L}_{recon,i} \right) \tag{4.15}$$

where ρ_i and θ_i define the significance of the prediction and reconstruction at each stage. While minimizing $\mathcal{L}_{pred,i}$ is our primary goal, the reconstruction error serves as a regularization term that helps mitigate overfitting.

4.4.5 Stochastic Deep Koopman Model (SDK)

In manufacturing systems, the same operation setting usually leads to varying product quality due to various sources of process noise. With such considerations, the base model may not capture the random deviations present in realistic processes. We propose an augmentation that

improves the performance of the model to deal with uncertainties. In this stochastic approach, we replace the AE with VAE and model the quality indicators as Gaussian variables. The updated framework is shown in Figure 4.6. In the stochastic framework, the encoding module first encodes the state into latent variables $\hat{H}_k$ as in Section 4.4.1. Then, we learn the Gaussian distribution of $\hat{H}_k$ using two single-layer networks, which gives:

$$P(\hat{H}_k \mid X_k) \sim \mathcal{N}(\hat{\mu}_k(X_k), \hat{\sigma}_k^2(X_k)) \tag{4.16}$$

where $\hat{\mu}_k$ is the vector of temporal mean values and $\hat{\sigma}_k$ is the vector of temporal variance. One can refer to [122] for implementation details of VAE.

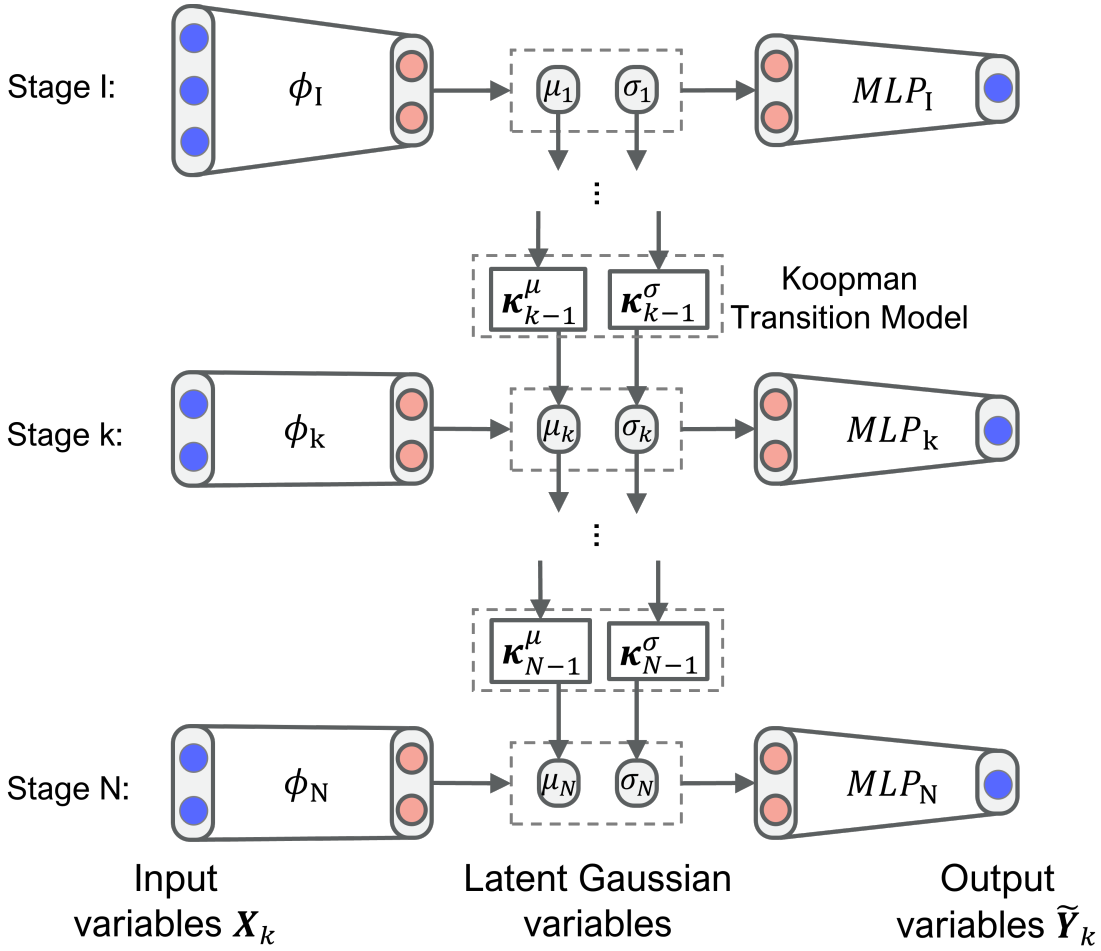

Figure 4.6: In the stochastic framework, quality indicators are modeled as Gaussian variables.

Following Eq. (4.11), one can derive a similar expression of the transition of the Gaussian variables. If $P(\hat{H}_k) \sim \mathcal{N}(\hat{\mu}_k, \hat{\sigma}_k^2)$ and $P(H_{k-1}) \sim \mathcal{N}(\mu_{k-1}, \sigma_{k-1}^2)$ are independent distributions, then $P(H_k) \sim \mathcal{N}(\mu_k, \sigma_k^2) = \mathcal{N}(\hat{\mu}_k + \mathcal{K}_{k-1}\mu_{k-1}, \hat{\sigma}_k^2 + \mathcal{K}_{k-1}\sigma_{k-1}^2)$. However, the distributional dependency is often unclear. Once again, we use Koopman operators to approximate the transition of $P(H_k)$. The propagation of the Gaussian variables is given by [121]:

$$\mu_k = \hat{\mu}_k + \mathcal{K}_{k-1}^{\mu}\mu_{k-1} \tag{4.17}$$

$$\ln \sigma_k = \ln \hat{\sigma}_k + \mathcal{K}_{k-1}^{\sigma} \ln \sigma_{k-1} \tag{4.18}$$

For the case where VAE is applied, the design of Koopman matrices is similar, except that two distinguished auxiliary networks need to be introduced. Outputs from the two networks are used to construct $\mathbf{K}_{k-1}^{\mu}, \mathbf{K}_{k-1}^{\sigma} \in \mathbb{R}^{d_{h,k-1} \times d_{h,k}}$, correspondingly. Once the distribution of the Gaussian variable is obtained, one can use the reparameterization trick to reconstruct exact local quality indicators. That is, generate a random variable $\epsilon \sim \mathcal{N}(0, 1)$ to sample $H_k = \mu_k + \epsilon\sigma_k$.

When pre-training the stochastic model, the reconstruction loss will follow the same expression in Eq. (4.9). However, another regularization term needs to be introduced in the training phase to enforce the Gaussian distribution in the latent space:

$$\mathcal{L}_{KLD,k} = D_{KL}\left(P(\hat{H}_k \mid X_k) \| \mathcal{N}(0, I)\right) \tag{4.19}$$

where D_{KL} is the Kullback-Leibler divergence and $\mathcal{N}(0, I)$ is the standard normal distribution. To fine-tune the model, the complete loss function becomes:

$$\mathcal{L}_{total} = \sum_{i=1}^{N} \left(\rho_i \mathcal{L}_{pred,i} + \theta_i \big(\mathcal{L}_{recon,i} + \omega_i \mathcal{L}_{KLD,i} \big) \right) \tag{4.20}$$

where ω_i is the weight of $\mathcal{L}_{KLD,i}$.

4.4.6 Supervisory Control for Set Point Optimization

Without loss of generality, we assume that a product has already undergone processing operations from 1 to k, and the goal of designing a supervisory controller is to optimize the downstream settings in operations $k+1$ to N to minimize variation in product quality.

Given that a deep Koopman model (either the base model or SDK) has been constructed, the following equations (from previous sections) can be used to predict product quality in MMSs:

$$\begin{aligned} H_0 &= \phi_0(X_0) && \text{(Initialization)} \\ H_k &= f_k(H_{k-1}, X_k) && \text{(Propagation)} \\ Y_k &= \psi_k(H_k) && \text{(Prediction)} \end{aligned}$$

Assume we need to compensate for a process fluctuation δX_k, where its impact on the local product quality can be characterized as:

$$\begin{aligned} H_k &= f_k(H_{k-1}, X_{\text{nom},k} + \delta X_k) \\ \Delta Y_k &= \psi_k(H_k) - \psi_k(H_{\text{nom},k}) \end{aligned} \tag{4.21}$$

where $H_{\text{nom},k}$ is the quality indicator under the nominal operation. Given the information up to stage S_k, the impact of δX_k on the final product quality is predicted to be:

$$\begin{aligned} H_{k\to N} &= f_k \circ f_{k+1} \circ \ldots \circ f_N(H_{k-1}, X_k + \delta X_k, X_{\text{nom},k+1}, \ldots, X_{\text{nom},N}) \\ \Delta Y_N &= \psi_N(H_{k\to N}) - \psi_N(H_{\text{nom},N}) \end{aligned} \tag{4.22}$$

Note Eq. (4.22) is based on the assumption that the downstream operations beyond S_k will still follow the nominal settings. Also, Eq. (4.22) can be evaluated recursively at each stage, allowing for the consideration of multiple disturbances being introduced to the final product quality. To compensate for the quality variation caused by δX_k, one needs to seek for a control sequence $\boldsymbol{\Delta}_X = [\Delta X_{k+1}, \ldots, \Delta X_N]$ to adjust the downstream set points. A feedforward control sequence

could be obtained by solving the following optimization problem:

$$\begin{aligned}
\min_{\Delta X_{k+1},\ldots,\Delta X_N} \quad & (\Delta Y_N)^{\mathrm{T}} Q \Delta Y_N + \boldsymbol{\Delta}_X^{\mathrm{T}} R \boldsymbol{\Delta}_X \\
\text{subject to} \quad & H_{k\to N} = f_k \circ \ldots \circ f_N(H_{k-1}, X_k + \delta X_k, X_{\text{nom},k+1} + \Delta X_{k+1}, \ldots, X_{\text{nom},N} + \Delta X_N) \\
& \Delta Y_N = \psi_N(H_{k\to N}) - \psi_N(H_{\text{nom},N}) \\
& \Delta X_i \in \mathcal{X}_i
\end{aligned} \tag{4.23}$$

Here, Q and R are positive semi-definite weighting matrices, and $\mathcal{X}_i$ defines the admissible adjustments for the set points at each stage. Due to the nonlinearity in the NN modules, (4.23) presents a nonlinear programming problem, which can be solved by using interior point methods (such as IPOPT [123]) or sequential quadratic programming.

Formulation (4.23) builds upon the same idea as presented in [124, 125]. However, the proposed feedforward control strategy is extended to nonlinear MMSs using the deep Koopman models. One can also observe that this formulation can be viewed as an MPC problem, albeit with a different focus. Instead of using models to propagate states over time, our formulation uses the deep Koopman model to propagate quality information across stages in MMSs. When implementing the algorithm in real production, the optimization problem needs to be solved recursively as the product reaches each new stage. This is necessary to refine the adjustments based on the new process and quality information obtained at each stage. After the optimization problem is solved, the adjustments are communicated to the process-level controllers, which will then accommodate the changes. For example, if a change in tension reference is commanded in a R2R process, the tension controller should be activated to follow the new set point.

4.5 Case Study

In this section, two case studies will be presented to illustrate the effectiveness of the proposed methods. The first case study involves validating the Deep Koopman modeling

algorithms using a dataset obtained from a real R2R production line. The second case study focuses on validating the control algorithms through a simulation study.

4.5.1 Validation of the Koopman Models

The dataset used in this case study was initially introduced in [92] and is derived from a web handling process in an actual R2R manufacturing system. To ensure confidentiality, all results have been normalized. The configuration of the process is depicted in Figure 4.7.

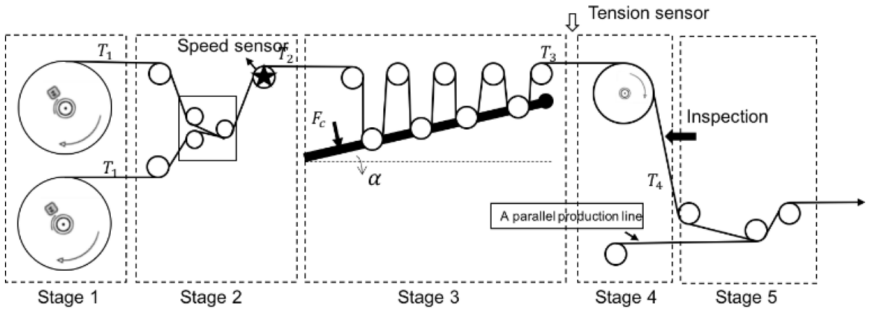

Figure 4.7: Layout of the R2R testbed.

The R2R system under consideration is composed of five distinct stages: 1) unwinding, 2) splicing, 3) dancer, 4) driven roller, and 5) registration. The process involves releasing the substrate from the unwind section, performing various intermediate processes, and ultimately stacking the substrate into a multi-layer product at stage 5. Maintaining good product quality requires monitoring the pitch length of each substrate span at stage 5. A closed-loop control system utilizes this monitoring data to regulate substrate tension and roller speeds, ensuring consistent pitch lengths across all product spans. To facilitate proactive control actions, it is desirable to establish a model for predicting the pitch length of each substrate.

In this particular testbed, a tension sensor is installed at the end of stage 2 to monitor intermediate process characteristics, while a 2D vision system is positioned between stages 4 and 5 to capture pitch length information. From a modeling perspective, the measurements obtained from these two sensors serve as quality metrics. Consequently, our modeling task involves using process measurements to predict the intermediate tension value and the final pitch length value (labels).

Specifically, 16 sensor measurements are collected from stages 1 and 2 for tension prediction, and an additional 11 sensor measurements are gathered from stages 3 and 4 for pitch length prediction. It is worth noting that, in order to train the Koopman model, stages 1 and 2 from the original production line are considered stage I, while stages 3 and 4 are considered stage II. This distinction helps in modeling the dynamics of the R2R system more effectively.

4.5.1.1 Implementation Details

The dataset used in this study consists of data collected from 7 trials of operations. To prepare the sensor signals for modeling, a wavelet filter is applied to remove noise from the signals. The dataset is then divided into a training set (comprising 4 trials) and a testing set (comprising 3 trials). The training set is randomly shuffled, and 10% of the shuffled data is separated as a validation set for monitoring the model's performance during training. The architecture of the stochastic Koopman model is selected based on its performance on the validation set. In this implementation, all stages share the same latent size, denoted as $d_{h,1} = d_{h,2} = 40$. This choice is reasonable because a sufficiently large latent space is created, and each operation stage only affects a subset of the latent variables. Several hyper-parameters are defined for the training process. The batch size is set to 200, and the learning rate is set to 10^{-3} for the pre-training phase and 5×10^{-4} for the fine-tuning phase. Constant weights are assigned as $\theta_1 = \theta_2 = 0.01$, $\omega_1 = \omega_2 = 5 \times 10^{-5}$, and $\rho_1 = 1$ and $\rho_2 = 10$. The algorithm is implemented using the Pytorch library, and the stochastic gradient descent (SGD) optimizer is employed to train the model.

4.5.1.2 Performance Evaluation

We demonstrate the performance of the proposed deep Koopman model through a comparison study between different regression models. The algorithms implemented in this study include:

1. A hybrid approach from [92] that combines a physical model and a censored regression model. It serves as a reference for all other data-driven algorithms.

2. ANN refers to the fully connected feedforward neural network. A two-layer ANN is implemented with 64 hidden units. The rectified linear unit (ReLU) activation function is chosen for the intermediate layer.

3. Random forest (RF) is an ensemble of decision trees widely used in data challenges. To avoid overfitting, the RF hyperparameters are set to be: number of estimators $= 30$, maximum depth $= 10$, minimum samples at a leaf (fractional) $= 0.01$.

4. Static AE-Koopman (S-AEK) refers to the proposed base model, whose transition models are static dense Koopman matrices.

5. Stochastic Deep Koopman (SDK) is the augmented Koopman model that is introduced in Section 4.4.5

Root mean squared errors (RMSE) on labels (Ys) are used to evaluate the prediction performance of the above algorithms. During the experiments, ANN and RF use individual models to predict the quality measures from different stages, whereas the others can obtain predictions under a unified framework. The prediction errors on the testing set are shown in Table 4.1. The experiments are repeated 10 times with different random seeds to obtain reproducible results. In addition, visualizations of the prediction results are shown in Figures 4.8 to 4.11.

The physics-based method (the first row in Table 4.1, as reported in [92]) achieves the lowest prediction error for both stages, which aligns with our expectations as it is derived from high-fidelity models from the literature. The proposed Stochastic Deep Koopman (SDK) algorithm performs the best among the data-driven algorithms, reaching a similar level of accuracy in predicting tension compared to the physics-based method. However, it performs less effectively in predicting pitch lengths.

Figure 4.8 demonstrates that the S-AEK algorithm captures the general trend of tension variations, while Figure 4.9 shows that the SDK algorithm has a different prediction pattern. Due to its embedded stochasticity, the predictions from SDK are distributed between the upper and lower

Table 4.1: Comparison of Prediction Errors

Model	**Tension RMSE**	**Pitch Length RMSE**
Hybrid [92]	0.2214	0.0102
ANN	0.2392 ± 0.0044	0.0251 ± 0.0021
RF	0.2814 ± 0.0052	0.0240 ± 0.0002
S-AEK	0.2454 ± 0.0149	0.0228 ± 0.0023
SDK	$\mathbf{0.2254 \pm 0.0101}$	$\mathbf{0.0192 \pm 0.0016}$

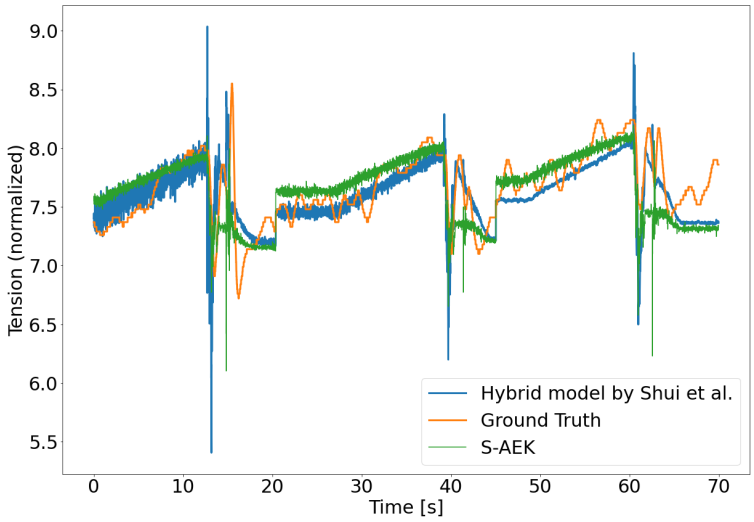

Figure 4.8: The base Koopman model reaches a comparable prediction accuracy compared to the hybrid approach.

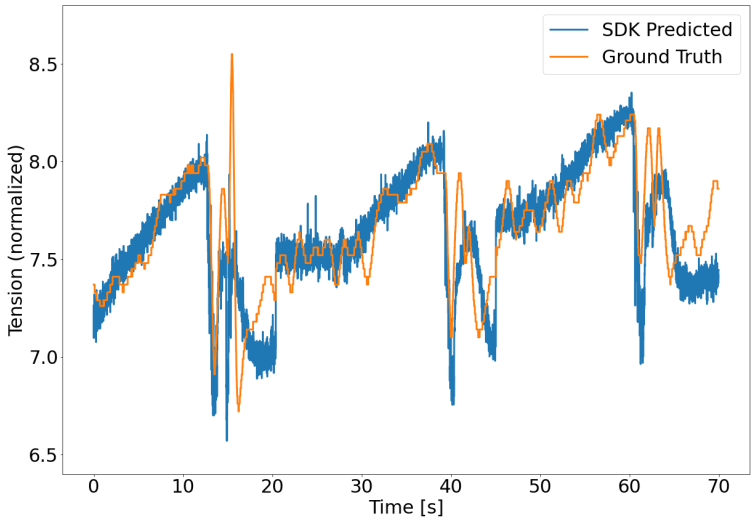

Figure 4.9: Stochasticity improves the robustness of the prediction.

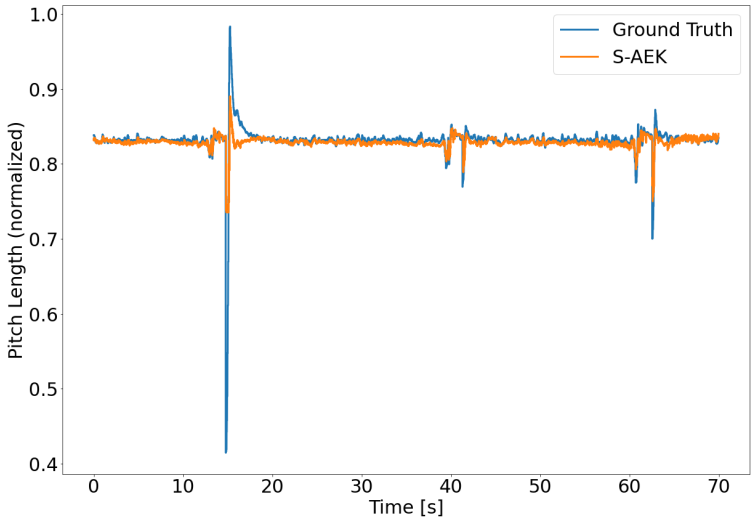

Figure 4.10: Prediction of pitch length reaches a fairly high accuracy.

envelope curves that surround the actual tension measurements, covering a significant portion of the tension measurements.

From Figures 4.10 and 4.11, it can be observed that the proposed Koopman algorithm produces reasonably accurate pitch length predictions. However, it is important to note that the data-driven algorithms do not surpass the performance of the physics-based method. This can be attributed to the fact that pitch length is influenced by a small subset of features from the dataset, making it challenging to conduct effective feature engineering without access to physical information. Specifically, two phenomena are worth noting:

1. In Figure 4.10, the data-driven model exhibits lower accuracy in predicting quality variations when significant impulse-like disturbances occur. Note that the significant quality variation in Figure 4.10 is caused by the splicing process, where the material roll is cut and connected to a redundant roll before it is completely used up.

2. In Figure 4.11, a trending offset can be noticed between the ground truth and the model prediction. It is deduced that the time-varying dynamics of the R2R process caused this inaccurate prediction.

These limitations can be effectively addressed by the physics-based model, as it accurately captures

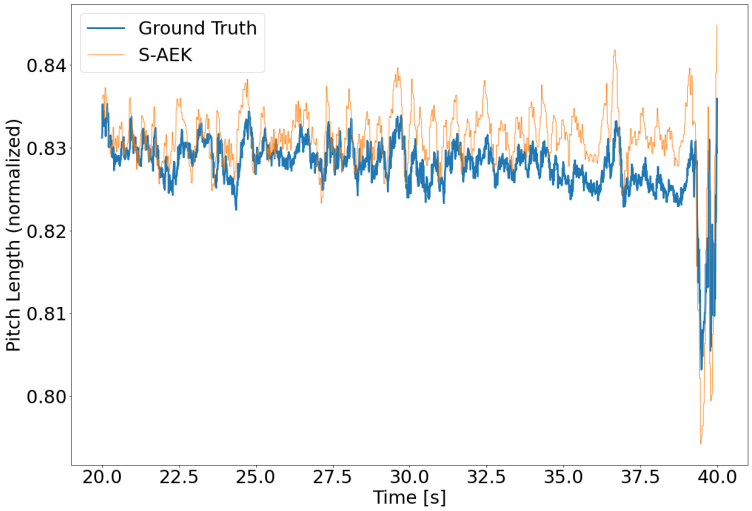

Figure 4.11: Drifting in the pitch length prediction.

the system dynamics in this simplified scenario. Therefore, one future direction is to explore the integration of physical knowledge, if available, into the deep Koopman model. Despite the limitations, the proposed SDK algorithm demonstrates promising results in predicting tension and performs reasonably well in predicting pitch lengths compared to the other data-driven algorithms.

4.5.1.3 Analysis in the Latent Space

Operators can perform analytics directly on the latent variables instead of the raw data to understand how quality evolves as the products are transmitted along the production line.

It is critical to decide the latent space dimension. Unlike many other DNN models where autoencoders are used to learn a compact subset of features, the Koopman-based architectures usually require autoencoders to lift the dimension of features so that the linear approximation can be well enforced. However, setting excessively large latent sizes can cause the model to encounter problems such as high computational expense and vanishing gradients. In our work, the latent space dimension is decided to be $d_{h,k} = 40$ for all stages according to the stage II RMSE on the validation set using the base model, as shown in Figure 4.12. In this test, the SDK model uses the same dimension for the latent variables.

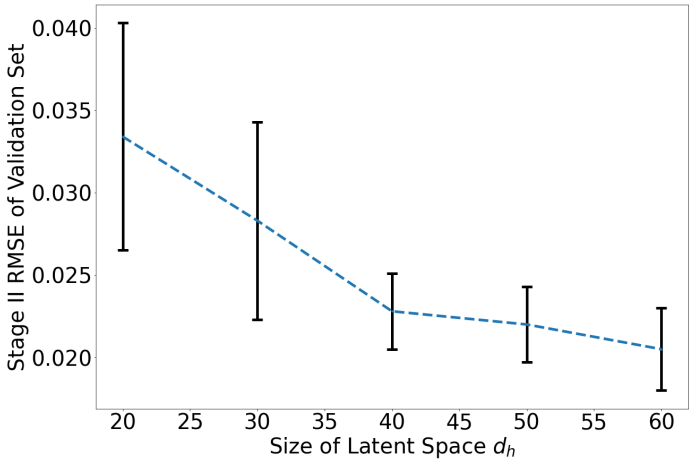

Figure 4.12: The latent size is decided to be 40 using the elbow method.

Once an SDK (or the base models) is trained, the Koopman transition matrices provide direct visualization of how the critical quality indicators are propagated to the downstream stations, as shown in Figure 4.13. The matrices are normalized so that the diagonal terms are scaled within $[0, 1]$. It can be observed that $\mathcal{K}_1^{\mu}$ and $\mathcal{K}_1^{\sigma}$ have 17 and 18 non-zero eigenvalues, respectively. The sparsity indicates that only a subset of the quality indicators from stage I significantly impact the quality at stage II under the nominal operating condition. The rest of the quality indicators will not significantly influence the operation at stage II, but they are critical for performing local quality predictions at stage I. The simple structure of the devised Koopman matrices allows for streamlined process monitoring. For example, operators can quickly locate the root causes by backtracking through the latent space when unexpected quality disruptions occur. We highlight this additional interpretability to be an important advantage of our approach over the other benchmarks. In the next case study, we will further demonstrate that the linear propagation in the latent space can also be applied to R2R systems involving more than two stages. This will showcase the scalability and effectiveness of the proposed approach in capturing the dynamics of complex multistage R2R systems.

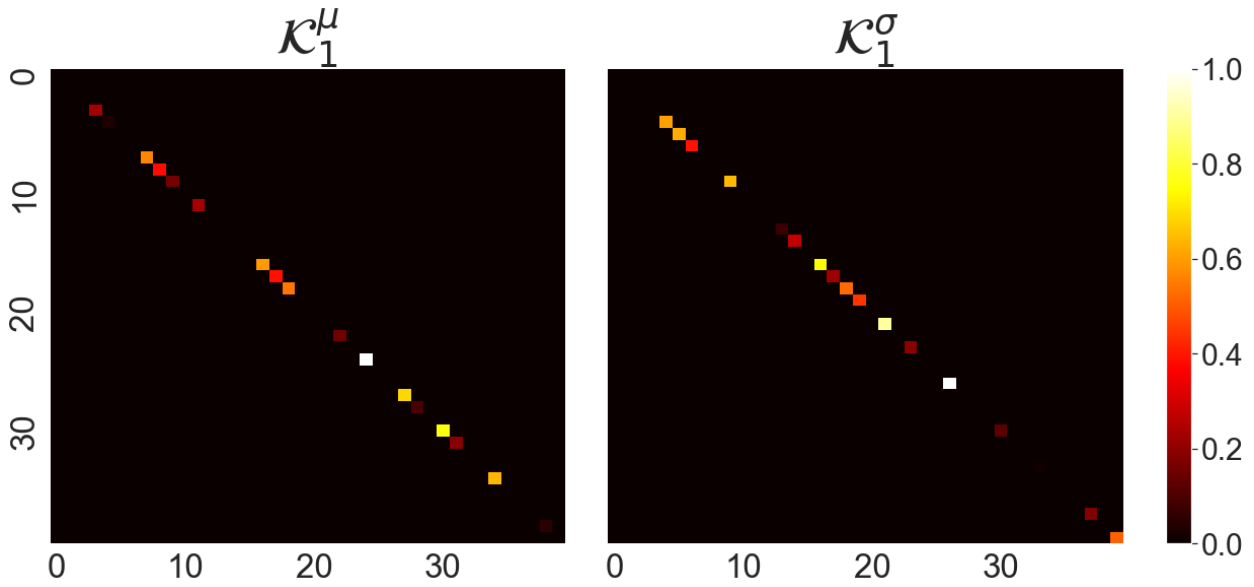

Figure 4.13: The layout of the Koopman transition matrices under the nominal operating condition.

The proposed approach has an inseparable connection with SoV methods. By constructing propagation models, we both attempt to represent product quality indices in terms of process measurements from all prior stages. However, our method resolves some key challenges under the SoV framework while preserving its per-stage structure. In SoV, it is usually assumed that there is prior knowledge of the key process characteristics and propagation mechanisms, which is not always the case. Without the availability of physical information, it can be challenging for engineers to define the key process and quality characteristics, which are necessary for the conventional SoV analysis. In contrast, our method efficiently learns the key quality indicators and Koopman matrices from data. The latent, decoupled transition model in SDK is precisely a variant of SoV. Therefore, SoV-based methods can potentially be adapted to our framework.

4.5.2 Validation of the Supervisory Control

A simulation study is conducted on a five-roller R2R process to validate the performance of the proposed supervisory controller. The system consists of three processing stages, each equipped with a heating chamber, as illustrated in Figure 4.14.

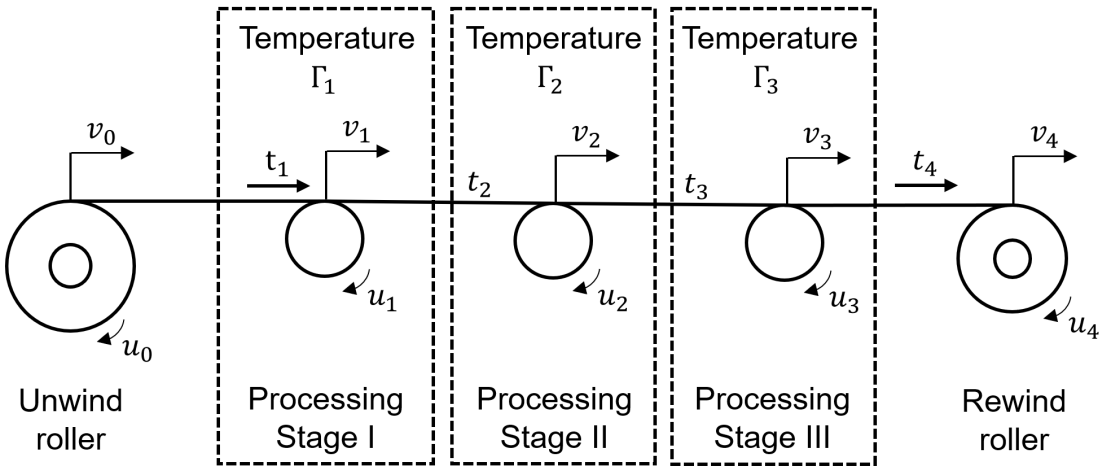

Figure 4.14: Schematic of the simulated R2R system.

The control objective is to maintain the pitch length of each substrate within a consistent range throughout the entire process. It is assumed that the pitch length will be affected by tension and temperature variations. The simulation includes the tension and speed models described in Eqs. (2.1) to (2.7). Additionally, the thermal behavior of the substrate is taken into account, accounting for pitch expansion under different temperature profiles. Specifically, the quality metric used in this case study follows:

$$l_i = (\frac{t_i}{AE} + 1)l_0 + \alpha(\Gamma_i - \Gamma_0)l_0 \tag{4.24}$$

where l_i is the actual pitch length, l_0 is the unstretched pitch length, Γ_i is the actual temperature and Γ_0 is room temperature. t_i, A, E, α are tension, cross-sectional area, Young's modulus, and thermal expansion coefficient of the substrates. The simulation settings align with those used in Chapter 2. In addition, the unstretched pitch length is assumed to be 10 cm, and $\alpha = 6 \times 10^{-5}/\mathrm{K}$.

The simulation is performed in MATLAB using the ode45 function. A total of 200 independent trials are conducted, with each trial lasting for 100 s. In each trial, the system starts from a steady state, and then increments of substrate tension are applied to different stages of the system. A temperature change is also commanded to the chamber starting at $60-70$ s. Throughout

Table 4.2: Inputs and outputs of the deep Koopman model.

Stage	**Inputs**	**Outputs**
Stage I	$v_0, u_0, v_1, \delta v_1, u_1, \Gamma_1$	t_1, l_1
Stage II	$v_2, \delta v_2, u_2, \Gamma_2$	t_2, l_2
Stage III	$v_3, \delta v_3, u_3, \Gamma_3$	t_3, l_3
Rewind stage	$v_4, \delta v4, u_4$	t_4, l_4

this process, the pitch length of the substrates is continuously monitored and recorded as a quality measurement. Notice that $\pm 1\%$ process noise is added to the simulation.

The collected data from the simulations are then utilized for training a deep Koopman model, which aims to learn the stagewise quality propagation of the R2R system. The focus is on understanding how the pitch length is affected by the tension and temperature at each stage, without relying on the underlying physics described by Eq. (4.24). Additionally, we also enforce the Koopman model to learn the influence of other process parameters on tensions. The features provided to the Koopman model are listed in Table 4.2. The latent size of the Koopman model is decided to be 16.

In our implementation, 80% of the data are used for training and the rest are used for validating the model. The prediction results are illustrated in Figure 4.15. The second row of figures represents the elongation of pitch lengths due to the applied tension and temperature change, compared to the unstretched substrates. It is evident that even without explicit knowledge of the underlying physics, the Koopman model can accurately predict the tension and pitch length measurements using the provided process information for both stages II and III. This precise prediction of process and quality characteristics is crucial for the development of the supervisory controller in the subsequent steps.

To evaluate the performance of the proposed set-point optimization scheme, three new simulation trials are conducted, each lasting for 300 s. In these trials, changes in the temperature profile Γ_1 of the first printing chamber are commanded, while keeping other process parameters at the steady state. As depicted by the blue curves in Figure 4.16, the temperature variation induces

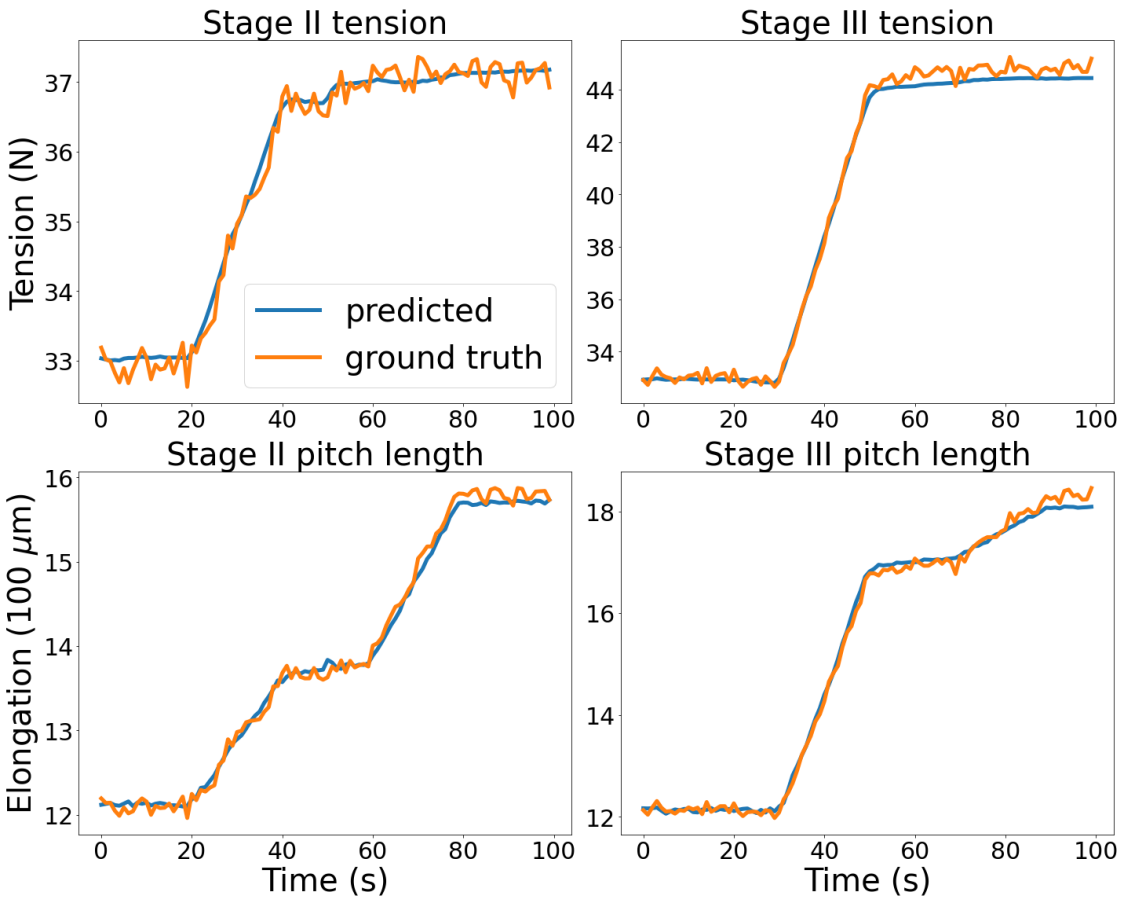

Figure 4.15: The deep Koopman model can accurately predict tension and pitch length elongation at Stages II and III.

a change in the pitch length at processing stage I, subsequently resulting in pitch length deviations across different processing stages. The control objective is to compensate for these deviations by adjusting the tension references. Specifically, the supervisory controller periodically evaluates the quality metrics and suggests adjusted set points for the motor torques in the downstream stages every 10 s. The nonlinear programming problem in (4.23) is solved by using the CasADi package in Python [123]. It is important to note that the supervisory controller operates at a much lower control frequency compared to the lower-level process controllers. After the adjusted process parameters are provided by the supervisory controller, the behavior of the system incorporating these adjustments is computed using a physical model. This approach allows us to assess whether the controller can offer valuable insights to actually improve the operation of the R2R system.

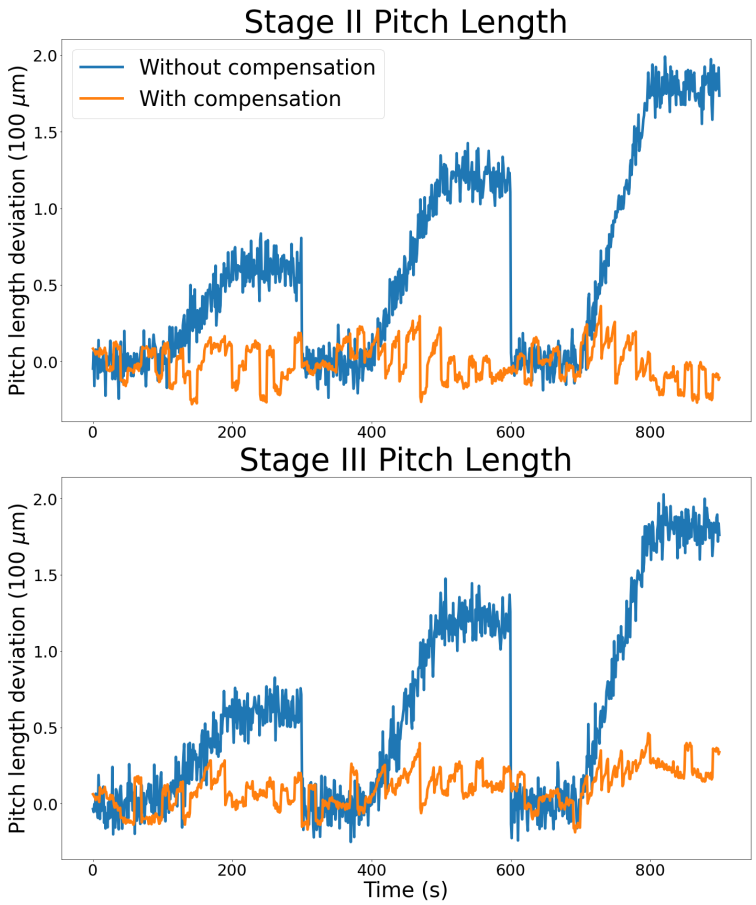

Figure 4.16: The supervisory controller compensates for pitch length deviations when disturbances occur. This deviation measures the variations of pitch length at different stages.

From Figure 4.16, it is evident that without active compensations from the supervisory controller, disturbances can result in pitch length deviations of 60, 120, and 180μm for both stages II and III in the three test trials. However, with the introduction of the supervisory controller, this trend can be predicted and then eliminated. Specifically, the deviation of pitch lengths is regulated within 40μm even when different levels of temperature changes are present. Furthermore, Figure 4.17 demonstrates the collaborative behavior of the motors at stages II and III in response to disturbances. The supervisory controller enables the motors to work in cooperation, dynamically adjusting their set points to counteract the effects of temperature changes and maintain the desired pitch lengths. This showcases the capability of the proposed supervisory controller to optimize the overall performance of the production line by considering the interdependencies between different

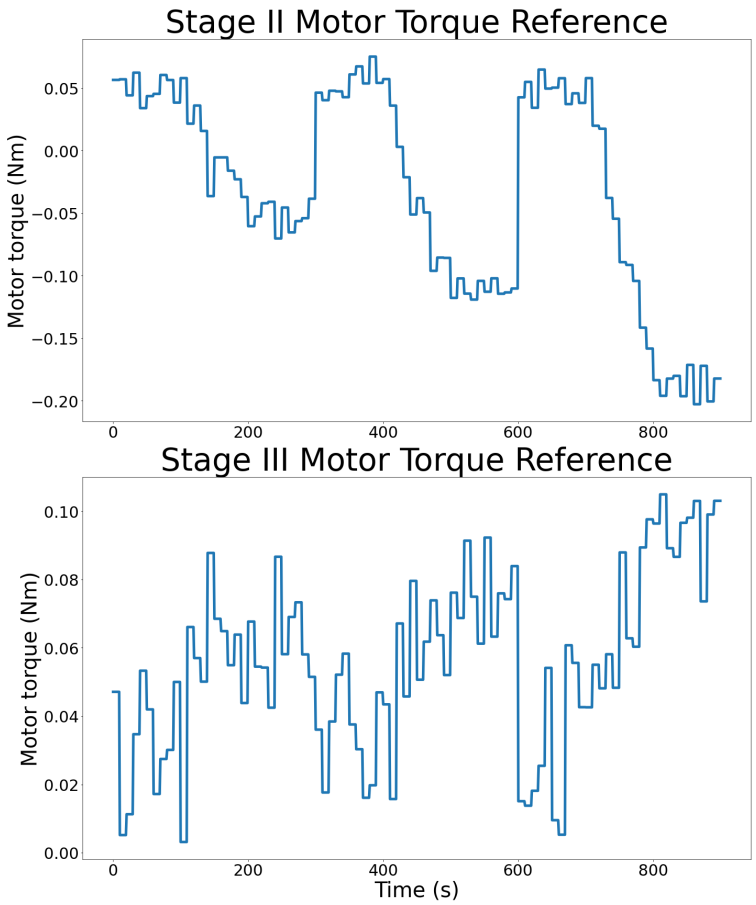

Figure 4.17: The motor torque set points are adjusted every 10 s.

stages. In this case, the interdependencies among stages are learned directly from the data and captured in the Koopman transition matrices, minimizing the reliance on human knowledge.

4.6 Conclusion of the Chapter

This chapter presents a deep Koopman approach to model the quality propagation in MMSs and develops a feedforward supervisory controller to optimize the system settings. Two R2R case studies validate the effectiveness of the proposed method and highlight its potential for improving the operation of R2R production lines. The following conclusions are drawn from the study:

1. The proposed modeling method achieves high prediction accuracy by utilizing an autoencoder-based framework. This approach extracts critical latent variables from the data,

allowing for more robust predictions even in the presence of high-dimensional data and industrial noise.

2. The stage-by-stage modeling scheme enhances the interpretability of the model without sacrificing accuracy. By applying the Koopman operator theory, the framework approximates the nonlinear dynamics of R2R processes by enforcing linear transitions of latent variables between stages. This approach provides insights into the system's behavior at each stage and facilitates decision-making in process optimization.

3. The proposed control scheme effectively optimizes the settings of R2R processes in a dynamic manner. By leveraging the learned model, the feedforward supervisory controller adjusts the system parameters to minimize quality deviations and improve overall performance.

The proposed Koopman framework exhibits several limitations. Firstly, the drifting phenomenon observed in Figure 4.11 may be attributed to the model's inability to capture the changing dynamics of R2R systems. In contrast, the physics-based model can accommodate such characteristics. This indicates a drawback of most data-driven models (including the Koopman models) - they are often trained with fixed model parameters. Adapting to evolving system dynamics becomes challenging in such cases. To address this issue, potential solutions may involve introducing online learning mechanisms or integrating the Koopman model with physics knowledge to eliminate residues from drifting phenomena.

Secondly, the Koopman operator theory suggests that an equivalent linear embedding may yield an infinite-dimensional feature space. However, in practice, dimension truncation is necessary due to the limitations of numerical methods. This worsens the capability of Koopman models in capturing highly nonlinear dynamics. Further research is needed to devise smart truncation approaches and design suitable measurement functions for more accurate modeling.

Future work will focus on implementing the developed methods in real production lines to validate their practical applicability. Additionally, the scope of research can expand to explore

applications, including root cause analysis and anomaly detection, using the deep Koopman framework. Furthermore, enhancements to the supervisory control scheme are essential to tackle challenges related to process noise, model uncertainty, and limited data availability, thereby improving its robustness.

Scholarly Contribution of the Chapter

Zhiyi Chen, Harshal Maske, Huanyi Shui, Devesh Upadhyay, Michael Hopka, Joseph Cohen, Xingjian Lai, Xun Huan, and Jun Ni. "Stochastic deep Koopman model for quality propagation analysis in multistage manufacturing systems." (In submission to Journal of Manufacturing Systems)

Zhiyi Chen, Harshal Maske, Devesh Upadhyay, Michael Hopka, Huanyi Shui, and Xun Huan. "Systems and methods for monitoring and training a manufacturing system." (In submission to US Patent Office, prepared by Ford Motor Company in 2023)

Zhiyi Chen, Harshal Maske, Devesh Upadhyay, Xun Huan, and Jun Ni. "A deep Koopman approach for variation reduction in multistage manufacturing systems." (To be submitted to ACC 2024)

CHAPTER 5

Conclusions and Future Directions

5.1 Conclusions and Contributions

Over the past decades, roll-to-roll processes have gained great attraction in industry for the fabrication of fabric and sheet-metal-based products. Extensive research in the field has demonstrated the potential of R2R printing technology in enabling high-volume and cost-effective production of flexible thin-film devices. However, despite these promising prospects, substantial challenges persist, posing obstacles to the implementation of R2R printing for mass production. These challenges need to be addressed to demonstrate the capability of R2R processes to meet industrial demands.

In this dissertation, we have addressed the challenges associated with enhancing the performance of R2R printing systems. The objective is to overcome the limitations of R2R processes and enable their adoption in the production of flexible electronics. Three major research topics that are explored include robust tension control, safety-critical registration control, and modeling and control of quality propagation in R2R systems. Standing on the shoulders of existing R2R hardware designs, the proposed methodologies approach from algorithmic perspectives to improve the system reliability and finished product quality. Some major takeaways from the presented work are listed as follows.

Chapter 2 provides a thorough investigation into tension control within roll-to-roll (R2R) printing systems. The chapter highlights three critical challenges associated with the complex

dynamics of R2R systems: model uncertainties, time-varying dynamics, and system constraints, which can significantly degrade the performance of conventional tension control methods. To address these challenges, the proposed LPV-MPC algorithm is introduced, demonstrating its effectiveness in achieving rapid and precise tracking of tension set points. Acting as a process-level controller, the proposed algorithm enhances the stability of R2R processes, thereby advancing the state-of-the-art tension control for R2R systems.

The tension controller in Chapter 2 can be applied to R2R processes that require tight tension margins. However, this controller does not directly address the issue of product quality, particularly the challenge of poor registration accuracy in R2R printing processes. To tackle this limitation, Chapter 3 focuses on the design of a quality-level control scheme that eliminates registration errors while ensuring system safety. The chapter presents a primary controller based on a modified Algebraic Riccati Equation to stabilize the registration dynamics. Additionally, a safety controller is designed using the concept of control barrier functionals to ensure system safety. By implementing this control scheme, registration errors can be minimized in the presence of disturbances, while simultaneously keeping the substrate tension within desired control limits.

Instead of focusing on direct control of the process characteristics, Chapter 4 develops a modeling and supervisory control framework that dynamically adjust the set points for process parameters that are considered in the last two chapters. Specifically, R2R processes are modeled as multistage manufacturing systems, and a deep Koopman model is designed to capture the quality propagation between adjacent operation stages. By utilizing the Koopman model, potential disruptions in quality can be anticipated in the presence of disturbances. The supervisory controller then plans adjustments to the process parameters to mitigate these quality issues. Integrating this supervisory controller with the lower-level controllers from the previous chapters holds the potential for achieving an optimized performance in R2R printing systems.

Overall, this dissertation follows a bottom-up approach, progressing from the design of a dedicated tension controller, then to addressing the simultaneous control of registration and substrate tension. Finally, a system-level control scheme is proposed, which supervises the two

lower-level controllers. This incremental approach allows for a comprehensive and systematic exploration of control strategies, gradually addressing the challenges in R2R printing systems.

The contributions of this dissertation include:

1. The disturbance factors that can lead to degradation in tension control performance are identified. An algorithm that combines a tube-based MPC and an incremental model is proposed, which is shown to achieve better tension control performance compared to the benchmarks from the literature.

2. The importance of addressing safety concerns on tension variations, aside from the design of a regular registration controller, is extensively illustrated. Then, the control synthesis that includes a primary controller and a safety controller is designed to mitigate registration errors while enforcing tension constraints.

3. A system-level modeling scheme, which requires a minimal physical understanding of the underlying system, is proposed to model the nonlinear inter-stage correlation in R2R systems. In addition, a supervisory control formulation is designed to dynamically optimize the process setting during operations.

5.2 Limitations of the Presented Work

Limitations of the proposed methods have been discussed in each corresponding chapter. Here, we try to highlight the key issues that need further study. Firstly, it is important to validate the control methods on experimental setups, as most of the validation in this work was conducted via simulation studies for proof-of-concept. Specifically, the disturbance rejection performance of the tension controller and the convergence performance of the registration controller should be thoroughly examined, as these aspects were not extensively studied in this work. Additionally, considering the types of disturbances specific to different R2R systems and incorporating them into the controller designs would enhance their robustness, especially for the proposed registration

control scheme.

The Koopman-based modeling and control method proposed in the last chapter was developed under the assumption of minimal available physical knowledge of the underlying R2R system. Therefore, the integration of physical knowledge into the Koopman framework was not studied in this dissertation. Future research can explore incorporating physical knowledge or active learning techniques to accommodate highly nonlinear and time-varying systems. While the proposed Koopman model demonstrated promising results in predicting stagewise quality indices for MMSs, further analysis can be conducted on the latent variables to assist root cause analysis and anomaly detection. The proposed framework has great potential for improving the operation of manufacturing systems, even though these aspects were not fully explored in this dissertation.

5.3 Future Work

Future work should prioritize resolving the aforementioned limitations while also exploring the development of hierarchical approaches to further improve state-of-the-art R2R printing systems. As mentioned in Chapter 1, to develop high-performance R2R processes that satisfy the industrial demands for producing flexible thin-film devices, researchers need to conduct studies from four different levels. Each level will require significant effort in the future.

At the equipment and sensor level, future research should focus on the development of advanced R2R-related hardware components. This involves exploring new printing technologies that offer improved precision, speed, and versatility in handling different materials and substrates. Additionally, the design and optimization of equipment, such as rollers, tension control systems, and web guiding systems, should be enhanced to ensure reliable and efficient R2R processes. Advanced sensors capable of real-time monitoring and control of critical process parameters, such as tension, temperature, and registration accuracy, should also be developed to enable better process understanding and control. The integration of these advanced hardware components and sensors will contribute to the overall performance and productivity of R2R systems, enabling high-

quality and high-throughput production of flexible thin-film devices.

At the process level, advanced designs of R2R components are essential to enhance the overall controllability. For instance, studies such as [16] and [77] have suggested innovative designs for fixtures and guiding mechanisms that can significantly improve the performance of R2R processes. There is also a need for comprehensive modeling and simulation tools that accurately capture the dynamics and interactions within R2R systems. These tools can aid in the optimization of process parameters, improvement of the system design, and prediction of system behavior under different operating conditions. To enable this, efficient design of experiment methods can be employed to identify critical process parameters and understand their impact on the process intelligently. Developing advanced process control strategies, such as model predictive control, adaptive control, and intelligent control algorithms, is another crucial area for future research. These strategies should address the challenges posed by system nonlinearity, uncertainties, and disturbances, while ensuring precise control of critical process parameters and maintaining product quality. This dissertation proposed methods related to this direction and conducted simulations to perform proof-of-concept studies of the algorithms. In the future, these algorithms should be tested on large-scale R2R production systems to validate their effectiveness further.

At the system level, future research should focus on integrating and optimizing the interaction between different components and subsystems in R2R printing processes. This involves developing advanced control and coordination strategies to ensure seamless operation and synchronization of various process modules, including printing, drying, curing, and post-processing stages. This dissertation has proposed a modeling and control scheme that holds the potential to coordinate the lower-level process controllers. Future work could involve designing an architecture that integrates the system-level and process-level controllers, making it applicable to large-scale R2R systems.

Another important aspect of future work at the system level is the development of scalable and adaptable R2R printing platforms. This involves designing modular systems that accommodate

different printing techniques, substrates, and materials, providing flexibility and versatility in manufacturing a wide range of products. Scalable configurations should be considered to support both small-scale prototyping and large-scale production, allowing for seamless transition and scalability based on market demands.

At the plant level, one should consider the development of advanced planning and scheduling algorithms specifically tailored for R2R printing processes. These algorithms should consider the complexities and constraints of the system, such as substrate availability, processing time, and equipment utilization, to generate optimized production plans. By efficiently allocating resources and coordinating production sequences, these algorithms can help maximize throughput, minimize production time, and reduce energy consumption.

BIBLIOGRAPHY

[1] Department of Energy. Roll to roll (r2r) processing technology assessment. *Quadrennial Technology Review 2015*, 2016.

[2] KP Grenfell. Tension control paper-making and converting machinery. *IEEE Transactions on Applications and Industry*, 83(73):234–240, 1964.

[3] Lei Zhang, Jun Ni, and Xinmin Lai. Dimensional errors of rollers in the stream of variation modeling in cold roll forming process of quadrate steel tube. *The International Journal of Advanced Manufacturing Technology*, 37:1082–1092, 2008.

[4] Hui Xu, Sa Li, Can Zhang, Xinlong Chen, Wenjian Liu, Yuheng Zheng, Yong Xie, Yunhui Huang, and Ju Li. Roll-to-roll prelithiation of sn foil anode suppresses gassing and enables stable full-cell cycling of lithium ion batteries. *Energy & Environmental Science*, 12(10):2991–3000, 2019.

[5] Boning Qu and Stephen R Forrest. Continuous roll-to-roll fabrication of organic photovoltaic cells via interconnected high-vacuum and low-pressure organic vapor phase deposition systems. *Applied Physics Letters*, 113(5):053302, 2018.

[6] Roar R Søndergaard, Markus Hösel, and Frederik C Krebs. Roll-to-roll fabrication of large area functional organic materials. *Journal of Polymer Science Part B: Polymer Physics*, 51(1):16–34, 2013.

[7] Jürgen Willmann, Daniel Stocker, and Edgar Dörsam. Characteristics and evaluation criteria of substrate-based manufacturing. is roll-to-roll the best solution for printed electronics? *Organic Electronics*, 15(7):1631–1640, 2014.

[8] Boning Qu, Zhiyi Chen, Lucas Lahann, and Stephen R Forrest. Cost estimates of roll-to-roll production of organic light emitting devices for lighting. *ACS Photonics*, 2023.

[9] Stephen R Forrest. Waiting for act 2: what lies beyond organic light-emitting diode (oled) displays for organic electronics? *Nanophotonics*, 10(1):31–40, 2020.

[10] Taho Yang and Ronald Van Olmen. Robust design for a multilayer ceramic capacitor screen-printing process case study. *Journal of Engineering Design*, 15(5):447–457, 2004.

[11] CATL's intelligent factory. https://www.catl.com/en/manufacture/, 2023.

[12] Huanyi Shui. *Real-Time Monitoring and Fault Diagnostics in Roll-To-Roll Manufacturing Systems*. PhD thesis, University of Michigan, 2018.

[13] Andreja Rojko. Industry 4.0 concept: Background and overview. *International journal of interactive mobile technologies*, 11(5), 2017.

[14] Steven M George. Atomic layer deposition: an overview. *Chemical reviews*, 110(1):111–131, 2010.

[15] Se Hyun Ahn and L Jay Guo. Large-area roll-to-roll and roll-to-plate nanoimprint lithography: a step toward high-throughput application of continuous nanoimprinting. *ACS nano*, 3(8):2304–2310, 2009.

[16] Chenglin Li, Huihua Xu, and Shih-Chi Chen. Design of a precision multi-layer roll-to-roll printing system. *Precision Engineering*, 66:564–576, 2020.

[17] Xiaobing Feng, Rong Su, Tuomas Happonen, Jian Liu, and Richard Leach. Fast and cost-effective in-process defect inspection for printed electronics based on coherent optical processing. *Optics express*, 26(11):13927–13937, 2018.

[18] Dan Feng, Ryan B Wagner, and Arvind Raman. Measuring nonuniform web tension for roll-to-roll manufacturing of flexible and printed electronics. *Flexible and Printed Electronics*, 6(3):035006, 2021.

[19] J. J. Shelton and K. N. Reid. Lateral Dynamics of a Real Moving Web. *Journal of Dynamic Systems, Measurement, and Control*, 93(3):180–186, 09 1971.

[20] Prabhakar R Pagilla, Nilesh B Siraskar, and Ramamurthy V Dwivedula. Decentralized control of web processing lines. *IEEE Transactions on control systems technology*, 15(1):106–117, 2006.

[21] Zhiyi Chen, Boning Qu, Baoyang Jiang, Stephen R Forrest, and Jun Ni. Robust constrained tension control for high-precision roll-to-roll processes. *ISA transactions*, 2022.

[22] Hailiang Hou, Xiaohong Nian, Hongyun Xiong, Zhong Wang, and Zhi Peng. Robust decentralized coordinated control of a multimotor web-winding system. *IEEE Transactions on Control Systems Technology*, 24(4):1495–1503, 2015.

[23] Xingjian Lai. *Bottleneck Prediction and Resilience Improvement for Manufacturing Systems*. PhD thesis, University of Michigan, 2022.

[24] Shengkai Chen, Shuiliang Fang, and Renzhong Tang. A reinforcement learning based approach for multi-projects scheduling in cloud manufacturing. *International Journal of Production Research*, 57(10):3080–3098, 2019.

[25] Jianjun Shi. *Stream of variation modeling and analysis for multistage manufacturing processes*. CRC press, 2006.

[26] Amine Drira, Henri Pierreval, and Sonia Hajri-Gabouj. Facility layout problems: A survey. *Annual reviews in control*, 31(2):255–267, 2007.

[27] Hartmut Stadtler. Supply chain management: An overview. *Supply chain management and advanced planning: Concepts, models, software, and case studies*, pages 3–28, 2014.

[28] SL Adeyemi and AO Salami. Inventory management: A tool of optimizing resources in a manufacturing industry a case study of coca-cola bottling company, ilorin plant. *Journal of social Sciences*, 23(2):135–142, 2010.

[29] Seung Ryul Na, Xiaohan Wang, Richard D Piner, Rui Huang, C Grant Willson, and Kenneth M Liechti. Cracking of polycrystalline graphene on copper under tension. *ACS nano*, 10(10):9616–9625, 2016.

[30] Xi Zhou, Dien Wang, Ji Wang, and Shih-Chi Chen. Precision design and control of a flexure-based roll-to-roll printing system. *Precision Engineering*, 45:332–341, 2016.

[31] G. E. Young and K. N. Reid. Lateral and Longitudinal Dynamic Behavior and Control of Moving Webs. *Journal of Dynamic Systems, Measurement, and Control*, 115(2B):309–317, 06 1993.

[32] Changwoo Lee, Hyunkyoo Kang, and Keehyun Shin. A study on tension behavior considering thermal effects in roll-to-roll e-printing. *Journal of mechanical science and technology*, 24:1097–1103, 2010.

[33] Carlo Branca, Prabhakar R Pagilla, and Karl N Reid. Governing equations for web tension and web velocity in the presence of nonideal rollers. *Journal of Dynamic Systems, Measurement, and Control*, 135(1):011018, 2013.

[34] Hakan Koc, Dominique Knittel, Michel De Mathelin, and Gabriel Abba. Modeling and robust control of winding systems for elastic webs. *IEEE Transactions on control systems technology*, 10(2):197–208, 2002.

[35] Seung-Ho Song and Seung-Ki Sul. A new tension controller for continuous strip processing line. *IEEE Transactions on Industry Applications*, 36(2):633–639, 2000.

[36] Pramod R Raul and Prabhakar R Pagilla. Design and implementation of adaptive pi control schemes for web tension control in roll-to-roll (r2r) manufacturing. *ISA transactions*, 56:276–287, 2015.

[37] Hailiang Hou, Xiaohong Nian, Jie Chen, and Dengfeng Xiao. Decentralized coordinated control of elastic web winding systems without tension sensor. *ISA transactions*, 80:350–359, 2018.

[38] Shanhui Liu, Xuesong Mei, Fanfeng Kong, and Kui He. A decoupling control algorithm for unwinding tension system based on active disturbance rejection control. *Mathematical Problems in Engineering*, 2013, 2013. Article ID 439797.

[39] Yi Hou, Zhiqiang Gao, Fangjun Jiang, and Brian T Boulter. Active disturbance rejection control for web tension regulation. In *Proceedings of the 40th IEEE Conference on Decision and Control (Cat. No. 01CH37228)*, volume 5, pages 4974–4979. IEEE, 2001.

[40] Andrew Kadik and Wilson Wang. Adaptive force control of in web handling systems. *Intelligent Control and Automation*, 3:329–336, 2012.

[41] Youwei Lu and Prabhakar R Pagilla. Adaptive control of web tension in a heat transfer section of a roll-to-roll manufacturing process line. In *2014 American Control Conference*, pages 1799–1804. IEEE, 2014.

[42] Fabien Claveau, Philippe Chevrel, and K Knittel. A 2dof gain-scheduled controller design methodology for a multi-motor web transport system. *control engineering practice*, 16(5):609–622, 2008.

[43] Dominique Knittel, Edouard Laroche, Daniel Gigan, and Hakan Koç. Tension control for winding systems with two-degrees-of-freedom h/sub/spl infin//controllers. *IEEE Transactions on Industry Applications*, 39(1):113–120, 2003.

[44] Adlane Benlatreche, Dominique Knittel, and Eric Ostertag. Robust decentralised control strategies for large-scale web handling systems. *Control Engineering Practice*, 16(6):736–750, 2008.

[45] D Knittel, D Gigan, and E Laroche. Robust decentralized overlapping control of large scale winding systems. In *Proceedings of the 2002 American Control Conference (IEEE Cat. No. CH37301)*, volume 3, pages 1805–1810. IEEE, 2002.

[46] Anton Nailevich Gafurov, Jaehyeong Jeong, Pyoungwon Park, Inyoung Kim, Thanh Huy Phung, Hyun-Chang Kim, Dongwoo Kang, Dongho Oh, and Taik-Min Lee. Registration error analysis and compensation of roll-to-roll screen printing system for flexible electronics. *Flexible and Printed Electronics*, 6(2):024003, 2021.

[47] Davor Hrovat, Stefano Di Cairano, H Eric Tseng, and Ilya V Kolmanovsky. The development of model predictive control in automotive industry: A survey. In *2012 IEEE International Conference on Control Applications*, pages 295–302. IEEE, 2012.

[48] Gabriele Pannocchia. Offset-free tracking mpc: A tutorial review and comparison of different formulations. In *2015 European control conference (ECC)*, pages 527–532. IEEE, 2015.

[49] Zhiyi Chen, Baoyang Jiang, and Jun Ni. High Precision Tracking of Roll-to-Roll Manufacturing Processes. In *ASME*, volume 2: Manufacturing Processes; Manufacturing Systems; Nano/Micro/Meso Manufacturing; Quality and Reliability of *International Manufacturing Science and Engineering Conference*, 09 2020. V002T07A030.

[50] Davide Martino Raimondo, Daniel Limon, Mircea Lazar, Lalo Magni, and Eduardo Ferná ndez Camacho. Min-max model predictive control of nonlinear systems: A unifying overview on stability. *European Journal of Control*, 15(1):5–21, 2009.

[51] Wilbur Langson, Ioannis Chryssochoos, SV Raković, and David Q Mayne. Robust model predictive control using tubes. *Automatica*, 40(1):125–133, 2004.

[52] David Q Mayne, María M Seron, and SV Raković. Robust model predictive control of constrained linear systems with bounded disturbances. *Automatica*, 41(2):219–224, 2005.

[53] Pornchai Bumroongsri. Tube-based robust mpc for linear time-varying systems with bounded disturbances. *International Journal of Control, Automation and Systems*, 13:620–625, 2015.

[54] Ramón Gonzalez, Mirko Fiacchini, Teodoro Alamo, José Luis Guzmán, and Francisco Rodríguez. Online robust tube-based mpc for time-varying systems: A practical approach. *International Journal of Control*, 84(6):1157–1170, 2011.

[55] Giulio Betti, Marcello Farina, and Riccardo Scattolini. A robust mpc algorithm for offset-free tracking of constant reference signals. *IEEE Transactions on Automatic Control*, 58(9):2394–2400, 2013.

[56] Liuping Wang. A tutorial on model predictive control: Using a linear velocity-form model. *Developments in Chemical Engineering and Mineral Processing*, 12(5-6):573–614, 2004.

[57] Yujun Deng, Peiyun Yi, Linfa Peng, Xinmin Lai, and Zhongqin Lin. Experimental investigation on the large-area fabrication of micro-pyramid arrays by roll-to-roll hot embossing on pvc film. *Journal of Micromechanics and Microengineering*, 24(4):045023, 2014.

[58] Ilya Kolmanovsky and Elmer G Gilbert. Theory and computation of disturbance invariant sets for discrete-time linear systems. *Mathematical problems in engineering*, 4(4):317–367, 1998.

[59] David Q Mayne, James B Rawlings, Christopher V Rao, and Pierre OM Scokaert. Constrained model predictive control: Stability and optimality. *Automatica*, 36(6):789–814, 2000.

[60] JA Delgado-Aguiñaga, Vicenç Puig, and FI Becerra-López. Leak diagnosis in pipelines based on a kalman filter for linear parameter varying systems. *Control Engineering Practice*, 115:104888, 2021.

[61] Yang Su, Kok Kiong Tan, and Tong Heng Lee. Tube based quasi-min-max output feedback mpc for lpv systems. *IFAC Proceedings Volumes*, 45(15):186–191, 2012.

[62] Stefano Riverso, Marcello Farina, and Giancarlo Ferrari-Trecate. Plug-and-play decentralized model predictive control for linear systems. *IEEE Transactions on Automatic Control*, 58(10):2608–2614, 2013.

[63] Zhiyi Chen, Boning Qu, Baoyang Jiang, Stephen R Forrest, and Jun Ni. Robust constrained tension control for high-precision roll-to-roll processes. *ISA transactions*, 136:651–662, 2023.

[64] Monimoy Bujarbaruah, Ugo Rosolia, Yvonne R Stürz, and Francesco Borrelli. A simple robust mpc for linear systems with parametric and additive uncertainty. In *2021 American Control Conference (ACC)*, pages 2108–2113. IEEE, 2021.

[65] Aravind Seshadri, Prabhakar R Pagilla, and Jamie E Lynch. Modeling print registration in roll-to-roll printing presses. *Journal of dynamic systems, measurement, and control*, 135(3):031016, 2013.

[66] Tsuguaki Yoshida, Shinichiro Takagi, Yasuhiko Muto, and Teilong Shen. Register control of sectional drive rotogravure printing press. In *Manufacturing Systems and Technologies for the New Frontier: The 41 st CIRP Conference on Manufacturing Systems May 26–28, 2008, Tokyo, Japan*, pages 417–420. Springer, 2008.

[67] Tsuguaki Yoshida, Shinichiro Takagi, Yasuhiko Muto, and Teilong Shen. Register control of rotogravure printing press. application of nonlinear control theory to sectional drive printing press. *Electronics and Communications in Japan*, 94(1):17–24, 2011.

[68] Shanhui Liu, Xuesong Mei, Jian Li, and Li'e Ma. Machine directional register system modeling for shaft-less drive gravure printing machines. *Mathematical Problems in Engineering*, 2013, 2013.

[69] Hyunkyoo Kang, Changwoo Lee, and Keehyun Shin. Modeling and compensation of the machine directional register in roll-to-roll printing. *Control Engineering Practice*, 21(5):645–654, 2013.

[70] Jongsu Lee, Keehyun Shin, and Changwoo Lee. Analysis of dynamic thermal characteristic of register of roll-to-roll multi-layer printing systems. *Robotics and Computer-Integrated Manufacturing*, 35:77–83, 2015.

[71] Karan Shah, Anqi He, Zifeng Wang, Xian Du, and Xiaoning Jin. Data-driven model predictive control for roll-to-roll process register error. In *International Manufacturing Science and Engineering Conference*, volume 86601, page V001T03A006. American Society of Mechanical Engineers, 2022.

[72] Kyung-Hyun Choi, Tran Trung Tran, P Ganeshthangaraj, KH Lee, MN Nguyen, Jong-Dae Jo, and Dong-Soo Kim. Web register control algorithm for roll-to-roll system based printed electronics. In *2010 IEEE International Conference on Automation Science and Engineering*, pages 867–872. IEEE, 2010.

[73] Aravind Seshadri and Prabhakar R Pagilla. Decentralized control of print registration in roll-to-roll printing presses. In *Dynamic Systems and Control Conference*, volume 56123, page V001T14A006. American Society of Mechanical Engineers, 2013.

[74] Tao Zhang, Zhanpeng He, and Zhihua Chen. A decoupling matrix-based learning control scheme for the machine directional register of roll-to-roll systems. *IEEE Transactions on Industrial Electronics*, 70(8):8398–8407, 2023.

[75] Zhihua Chen, Tao Zhang, Ying Zheng, David Shan-Hill Wong, and Zhonghua Deng. Fully decoupled control of the machine directional register in roll-to-roll printing system. *IEEE Transactions on Industrial Electronics*, 68(10):10007–10018, 2020.

[76] Shanhui Liu, Bingzheng Yin, Li'e Ma, Hongwei Xu, and Geshun Zhu. A decoupling control strategy for multilayer register system in printed electronic equipment. *Mathematical Problems in Engineering*, 2016, 2016.

[77] Jongsu Lee, Junhyeon Byeon, and Changwoo Lee. Theories and control technologies for web handling in the roll-to-roll manufacturing process. *International Journal of Precision Engineering and Manufacturing-Green Technology*, 7:525–544, 2020.

[78] Marco M Nicotra, Tam W Nguyen, Emanuele Garone, and Ilya V Kolmanovsky. Explicit reference governor for the constrained control of linear time-delay systems. *IEEE Transactions on Automatic Control*, 64(7):2883–2889, 2018.

[79] Nan Li, Sijia Geng, Ilya Kolmanovsky, and Anouck Girard. An explicit reference governor for linear sampled-data systems with disturbance inputs and uncertain time delays. *IEEE Transactions on Automatic Control*, 68(1):440–447, 2022.

[80] Gábor Orosz and Aaron D Ames. Safety functionals for time delay systems. In *2019 American Control Conference (ACC)*, pages 4374–4379. IEEE, 2019.

[81] Adam K Kiss, Tamas G Molnar, Daniel Bachrathy, Aaron D Ames, and Gábor Orosz. Certifying safety for nonlinear time delay systems via safety functionals: a discretization based approach. In *2021 American Control Conference (ACC)*, pages 1058–1063. IEEE, 2021.

[82] Adam K Kiss, Tamas G Molnar, Aaron D Ames, and Gábor Orosz. Control barrier functionals: Safety-critical control for time delay systems. *arXiv preprint arXiv:2206.08409*, 2022.

[83] Wenyou Liu, Yunjun Bai, Li Jiao, and Naijun Zhan. Safety guarantee for time-delay systems with disturbances by control barrier functionals. *Science China Information Sciences*, pages 1–15, 2021.

[84] Zhihua Chen, Ying Zheng, Tao Zhang, David Shan-Hill Wong, and Zhonghua Deng. Modeling and register control of the speed-up phase in roll-to-roll printing systems. *IEEE Transactions on Automation Science and Engineering*, 16(3):1438–1449, 2018.

[85] Keqin Gu, Jie Chen, and Vladimir L Kharitonov. *Stability of time-delay systems*. Springer Science & Business Media, 2003.

[86] Emilia Fridman. Tutorial on lyapunov-based methods for time-delay systems. *European Journal of Control*, 20(6):271–283, 2014.

[87] Aravind Seshadri and Prabhakar R Pagilla. Design of delay independent state feedback control for roll-to-roll printing applications. In *Dynamic Systems and Control Conference*, volume 46209, page V003T28A004. American Society of Mechanical Engineers, 2014.

[88] Jian-Hua Ge, Paul Martin Frank, and Ching-Fang Lin. Robust h_∞ state feedback control for linear systems with state delay and parameter uncertainty. *Automatica*, 32(8):1183–1185, 1996.

[89] Arthur B Yeh, Dennis KJ Lin, and Richard N McGrath. Multivariate control charts for monitoring covariance matrix: a review. *Quality Technology & Quantitative Management*, 3(4):415–436, 2006.

[90] Cynthia A Lowry and Douglas C Montgomery. A review of multivariate control charts. *IIE Transactions*, 27(6):800–810, 1995.

[91] Sampatraj S Mandroli, Abhishek K Shrivastava, and Yu Ding. A survey of inspection strategy and sensor distribution studies in discrete-part manufacturing processes. *IIE Transactions*, 38(4):309–328, 2006.

[92] Huanyi Shui, Xiaoning Jin, and Jun Ni. Twofold variation propagation modeling and analysis for roll-to-roll manufacturing systems. *IEEE Transactions on Automation Science and Engineering*, 16(2):599–612, 2018.

[93] Le Yao and Zhiqiang Ge. Cooperative deep dynamic feature extraction and variable time-delay estimation for industrial quality prediction. *IEEE Transactions on Industrial Informatics*, 17(6):3782–3792, 2020.

[94] Yun Bai, Zhenzhong Sun, Bo Zeng, Jianyu Long, Lin Li, José Valente de Oliveira, and Chuan Li. A comparison of dimension reduction techniques for support vector machine modeling of multi-parameter manufacturing quality prediction. *Journal of Intelligent Manufacturing*, 30(5):2245–2256, 2019.

[95] Xiaofeng Yuan, Lin Li, and Yalin Wang. Nonlinear dynamic soft sensor modeling with supervised long short-term memory network. *IEEE Transactions on Industrial Informatics*, 16(5):3168–3176, 2019.

[96] Lei Ren, Zihao Meng, Xiaokang Wang, Renquan Lu, and Laurence T Yang. A wide-deep-sequence model-based quality prediction method in industrial process analysis. *IEEE Transactions on Neural Networks and Learning Systems*, 31(9):3721–3731, 2020.

[97] Xiang Li, Xiaodong Jia, Qibo Yang, and Jay Lee. Quality analysis in metal additive manufacturing with deep learning. *Journal of Intelligent Manufacturing*, 31(8):2003–2017, 2020.

[98] Jinjiang Wang, Yilin Li, Robert X Gao, and Fengli Zhang. Hybrid physics-based and data-driven models for smart manufacturing: Modelling, simulation, and explainability. *Journal of Manufacturing Systems*, 63:381–391, 2022.

[99] Jian Liu. Variation reduction for multistage manufacturing processes: a comparison survey of statistical-process-control vs stream-of-variation methodologies. *Quality and Reliability Engineering International*, 26(7):645–661, 2010.

[100] Marc-André Filz, Sebastian Gellrich, Christoph Herrmann, and Sebastian Thiede. Data-driven analysis of product state propagation in manufacturing systems using visual analytics and machine learning. *Procedia CIRP*, 93:449–454, 2020.

[101] Fahmi Arif, Nanna Suryana, and Burairah Hussin. Cascade quality prediction method using multiple pca+ id3 for multi-stage manufacturing system. *Ieri Procedia*, 4:201–207, 2013.

[102] Zhenyu Liu, Donghao Zhang, Weiqiang Jia, Xianke Lin, and Hui Liu. An adversarial bidirectional serial–parallel lstm-based qtd framework for product quality prediction. *Journal of Intelligent Manufacturing*, 31(6):1511–1529, 2020.

[103] Donghao Zhang, Zhenyu Liu, Weiqiang Jia, Hui Liu, and Jianrong Tan. Path enhanced bidirectional graph attention network for quality prediction in multistage manufacturing process. *IEEE Transactions on Industrial Informatics*, 18(2):1018–1027, 2021.

[104] Pei Wang, Hai Qu, Qianle Zhang, Xun Xu, and Sheng Yang. Production quality prediction of multistage manufacturing systems using multi-task joint deep learning. *Journal of Manufacturing Systems*, 70:48–68, 2023.

[105] Moschos Papananias, Thomas E McLeay, Mahdi Mahfouf, and Visakan Kadirkamanathan. A bayesian framework to estimate part quality and associated uncertainties in multistage manufacturing. *computers in industry*, 105:35–47, 2019.

[106] Partha Protim Mondal, Placid Matthew Ferreira, Shiv Gopal Kapoor, and Patrick N Bless. Monitoring and diagnosis of multistage manufacturing processes using hierarchical bayesian networks. *Procedia Manufacturing*, 53:32–43, 2021.

[107] Li-Ping Zhao, Bo-Hao Li, and Yi-Yong Yao. A novel predict-prevention quality control method of multi-stage manufacturing process towards zero defect manufacturing. *Advances in Manufacturing*, pages 1–15, 2023.

[108] Jianjun Shi and Shiyu Zhou. Quality control and improvement for multistage systems: A survey. *IIE Transactions*, 41(9):744–753, 2009.

[109] Dragan Djurdjanovic and Jun Ni. Online stochastic control of dimensional quality in multistation manufacturing systems. *Proceedings of the Institution of Mechanical Engineers, Part B: Journal of Engineering Manufacture*, 221(5):865–880, 2007.

[110] Pingyu Jiang, Feng Jia, Yan Wang, and Mei Zheng. Real-time quality monitoring and predicting model based on error propagation networks for multistage machining processes. *Journal of Intelligent Manufacturing*, 25:521–538, 2014.

[111] Hao Yan, Nurettin Dorukhan Sergin, William A Brenneman, Stephen Joseph Lange, and Shan Ba. Deep multistage multi-task learning for quality prediction of multistage manufacturing systems. *Journal of Quality Technology*, 53(5):526–544, 2021.

[112] Jose V Abellan-Nebot, Jian Liu, and F Romero Subiron. Design of multi-station manufacturing processes by integrating the stream-of-variation model and shop-floor data. *Journal of Manufacturing Systems*, 30(2):70–82, 2011.

[113] YU Ding, Jionghua Jin, Dariusz Ceglarek, and Jianjun Shi. Process-oriented tolerancing for multi-station assembly systems. *IIE Transactions*, 37(6):493–508, 2005.

[114] Dragan Djurdjanović, Yibo Jiao, and Vidosav Majstorović. Multistage manufacturing process control robust to inaccurate knowledge about process noise. *CIRP Annals*, 66(1):437–440, 2017.

[115] José V Abellan-Nebot, Jian Liu, and F Romero Subirón. Quality prediction and compensation in multi-station machining processes using sensor-based fixtures. *Robotics and Computer-Integrated Manufacturing*, 28(2):208–219, 2012.

[116] Jay Lee, Prayag Gore, Xiaodong Jia, Shahin Siahpour, Pradeep Kundu, and Keyi Sun. Stream-of-quality methodology for industrial internet-based manufacturing system. *Manufacturing Letters*, 34:58–61, 2022.

[117] Bernard O Koopman. Hamiltonian systems and transformation in hilbert space. *Proceedings of the National Academy of Sciences*, 17(5):315–318, 1931.

[118] Peter J Schmid. Dynamic mode decomposition of numerical and experimental data. *Journal of Fluid Mechanics*, 656:5–28, 2010.

[119] Matthew O Williams, Ioannis G Kevrekidis, and Clarence W Rowley. A data–driven approximation of the koopman operator: Extending dynamic mode decomposition. *Journal of Nonlinear Science*, 25(6):1307–1346, 2015.

[120] Bethany Lusch, J Nathan Kutz, and Steven L Brunton. Deep learning for universal linear embeddings of nonlinear dynamics. *Nature Communications*, 9(1):1–10, 2018.

[121] Kaushik Balakrishnan and Devesh Upadhyay. Stochastic adversarial koopman model for dynamical systems. *arXiv preprint arXiv:2109.05095*, 2021.

[122] Diederik P Kingma and Max Welling. Auto-encoding variational bayes. *arXiv preprint arXiv:1312.6114*, 2013.

[123] Joel A E Andersson, Joris Gillis, Greg Horn, James B Rawlings, and Moritz Diehl. CasADi – A software framework for nonlinear optimization and optimal control. *Mathematical Programming Computation*, 11(1):1–36, 2019.

[124] L Eduardo Izquierdo, Jianjun Shi, S Jack Hu, and Charles W Wampler. Feedforward control of multistage assembly processes using programmable tooling. *Trans. NAMRI/SME*, 35:295–302, 2007.

[125] Xiaowei Yue and Jianjun Shi. Surrogate model–based optimal feed-forward control for dimensional-variation reduction in composite parts' assembly processes. *Journal of Quality Technology*, 50(3):279–289, 2018.